Development of nano-particle modified polymer matrices for improved fibre reinforced composites

Vom Promotionsausschuss der
Technischen Universität Hamburg-Harburg
zur Erlangung des akademischen Grades
Doktor-Ingenieur (Dr.-Ing.)
genehmigte Dissertation.

von
Swetha Chandrasekaran

aus
Ranipet, Tamil Nadu, India

2014

Gutachter: Prof. Dr.-Ing. Karl Schulte
(Technische Universität Hamburg-Harburg)
Prof. Dr. Gerold Schneider
(Technische Universität Hamburg-Harburg)
Vorsitzender des Prüfungsausschusses:
Prof. Dr.-Ing. habil. Norbert Huber
(Helmholtz-Zentrum Geesthacht)

Tag der mündlichen Prüfung: 14.07.2014

urn:nbn:de:gbv:830-tubdok-12870

Acknowledgement

At the outset, I express my deep sense of gratitude to my research advisor, *Prof. Karl Schulte* for his valuable and inspiring guidance throughout the course of this work and for giving me an opportunity to do it in the first place. His ideas, comments and healthy critics during our discussions enhanced my appreciation of the subject. Further, I express my sincere thanks to him for providing me with the required facilities and supporting me in all possible ways to the right shape to my doctoral work.

I take this opportunity to thank all my past teachers for their lessons without which I would not have been capable to complete this thesis. I would like to thank everyone who has helped me either directly or indirectly in my research. I would like to thank *Prof. Bodo Fiedler* for allowing me to continue this work. A special thanks to *Dr. rer. nat. Ravi Kumar NV* who encouraged me to pursue research in Germany and also for his motivation to proceed further.

I also place on record, my sense of gratitude to all my colleagues at this institute for their assistance in conducting experiments. I am extremely grateful to *Thea Schnoor, Mathias Mecklenburg, Luis Prado, Hans Wittich and Ingrid Hoffman* for their help and support in the day to day activities of my research and for providing a peaceful and joyful atmosphere in the lab during my work. Some of the experimental works could not have been completed without the assistance of my students *Adan Hernandez and Varun Gopal,* whom I thank for their contribution.

My sincere thanks to my friends *Agata Kopyniecka, Gabriella Faiella, Kaja Wnuk, Rashmi Canchi and Kish Palacios* for making my stay here a very fun filled and a memorable one.

No words will suffice to convey my heart-felt thanks to *Jean Baptiste Forien* for his unwavering support in good or bad times and patience to help me complete this work.

I am grateful to my beloved parents *S. Chandrasekaran and G. Meenakshi* for their blessings and unconditional love, support without which I would not have made this far. Thanks are due to my sister *Sripradha Chandrasekaran* for her care and concern as she constantly reminded me to stay focussed during hard times. Their continuous support and encouragement has brought me over here. Finally, I appreciate the financial support from DAAD-SIEMENS Scholarship (A/10/71620) that funded my research work and my stay in Germany.

Swetha Chandrasekaran

"கற்றது கைமண் அளவு, கல்லாதது உலகளவு"

- Tamil Saint Avvaiyar (1st - 2nd century CE)

Meaning

“What you have learnt is a mere handful; what you haven’t learned is the size of the world”.

Zussammenfassung

Graphen besteht aus einer zweidimensionale Monolage von kovalent gebundenen Kohlenstoffatomen und bildet die Grundeinheit von Graphit und Kohlenstoff-Nanotubes. Insbesondere deren hohe Steifigkeit in Ebenenrichtung (1 TPa), die hohe spezifische Oberfläche (2600 m^2/g) und die hervorragenden elektrischen Eigenschaften haben das Interesse der wissenschaftlichen Gemeinschaft geweckt. Deshalb wird Graphen als weiterer Kandidat neben den etablierten Nano-Füllstoffen, wie Kohlenstoffnanotubes, Ruße, Nano-Silika und Nano-Clay, angesehen. Obwohl kommerziell erhältliches Graphen bisher nicht die theoretischen Kennwerte erreicht, können durch die Dispergierung von Graphen in einem Polymer bereits Nanokomposite mit im Vergleich zu anderen Nano-Carbon gefüllten Systemen überlegenen Eigenschaften erreicht werden.

Diese Arbeit befasst sich mit der Herstellung und Charakterisierung von Epoxid- Kompositen, die mit drei verschiedenen Arten von Nano-Carbon Partikeln (thermisch reduziertes Graphen Oxid (TRGO), Graphit Nano Plättchen (GNP), mehrwandige Kohlenstoffnanotubes (MWCNT)) verstärkt wurden. Die Herstellung dieser gefüllten Komposite erfolgte bevorzugt in einem Dreiwalzwerk. Der Einfluss der unterschiedlichen Füllstoffe auf die mechanischen, elektrischen und thermischen Eigenschaften der Nanokomposite wurde systematisch untersucht. Die Graphen gefüllte Systeme konnten dabei in Bezug auf ihre mechanischen Eigenschaften die MWCNT/ Epoxid Komposite deutlich übertreffen. Um den Einfluss des Dispersionsverfahrens auf die Eigenschaften der ausgehärteten Nanokomposite zu klassifizieren wurde das GNP/ Epoxid System mit modifizierten Dispergierverfahren hergestellt und der Einfluss auf die elektrischen und mechanischen Eigenschaften eingehend untersucht.

Weiterführende Studien, die die Unterschiede insbesondere in der Bruchzähigkeit für die verschiedenen Füllmaterialen systematisch erfassten, wurden durchgeführt. Die Bruchzähigkeit wurde in single-edge notch Drei-Punkt-Biegeversuche gemessen. Die Bruchflächen wurden mittels Raster-Elektronen-Mikroskopie intensiv analysiert. Aus diesen Daten konnte ein mechanistisches Modell entwickelt werden, das aufzeigt, dass insbesondere in den Graphen gefüllten Systemen die Ablenkung der Risse an den Graphen Schichten und die Separierung einzelnen graphitischer Lagen als Hauptfaktoren für die Verstärkung anzusehen sind. Hinweise auf die Funktion als Rissstopper als auch auf eine Initiierung von sekundären Rissen an den Ecken der Graphenschichten könnten ebenfalls gefunden werden.

Aus den gesammelten Beobachtungen und Erkenntnissen wurde ein schematisches Modell für die Versagensmechanismen von Graphen basierten Epoxid-Nanokompositen entwickelt.

In kombinierten rheologischen und elektrischen Messungen wurde ebenfalls untersucht, wie sich die Zugabe von TRGO auf die elektrische Perkolationsschwelle von MWCNT/ Epoxid Kompositen auswirkt. Die Reduzierung der elektrischen Eigenschaften zusammen mit einer morphologischen Charakterisierung zeigen auf, dass es eine Interaktion von TRGO und MWCNTs in der Epoxid Matrix gibt.

Abstract

Graphene a two-dimensional monolayer of covalently bonded carbon atoms is the basic building block for graphite and carbon nanotubes. Having caught the attention of scientific community for its high stiffness (1 TPa), specific surface area (2600 m^2/g) and electronic properties, it has become a potential competitor to carbon nanotubes, carbon black, nano-silica and nano-clay in the field of nano-composites. Though commercially available graphene does not reach the theoretical values in terms of its intrinsic properties, dispersing graphene and its derivatives in polymers yield nano-composite with better properties when compared to other carbon filler based polymer nano-composites.

In this work, epoxy nano-composites reinforced with three different types of carbon nano-fillers (thermally reduced graphene oxide (TRGO), graphite nano-platelets (GNPs) and multiwall carbon nanotubes (MWCNTs)) are prepared by dispersing the fillers in epoxy matrix using a three roll mill. The effect of filler type on the mechanical, electrical and thermal properties of the nano-composite is studied. Graphene based nano-composites outperformed MWCNT/epoxy composites in terms of mechanical properties. Besides determining the effect of filler type on the final properties of nano-composite, the influence of different dispersion methods on electrical and mechanical properties was also studied for GNP/epoxy system.

In the aspect of mechanical properties, studies on the fracture resistance of epoxy nano-composites reinforced with graphene were investigated in depth. The fracture toughness of the nano-composites was measured using single edge notch three point bending test method. An extensive analysis was carried out on the fracture surface using scanning electron microscopy. Finally, a comprehensive investigation on graphene failure mechanisms shows that, crack deflection by the graphene sheets and separation between the graphitic layers are the prime factors that govern the toughening mechanism. Evidence of crack pinning and origination of secondary cracks from the edges of the graphene sheet were also found. Based on the observations a schematic on the failure mechanisms in graphene based epoxy nano-composites is proposed.

The study also investigates the effect of adding TRGO on the electrical percolation threshold of MWCNT/epoxy composites through combined rheological/electrical experiments. The reduction in electrical properties along with morphological investigations gave an insight to the TRGO-MWCNT interactions in the epoxy matrix.

Table of Contents

1 Introduction 1

1.1 Aim of the work 2

1.2 Structure of the thesis 2

2 Back ground and state of the art 3

2.1 History of graphene 3

2.2 Production of graphene 3

2.2.1 Mechanical exfoliation 4

2.2.2 Chemical exfoliation 6

2.3 Properties of graphene 8

2.4 Epoxy resin system 9

2.4.1 Chemistry of epoxy resins 10

2.4.2 Curing of epoxy resins 11

2.4.3 Graphene and epoxy resin used in this work 12

2.5 State of the art: Graphene in polymer composites 13

2.5.1 Preparation of graphene/polymer nano-composite 13

2.5.1.1 Solution mixing 13

2.5.1.2 Melt blending 14

2.5.1.3 In-situ polymerisation 14

2.5.2 Properties of graphene/polymer nano-composite 15

2.5.2.1 Electrical properties 15

2.5.2.2 Thermal properties 15

2.5.2.3 Mechanical properties 16

2.5.2.4 Fracture toughness: graphene/epoxy composite 17

3 Experimental procedure 19

3.1 Materials 19

3.2 Preparation of the nano-composite 20

3.3 Sample geometry 21

3.4 Notch preparation for fracture toughness 24

3.5 Experimental set-up 25

3.5.1 Microscopic analysis 25

3.5.2 Spectro-chemical analysis 25

3.5.3 Electrical studies 26

3.5.4 Thermal studies 26

3.5.5 Rheological studies 26

3.5.6 Mechanical studies 27

4 Results 29

4.1 Filler characterisation 29

4.2 Nano-composite characterisation 35

4.2.1 Dispersion quality: Different dispersion method 37

4.2.2 Microscopic analysis of cured composite 40

4.3 Electrical conductivity 43

4.3.1 Electrical percolation curves of cured nano-composite 45

4.3.2 Effect of dispersion method on electrical conductivity of GNP/epoxy 46

4.3.3 Effect of addition of TRGO on the electrical conductivity of MWCNT/epoxy . 47

4.4 Rheological measurements 49

4.4.1 Steady shear rate sweep measurements 49

4.4.2 Steady shear rate sweep measurements: Effect of different processing technique 51

4.4.3 Combined electro-rheological studies of TRGO_MWCNT/epoxy (shear rate step test) 52

4.5 Thermal conductivity of GNP/epoxy nano-composite 55

4.6 Dynamic thermo-mechanical analysis: Storage modulus and T_g 57

4.6.1 Storage modulus and T_g as a function of temperature for MWCNT/epoxy, TRGO/epoxy and GNP/epoxy 57

4.7 Fracture toughness and R-curve 61

4.7.1 Fracture toughness measurements (SEN-3PB) 62

4.7.2 R-curve behaviour (SEN-4PB) 63

5 Discussions 66

5.1 Filler characterisation 66

5.2 Bi-filler nano-composite TRGO_MWCNT/epoxy 69

5.2.1 Proposed theory for reduced conductivity of bi-filler nano-composite 71

5.3 Mechanical, thermal and electrical characterisation of GNP/epoxy composite 73

5.4 Fractographic analysis 76

5.4.1 Fracture surface observation through SEM after (SEN-3PB) tests 76

5.4.2 Failure mechanism in GNP and TRGO/epoxy after (SEN-3PB) tests 78

5.4.3 Fracture surface analysis GNP/epoxy after cryo-fracture 87

5.5 R-curve 88

6 Conclusion 91

7 Outlook 95

Annexure 97

Publications from this work 103

References ..... Error! Bookmark not defined.5

List of Figures

Figure 2.1: A flow chart on graphene production methods [45]; mechanical exfoliation [20], epitaxial growth [46], CVD [47], thermally reduced graphene [48]. 4

Figure 2.2: Crystal structure of graphite [49]. 5

Figure 2.3: Chemical structure of graphite [56-57]. 6

Figure 2.4: Chemical structure of reduced graphene oxide [48]. 8

Figure 2.5: Schematic of reaction between the Epichlorohydrin and Bisphenol A yielding DGEBA. 10

Figure 2.6: Curing reaction for epoxy resin with anhydride hardener [83]. 12

Figure 2.7: Normalised fracture toughness as a function of filler content for different nano-filler reinforced epoxies. References used in the plot [8], [118], [134], [139-148]. 18

Figure 3.1: A flow chart of the dispersion methods used for preparation of the nano-composite. 21

Figure 3.2: Sample geometries for different test methods. 23

Figure 3.3: Specimen geometry and notch preparation for fracture toughness tests. 24

Figure 4.1: Scanning electron micrograph of carbon nano-fillers MWCNT,TRGO and GNP - (a, c and e) as-received powders; (b, d and f) pelletized fillers. 30

Figure 4.2: TGA mass loss curve for MWCNT, GNP, TRGO fillers under nitrogen and synthetic air atmosphere. 31

Figure 4.3: X-ray diffractogram of the as-received nano-fillers. 32

Figure 4.4: Raman spectra of the as-received nano-fillers taken using He-Ne laser. 33

Figure 4.5: Volume conductivity of the pelletized nano-fillers. 34

Figure 4.6: Schematic that relates the dispersion state and distribution of nano-fillers to the subequent mechanical and electrical properties of nano-composite. 36

Figure 4.7: Transmission light microscopic images of (a-c) 0.29wt% MWCNT/epoxy after different dispersion cycle in 3RM; (d-f) the same for 0.29wt% TRGO/epoxy respectively. ..38

Figure 4.8: Transmission light microscopic images of 0.57wt% GNP/epoxy prepared by different dispersion methods (a) 3RM; (b) Soni_hsm and (c) Soni_3RM.....39

Figure 4.9: Transmission optical micrograph of mono-filler and bi-filler systems (a) 0.29wt% TRGO/epoxy; (b) 0.29wt% MWCNT/epoxy and (c) 0.29_0.29wt% TRGO_MWCNT/epoxy. 40

Figure 4.10: Scanning electron micrograph in "in-lens" mode of cryo-fractured cured composites containing (a) 0.3wt% MWCNT/epoxy; (b) 0.3wt% TRGO/epoxy and (c) 0.3wt% GNP/epoxy, showing the distribution of fillers in matrix.....41

Figure 4.11: Scanning electron micrographs of thin slices (500nm thick on Si wafer) of cured composite in "in-lens" mode (a-c) 0.1-0.5wt% of MWCNT/epoxy and (d-f) 0.1-0.5wt% TRGO/epoxy.....42

Figure 4.12: Schematic representation of filler dispersion by varying the filler loading and its corresponding electrical conductivity.....44

Figure 4.13: Electrical percolation curves for MWCNT/epoxy, TRGO/epoxy and GNP/epoxy. 45

Figure 4.14: Electrical percolation curve for GNP/epoxy system prepared via different dispersion methods.....47

Figure 4.15: Comparison of the electrical conductivity between bi-filler 0.01wt% TRGO_MWCNT/epoxy and mono-filler MWCNT/epoxy cured composite. Insert shows the electrical percolation curve for mono-filler TRGO/epoxy composite.....48

Figure 4.16: Viscosity of different nano-composite suspensions as a function of shear rate. 50

Figure 4.17: Viscosity as a function of shear rate for 0.57wt% GNP/epoxy composite suspension prepared via different dispersion methods measured under steady state. 51

Figure 4.18: Electrical conductivity at different shear rates for the MWCNT/epoxy and TRGO_MWCNT/epoxy suspensions at lower filler concentration.....52

Figure 4.19: Optical micrographs of (a–c) 0.02_0.02wt% TRGO_MWCNT/epoxy; (d-f) 0.02_0.05wt% TRGO_MWCNT/epoxy; (g-i) 0.02wt% MWCNT/epoxy and (j-l) 0.05wt% MWCNT/epoxy. 54

Figure 4.20: Thermal conductivity of GNP/epoxy nano-composite as a function of weight percentage of filler. 56

Figure 4.21: Storage modulus curve as a function of temperature for different nano-composite systems. 58

Figure 4.22: Loss factor as a function of temperature for three different nano-composite systems. 59

Figure 4.23: Storage modulus of 0.3wt% GNP/epoxy systems using three different dispersion methods. 60

Figure 4.24: Loss factor curve for 0.3wt% GNP/epoxy systems via different processing methods. 60

Figure 4.25: Fracture toughness by (SEN-3PB test) as a function of weight percentage of filler for MWCNT, TRGO and GNP reinforced epoxy nano-composite. 63

Figure 4.26: R-curve for 0.1wt% and 0.5wt% of TRGO/epoxy exhibiting an increasing trend. 64

Figure 4.27: Comparing the crack resistance curve for 0.3wt% of TRGO/epoxy and MWCNT/epoxy nano-composite [197]. 65

Figure 5.1: Scanning electron micrographs of 500 nm thin slices of composite deposited on Si substrate. (a-c) SEM of mono-filler 0.035wt% MWCNT/epoxy; (d-f) SEM of mono-filler 0.01wt% TRGO/epoxy; (g-i) SEM of bi-filler 0.01_0.035wt% TRGO_MWCNT/epoxy. 70

Figure 5.2: Morphological model for TRGO_MWCNT/epoxy cured composite; (a) cross-sectional view and (b) top-view respectively. 71

Figure 5.3: Scanning electron micrographs in-lens mode of cryo-fractured surface of bi-filler 0.3_0.3wt% TRGO_MWCNT/epoxy cured composite; (a) MWCNT agglomerates are surrounded by TRGO agglomerates and (b) MWCNTs pinned onto the TRGO sheets respectively. 72

Figure 5.4: Cryo-fractured SEM images of 0.3wt% GNP/epoxy prepared by (a) 3RM technique; (b) Soni_hsm technique and (c) Soni_3RM technique respectively. Dotted lines indicate the crack propagation direction. 74

Figure 5.5: Mechanical, thermal and electrical properties of GNP/epoxy composite prepared via 3RM technique as a function of filler content. 75

Figure 5.6: Effect of filler type on storage modulus, glass transition temperature and fracture toughness on epoxy based nano-composites. 76

Figure 5.7: Representative fracture surfaces of 0.1wt% nano-filler/epoxy after SEN-3PB test, (a) pure epoxy, (b) MWCNT/epoxy, (c) GNP/epoxy and (d) TRGO/epoxy. Insets in (a) and (b) show higher magnification micrographs. 77

Figure 5.8: Examples of crack pinning failure (a), (b) GNP/epoxy and (c), (d) TRGO/epoxy on both the fracture sides. Dotted lines indicate crack propagation direction. 79

Figure 5.9: Examples of failure by separation in between the GNPs on both fracture sides (a), (b) and TRGO (c), (d) where the white arrows indicate the delaminated surface of nano-filler. 80

Figure 5.10: Examples of GNP/TRGO separation in between the graphitic layers: (a) GNP /epoxy and (c) TRGO/epoxy through SE2 detector; (b) GNP/epoxy and (d) TRGO/epoxy through in-lens detector (arrows indicate the nano-filler layers oriented perpendicular to crack front). 81

Figure 5.11: Schematic of the observed crack propagation mechanism in TRGO/GNP epoxy composite. 82

Figure 5.12: Schematic on the interaction of crack front with GNP/TRGO particles. 83

Figure 5.13: Scanning electron micrograph of fracture surface of GNP/epoxy (a) 0.1wt%; (b) 0.3wt%; (c) 0.5wt%; (g) 1.0wt%; (h) 2.0wt%; and of TRGO/epoxy (d) 0.1wt%; (e) 0.3wt% and (f) 0.5wt% respectively (dotted arrows indicate crack propagation direction). 84

Figure 5.14: Scanning electron micrographs of fracture surface of TRGO/epoxy (a) shows wrinkled morphology of filler; (b) secondary cracks emerging beneath the TRGO sheet and (c) formation of multiple cracks respectively. Dotted lines indicate crack propagation direction. 85

Figure 5.15: (a) Fracture toughness of TRGO/epoxy and GNP/epoxy as a function of filler content; (b) schematic of crack propagation that accounts for the fracture toughness variation with filler content for GNP/epoxy system. 86

Figure 5.16: Scanning electron micrographs of cryo-fractured 0.3wt% GNP/epoxy; (a) hindering of crack propagation by GNP agglomerate, (b) trace from separation between the graphene layers. 87

Figure 5.17: Scanning electron micrographs of the fracture surface near the raw notch of (a) pure epoxy; (b) 0.3wt% MWCNT/epoxy; (c) 0.3wt% TRGO/epoxy. Insets show the beach marks (white solid arrows). Dotted lines indicate the crack propagation direction.....89

Figure 6.1: Mechanical and electrical property of 0.5wt% MWCNT/epoxy, TRGO/epoxy and GNP/epoxy nano-composites.....92

Figure 6.2: Effect of dispersion method on electrical conductivity, storage modulus and glass transition temperature of 0.3wt% GNP/epoxy.....92

Figure A.1: Notch preparation for SEN-4PB tests; raw notch using diamond saw blade and V-notch using blade runner.....97

Figure A.2: Electrical conductivity of 0.3_0.3wt% TRGO_MWCNT/epoxy bi-filler composite compared with respective mono-filler composites as a function of frequency. 97

Figure A.3: Viscosity of 0.3wt% MWCNT/epoxy suspension prepared by 3RM process as a function of shear rate after each milling cycle.....98

Figure A.4: Electrical conductivity at different shear rates for the MWCNT/epoxy, TRGO/epoxy and TRGO_MWCNT/epoxy suspensions at higher filler concentration respectively. 98

Figure A.5: Electrical conductivity and viscosity of 0.02wt% TRGO/epoxy suspensions as a function of shear rate and time.....99

Figure A.6: Optical micrograph of 0.02wt% TRGO/epoxy suspension after 10 minute at (a) initial suspension (b) at 10 s^{-1} shear rate and (c) at 0.1 s^{-1} shear rate respectively. 99

Figure A.7: Energy dispersive spectrum for the as-received TRGO and GNP nano-fillers.102

Figure A.8: Scanning electron micrograph of cryo-fractured 0.3_0.3wt% TRGO_CB/epoxy in "in-lens" mode where (a) impression of CB agglomerates on graphene sheets and (b) higher magnification micrograph. Dotted lines indicate crack propagation direction.....102

List of Tables

Table 3.1: Datasheet of as-received MWCNT, TRGO and GNP nano-fillers. 19

Table 5.1: Consolidated parameters obtained from filler characterisation. 68

Table A.1: Thermo-mechanical properties of the nano-composite from DMTA analysis. .. 100

Table A.2: Fracture toughness values of nano-composite from SEN-3PB test. 101

List of Abbreviations

1D/2D	-	One-dimensional/Two-dimensional
3PB	-	Three point bending
3RM	-	Three roll-mill
4PB	-	Four point bending
AFM	-	Atomic force microscope
CB	-	Carbon black
CCG/CRG	-	Chemically converted/Reduced graphene
CNT	-	Carbon nano-tube
DENB	-	Double edge notch bending
DMTA	-	Dynamic thermo-mechanical analysis
FWHM	-	Full width at half maximum
GIC	-	Graphite intercalated compounds
GNP	-	Graphite nano-platelet
GO	-	Graphite oxide
HOPG	-	Highly ordered pyrolytic graphite
LM	-	Light microscope
MEG/MEGO	-	Microwave exfoliated graphene/Microwave exfoliated graphene oxide
MWCNT	-	Multi-wall carbon nano-tube
PNC	-	Polymer nano-composite
R-curve	-	Crack resistance curve
SEM	-	Scanning electron microscopy
SEN-3PB/SEN-4PB	-	Single edge notch-three/four point bending
SENB	-	Single edge notch bending
Soni_3RM	-	Sonication combined with three-roll mill
Soni_hsm	-	Sonication combined with high speed shear mixing
SSA	-	Specific surface area
TGA	-	Thermo-gravimetric analysis
TRG/TRGO	-	Thermally reduced graphene/Thermally reduced graphene oxide
wt%	-	Weight percentage
XRD	-	X-ray diffraction

List of Symbols

Symbol		Quantity	Unit
T_g	-	Glass transition temperature	°C
E'_g	-	Glassy storage modulus	GPa
E'_r	-	Rubbery storage modulus	GPa
E”	-	Loss modulus	GPa
tan δ	-	Loss factor	-
K_{IC}	-	Fracture toughness	$MPa \cdot m^{1/2}$
σ	-	Electrical conductivity	S/m
η	-	Viscosity	Pa·s
θ	-	Degree	°
λ	-	Wavelength	Å
g	-	Degree of graphitisation	%
ρ_{th}	-	Theoretical density	g/cc
ρ_{exp}	-	Experimental density	g/cc
V_f	-	Volume fraction of filler	-
p_f	-	Packing fraction	-
$d_{(0\,0\,2)}$	-	Inter-layer spacing	Å
$D_{(0\,0\,2)}$	-	Crystalline thickness	nm
I_D/I_G	-	Intensity ratio of D band to G band	-
L_a	-	Crystalline width	nm
R_s	-	Sheet resistance	Ω
φ_c	-	Percolation threshold	wt%

1 Introduction

Composites are multi-phase materials that exhibit all the properties of its constituent phases. Over the recent years, a strong emphasis is being given for polymeric nano-composites (PNCs) where the dispersed phase shall be in nano-meter scale and of any shape. The use of nano-scale over micron-scale materials has an advantage of exhibiting better physical and chemical properties because of their large surface area. Different types of nano-particles can be incorporated into the polymeric matrix depending on the application [1]. Typical materials used are nano particles, nano-platelets, nano tubes, fullerenes and nano-wires. Among the nano-fillers, carbon based nano-fillers dominate as reinforcements as they exhibit better mechanical, electrical and thermal properties and have opened the floodgates in the field of polymer nano-composites [2-6].

The development of PNCs has two major issues; first is the selection of nano-filler so that it is compatible with the polymeric matrix and the second is the processing technique through which it is dispersed in the polymeric matrix. The dispersion state of nano-fillers in the polymeric matrix often has a huge impact on the properties of polymeric materials [7]. Earlier studies have shown that a reasonable degree of dispersion is achieved either by means of high shear mixing where the polymer is subjected to very high shear forces or through sonication. [8-11].

Polymers reinforced with carbon nanotubes exhibit a substantial improvement in modulus, toughness, electrical conductivity, glass transition temperature of the polymer [12-16]. There are studies on estimation of the maximum reinforcement given by carbon nanotubes on polymers. According to this estimation, the efficiency of reinforcement is based on the percolation behaviour and stress transfer theory in large aspect ratio fillers [17,18].

A recent addition to the family of carbon nano-fillers is graphene and its derivatives - a honeycomb like structure which consists of one monolayer of carbon. Similar to carbon nanotubes (CNTs), these two-dimensional layered structures also possess excellent electrical and thermal conductivities along with high modulus [19,20]. When compared with carbon nanotubes, graphene and functionalized graphene sheets have less entanglement, if any and large specific surface area thus making them an ideal substitute for mechanical reinforcement in the matrix [21-23]. The addition of thermally reduced graphene to polymer matrices provides composites with either lower or higher electrical conductivity depending on the matrix [24,25].

1.1 Aim of the work

The utilization of epoxy resins in engineering application is often restricted due to its brittle nature (low fracture toughness). Hence, loading the polymeric matrix with nano-fillers such as carbon nanotubes or graphene is an alternative solution to enhance the facture toughness without compromising its mechanical properties. Recent literature suggests that the use of graphene as filler in epoxy matrix yields to nano-composites with better mechanical properties than those reinforced with carbon nanotubes. However, there has been little discussion about the toughening mechanisms in graphene based epoxy composites so far.

In this work, different types of graphene filler were dispersed in epoxy matrix using a three roll-mill, to prepare a graphene based epoxy nano-composite and compared with carbon nanotube reinforced epoxy system. The object of the work is to study the effect of filler on storage modulus, glass transition temperature, fracture toughness and electrical conductivity of nano-composites by varying the filler concentrations. The potential of intermixing different fillers was also studied using bi-filler epoxy composites containing nanotubes and thermally reduced graphene oxide through combined electro-rheological measurements. The main object of the current study is to understand the failure mechanisms and toughening effects of graphene based fillers in epoxy composites.

1.2 Structure of the thesis

The thesis has been well structured so as to present a detailed account of the study. The first chapter introduces the reader to the object of this research and Chapter 2 lays out the theoretical dimensions of the research, especially on the production, properties of graphene and graphene based polymer composites. Chapter 3 describes the design of the experiments, materials used, preparation of samples and details of the experiments performed. The main results are presented and discussed in Chapter 4. Since the current study compares epoxy nano-composites based on different fillers, a detailed discussion on the potentiality of using graphene and its derivatives as filler is presented in Chapter 5. The chapter also focuses on the failure mechanism on graphene based epoxy nano-composites which is the aim of this research work. The final chapters summarise the main findings of the current study and the implications of this work for further research pertaining to this field.

2 Back ground and state of the art

2.1 History of graphene

Carbon which is one of the essential elements, as it forms the basic building block of life, is known to exist in several allotropes due to its valency. Until 1985 only two allotropes of carbon were found to exist which are diamond and graphite. The field of carbon allotropes received attention with the discovery of buckyballs (C_{60}) - also named fullerenes. This was later followed by several other forms of buckyballs (from C_{20} to C_{80}) and in 1991 another break through was seen with the first description of carbon nano-tubes.

Graphite an early allotrope of carbon known to exist got its name from the Greek word "graphein". It is known for its lamellar structure and stacked by several mono layers of carbon which are held together by weak van der Waals forces. Since early 1940's it was predicted that when these mono layers, if isolated, can be bestowed with unique electrical and mechanical properties [26]. This monolayer of carbon when isolated from graphite is called "graphene". The name was coined in 1986 by Boehm [27]. However, graphene like materials were derived from graphite oxide via chemical methods in 1960s [28]. While the exfoliation of graphite is known for several decades, it was only in 2004 that graphene monolayer was isolated at room temperature by A. Geim and K. Novoselov who later were awarded the Nobel Prize in Physics in 2010 [29-31].

2.2 Production of graphene

Ever since its discovery, scientists have always been looking for effective and efficient methods for large scale production of high purity graphene [32]. In fact most research on production of graphene is focused on finding a cost effective way of harvesting graphene for commercial use. Most of the graphene production methods available today could be classified under two main approaches.

Top down approach:

The production process of the top down approach commences with the use of graphite or graphite derivatives (graphite oxide (GO) or graphite intercalated compounds (GIC)) and finally ends with graphene. The methods used in this approach are typically exfoliation techniques that separate the individual layers of graphite in order to arrive at graphene.

Bottom up approach:

Another route to synthesise graphene is to grow it on a substrate. Chemical vapour deposition (CVD) [33-36], epitaxial growth on SiC [37-39], chemical unzipping of nanotubes [40,41], arc discharge[42-44] are some examples of bottom up approach.

Among these several techniques which are established for graphene synthesis, mechanical cleavage, chemical exfoliation and thermal chemical vapour deposition are widely used. An overview of graphene synthesis techniques is shown in the flow chart Fig. 2.1.

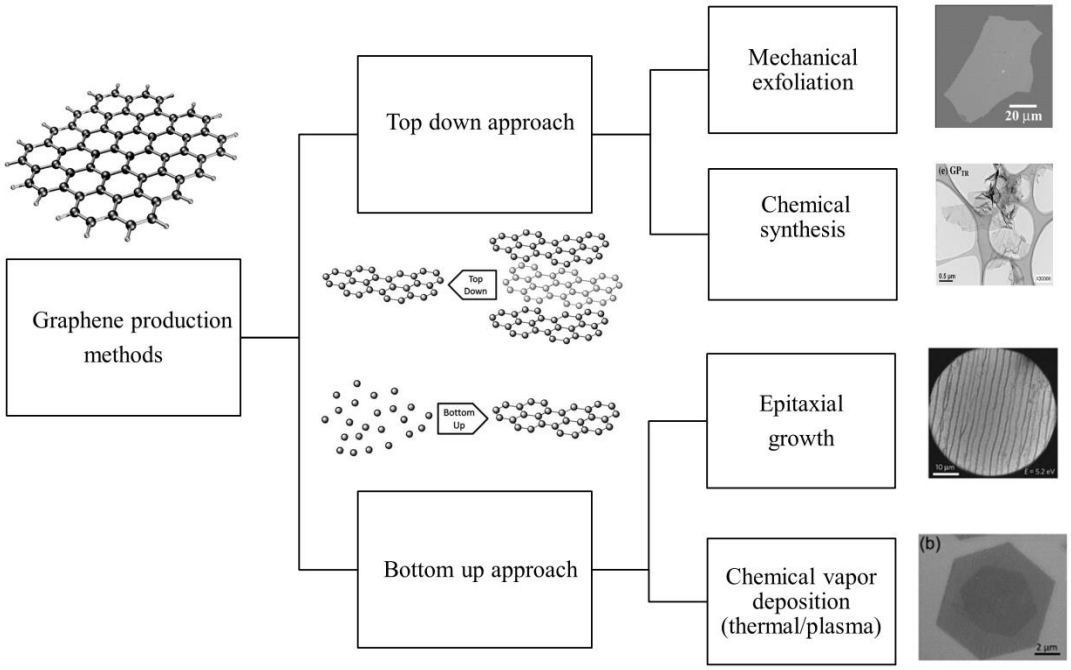

Figure 2.1: A flow chart on graphene production methods [45]; mechanical exfoliation [20], epitaxial growth [46], CVD [47], thermally reduced graphene [48].

Out of the several methods reported in literature, this section discusses in detail two main methods viz., the mechanical exfoliation as this method paved way for graphene discovery and the chemical exfoliation as the material used in this study was prepared by this method.

2.2.1 Mechanical exfoliation

It is the first recognised method to produce monolayer graphene where a longitudinal or transverse force is generated on the surface of layered material by means of any mechanical energy. Graphite which is an allotrope of carbon is formed by stacking several mono-layers of graphene and is held by weak van der Waals forces in the transverse axis (c-axis), having an interlayer spacing of 3.34 Å between the graphitic sheets.

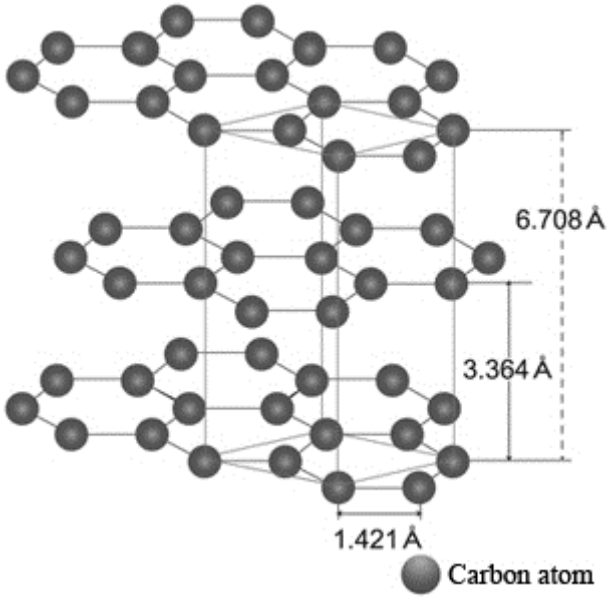

Figure 2.2: Crystal structure of graphite [49].

The external force required to mechanically cleave a mono-layer is ~300 nN/μm^2 [50]. Novoselov et al., used laboratory grade scotch tape (less glue content) to produce single layer graphene from 1mm thick highly ordered pyrolytic graphite (HOPG) by mechanical cleaving. HOPG which is stuck on to the scotch tape is peeled repeatedly for a few times and the final transfer is made on Si wafer which is cleaned using solvents. Once the scotch tape with few graphite layers is stuck to the Si wafer, the scotch tape is then peeled very slowly for better cleavage and a final peeling is done with a fresh scotch tape and peeled rapidly. The silicon wafer now consists of graphene flakes varying from mono-layer, bi-layer and few-layer graphene, which is again washed with solvents.

The HOPG is first dry etched using oxygen plasma and the resulting graphite surface is transferred on to a photoresist layer on a glass substrate. Then repeated peeling is carried out using the scotch tape and is then released into acetone. Si wafer is then used to transfer these single and few layer graphene from acetone, which is then cleaned with water and propanol.

Apart from the adhesive tape method, several micro mechanical cleaving techniques using atomic force microscope (AFM cantilever) [51], cleaving aided by ultrasonic oscillations along the wedge [52], and direct sonication of graphite in appropriate solvents [53-54]. Graphene obtained from mechanical exfoliation has fewer defects and hence are used for fabrication of electronic devices but only at the laboratory scale.

2.2.2 Chemical exfoliation

Large scale production method of graphene is envisaged through liquid phase exfoliation using chemicals which is a well-established chemical process developed by Brodie, later modified by Hummer [55]. The method is based on the principle of oxidising graphite in the presence of strong acids and oxidising agents. The oxide functionalities that are formed during the chemical process decorate the edges and surface of the graphite sheets to yield graphite oxide. Graphite oxide is prepared by treating graphite with a mixture of sulphuric acid (H_2SO_4), sodium nitrate ($NaNO_2$) and potassium permanganate ($KMnO_4$) for two hours at a temperature below 45 °C. After completion of the reaction, the mixture is then washed in ice-bath with hydrogen peroxide (H_2O_2) to reduce residual $KMnO_4$ to manganese dioxide MnO_2. Repeated washing in distilled water yields graphite oxide as a brownish yellow liquid. The presence of several functional groups like epoxide, hydroxyl, etc., in graphene oxide is hydrophilic and can be dissolved in water by sonication. Now the layers become negatively charged and therefore recombination of layers is inhibited. Graphite oxide is then dissolved either in water or organic solvents and is then subjected to ultra-sonication to further exfoliate the sheets and graphene oxide (GO) is obtained. The chemical structure of graphite oxide is shown in Fig. 2.2.

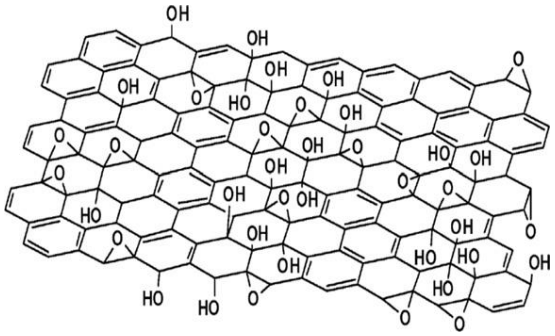

Figure 2.3: Chemical structure of graphite [56-57].

Natural graphite has an inter-layer spacing of 3.34 Å between the graphitic sheets; whereas graphite oxide has a spacing of 7.88 Å obtained from X-ray diffraction studies [58]. This increase in d-spacing is due to the presence of intercalated water molecule and various other oxide groups. Also during this chemical process there is reduction in the flake size of the parent graphite used and the C:O:H ratio is very less (~2:1:0.8). The presence of epoxy, carbonyl and carboxylic functional groups in GO which decorate the edges and surface provides reactive sites for various surface modifications on the GO thus enabling GO to be easily dispersed in

polymeric matrices where better filler matrix interaction could be envisaged via functionalization [59-60].

Oxidation of graphite by means of chemicals has its disadvantages too, as during the process, the sp^2 hybridised carbon structure is broken, causing lattice defects in the graphene monolayer. One of the key properties of graphene which attracted many researchers is its electrical conductivity which relies on the long range conjugated network in the graphite lattice. But, during oxidation, this long range order is broken, due to the presence of functionalities and the defects caused. As a result, the π-electrons are localised and decrease both conductivity and mobility of electrons in GO. Hence a reduction process is necessary not only to remove the oxide groups but also to remove the atomic scale defects in the GO lattice structure [61].

Reduction of GO is done using two ways; either by thermal treatment or by chemical treatment. During thermal treatment GO is heated rapidly up to 2000 °C in seconds under nitrogen or argon atmosphere. The mechanism of exfoliation is based on the pressure generated by the CO or CO_2 gases formed. This pressure was estimated to vary between 40 and 130 MPa depending on the temperature of annealing, whereas the actual pressure required was found to be 2.5 MPa (theoretical calculation) to exfoliate two GO sheets [62]. Hence the graphene obtained by thermal reduction is termed as "thermally reduced graphene/graphene oxide (TRG/TRGO)" and has a wrinkled morphology due to the thermal treatment. There are also reports where the thermal annealing is done by means of microwave radiation and the graphene obtained is termed as "microwave exfoliated graphene/graphene oxide (MEG/MEGO)" [63-64].

Chemical reduction involves removal of oxide functionalities by using chemical reduction reagents [65]. The most popular among these reagents is hydrazine and its derivatives as the yield from this process is very high. Due to the toxicity of this chemical, there are also other alternatives where hydride salts such as sodium borohydride ($NaBH_4$) [66] and lithium aluminium hydride ($LiAlH_4$) are used [67]. Other chemical reagents reported in literature involve ascorbic acid [68], hydro iodic acid [69], alcohols [70] and base reduction using NaOH [71]. Also in-situ polymerisation is used where the polymer acts as a reducing agent [72,73]. The use of photo catalysis method, electro-chemical method and solvo-thermal methods is also reported for the reduction of GO. The graphene prepared by chemical reduction is termed as "chemically converted/reduced graphene (CCG/CRG)" [74].

However, both thermal and chemical reduction does not fully reduce the GO and remove the lattice defects. The chemical structure of CCG/CRG and TRG/TRGO is still under

investigation and it was found that there is a difference in the structure as shown in Fig.2.3 and it affects the intrinsic property of the material prepared.

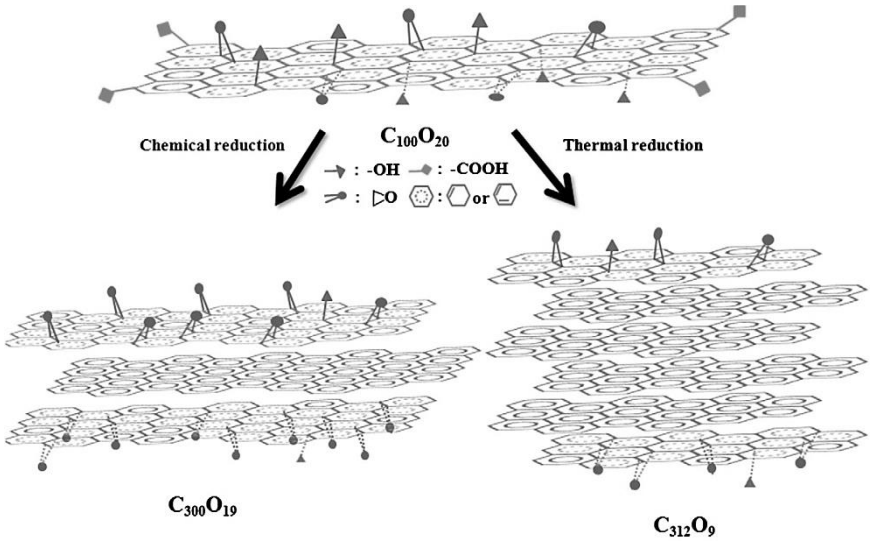

Figure 2.4: Chemical structure of reduced graphene oxide [48].

The above discussed chemical route uses graphite as its parent material to obtain graphene. But the same can be applied to obtain GO sheets from carbon nanotubes and is called chemical unzipping of the tubes to yield graphene nano ribbons (GNRs) [40]. Even carbon nano fibres (CNFs) having a cup and cone arrangement are used as apparent material to get graphene [75].

Another chemical exfoliation method used is by means of alkali metals that can form graphite intercalated structures with graphite. The most common metal used is potassium (K) which forms a KC_8 intercalated compound when reacted with graphite at 200 °C in helium atmosphere. This compound further reacts with aqueous solution of ethanol where the potassium ions dissolve in the solution [76]. This method yields few layered graphene which are further exfoliated by rapid thermal treatment. The graphene obtained from this method has less oxide functionalities and depending on the degree of exfoliation the graphene obtained is termed as "graphite/graphene nano-platelets (GNPs)".

2.3 Properties of graphene

Being one of the very few 2D materials known to man, graphene has a set of unique physical and chemical properties that makes it very attractive for a large number of potential applications.

Electronic properties

Theoretically, because of its honeycomb like structure, pure graphene has a high electrical conductivity. The mobility of the charge carriers is about 200,000 cm^2/Vs [77]. The electrons travel through the graphene sheet as if they carry no mass and by restricting the electrons to only two dimensions, they exhibit some interesting properties such as the 'anomalous quantum Hall effect' [78].

Thermal properties

Its thermal conductivity measured recently at room temperature is >5000 W/mK which is highest value measured among the other carbon allotropes [79]. The ballistic thermal conductance of graphene is isotropic in nature.

Mechanical properties

Ideal graphene is highly flexible. It can be stretched up to 20% elastically, thereby making it highly bendable and is tougher than diamond (and almost 300 times stronger than steel). It has Young's modulus values of around 1 TPa [80].

Optical properties

Despite being the thinnest material, it is still visible to naked eye. Due to its electronic band structure, it can absorb as high as 2.3% of visible light which is sufficient to see it in naked eye.

Chemical properties

Graphene has a very high surface area to weight ratio (greater than 2600 m^2/g.) making it extremely thin and light weight. Similar to the surface of graphite, graphene can adsorb and desorb various atoms and molecule. They can be easily functionalized either covalently or non-covalently by several chemical groups. Chemical reactions are focused either at the edge of graphene sheets or to the bulk lattice.

2.4 Epoxy resin system

Epoxy polymers that fall under the class of thermoset polymers are used as matrices for fibre reinforced composites and also as adhesives. In view of their cross-linked network structure, these polymers are used in structural engineering applications owing to their low moisture absorption, high modulus and high temperature performance [81]. Therefore, good mechanical properties and chemical resistance while providing relative low densities are obtained. While

processing, the components are mixed to produce a polymerization reaction, leading to a three dimensional cross-linked polymer network.

The applications for epoxy-based materials are widespread and include coatings, adhesives and composite materials such as those using carbon and glass fibre reinforcements (although polyester, vinyl ester, and other thermosetting resins are also used for glass-reinforced plastic). With chemistry of epoxies and the range of commercially available variations, cured polymers can be produced with a very broad range of properties. In general, epoxies are known for their excellent adhesion, chemical and heat resistance, good-to-excellent mechanical properties and very good electrical insulating properties.

2.4.1 Chemistry of epoxy resins

Epoxy is a monomer that is formed from two different chemicals that are referred to as the "resin" or "compound" and the "hardener" or "activator". The resin consists of monomers or short chain polymers with an epoxide group at either end. Most common epoxy resins are produced from a reaction between epichlorohydrin and bisphenol-A whose reaction mechanism is shown in Fig. 2.4, though the latter may be replaced by similar chemicals.

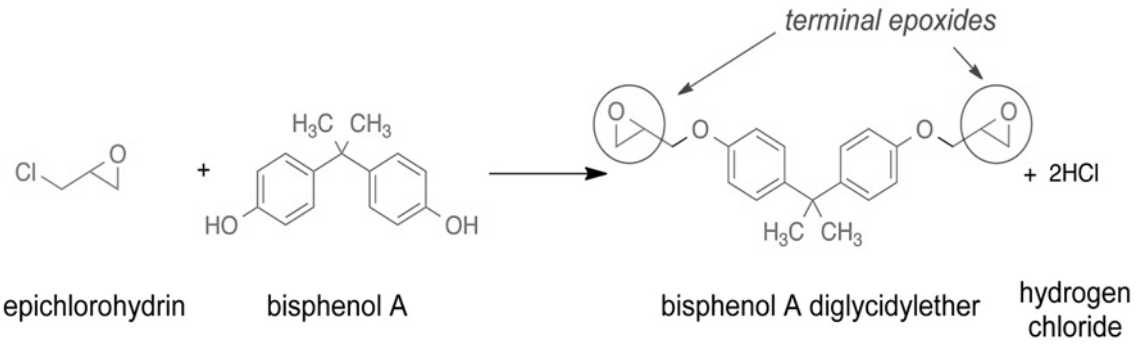

Figure 2.5: Schematic of reaction between the Epichlorohydrin and Bisphenol A yielding DGEBA.

The properties of the DGEBA resins depend on the value of n, which is the number of repeating units commonly known as degree of polymerization. The number of repeating units depends on the stoichiometry of synthesis reaction. Typically, it ranges from 0 to 25 in many commercial products.

Furthermore, the resins have a curing process so it can form a highly cross-linked, three-dimensional network. The curing process is a chemical reaction in which the epoxide groups in epoxy resin react with a curing agent (hardener). In order to convert epoxy resins into a hard,

infusible and rigid material, it is necessary to cure the resin with the hardener. Epoxy resins cure quickly and easily at practically any temperature from 5 to 180 °C depending on the choice of curing agent. A wide variety of curing agent for epoxy resins is available depending on the process and properties required. The commonly used curing agents for epoxies include amines, anhydrides, polyamides, phenolic resins, isocyanates and polythiols. Amines are the most commonly used curing agents for epoxy cure. Primary and secondary amines are highly reactive with epoxy. Tertiary amines are generally used as catalysts, commonly known as accelerators for cure reactions. Use of excessive amount of catalyst achieves faster curing, but usually at the expense of working life, and thermal stability.

Glass transition temperature or T_g is just the temperature in which the polymer goes from a hard and brittle state into a molten or rubber-like state. This temperature is always lower than the melting temperature, T_m (which normally does not exist). The choice of resin and hardeners depends on the application, the process selected, and the properties desired. The stoichiometry of the epoxy-hardener system also affects the properties of the cured material. The cure kinetics and the T_g of cured system are dependent on the molecular structure of the hardener; for example, the most commonly used curing agents for epoxies include amines, polyamides, phenolic resins and anhydrides. Employing different types and amounts of hardener tend to control the cross-link density and vary the structure of epoxy resins [82].

2.4.2 Curing of epoxy resins

The cure reaction of epoxy resins is highly dependent on temperature and the reactions that take place at elevated temperatures normally occur in a step-wise manner. Imidazole is usually used as accelerators that aid the reaction mechanism between epoxies and other curatives. Anhydride, a low viscous system, is one of the major classes of curing agents used along with epoxy. The reaction mechanism between epoxy resin and anhydride is very complex as three reactions compete with each other. The anhydride reacts with the hydroxyl groups present in epoxy to form a half ester which contains carboxyl groups. These carboxyl groups of half-ester further react with epoxy groups to produce hydroxyl groups which again react with anhydride and the reaction cycle proceeds.

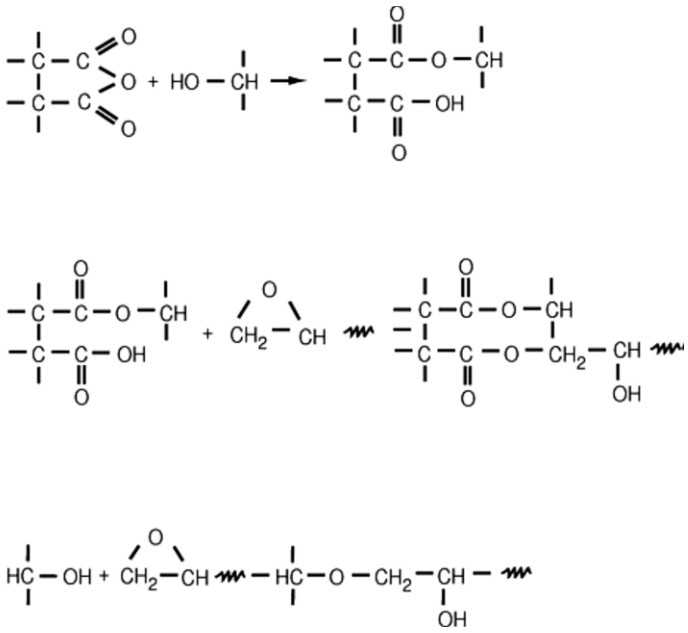

Figure 2.6: Curing reaction for epoxy resin with anhydride hardener [83].

The primary cure reaction occurs in the temperature range between 80 °C and 150 °C and post cures extend till 200 °C. Imidazole accelerators are used in the range of 0.5-3.0% to speed up the curing process.

2.4.3 Graphene and epoxy resin used in this work

Two types of graphene fillers are used for the current work which is thermally reduced graphene oxide (TRGO) and graphite nano-platelets (GNPs). The TRGO was prepared by hummer's method as explained in the chemical exfoliation process. The thermal annealing was done in nitrogen atmosphere at 700 °C. The GNPs prepared via intercalation method were also thermally annealed for better exfoliation. Further details of the material are given in Chapter 3 Section 3.1 Table 3.1.

The epoxy resin system used in this work consists of a high temperature curing system which provided by the Company Huntsman®, together with the resin called Araldite LY556, anhydride hardener Aradur CH917 and an imidazole accelerator DY070. The mixing ratio of the components in parts per weight is resin/hardener/accelerator: 100/90/1. The LY556 epoxy resin exhibit a viscosity of roughly 10 Pa·s, while the viscosity of the mixture is around 700 mPa·s. The hardener Aradur CH917 has an initial viscosity of 50-100 mPa·s and 50 mPa·s initial viscosity for the accelerator DY070. The three components are in a clear liquid state and the resin has a pale yellow colour. The cured resin system mixed in the above mentioned ratio

gives an epoxy having a tensile strength of 83-93 MPa with a modulus of 3.0-3.3 GPa and a fracture toughness in the range 0.56-0.6 $MPa \cdot m^{1/2}$ [84].

2.5 State of the art: Graphene in polymer composites

As one of the most important branches of current nanotechnology and composite science, the fabrication of polymer nano-composites is critical to realize the new generation materials with high performances and multi-functionalities. By incorporating nano-fillers in a polymer matrix, the properties of polymers such as density, flexibility, and transparency can be combined with mechanical, electrical, thermal and other properties of nano-materials. This simple mix and match approach has enabled engineers to use a selected set of polymers to yield nano-composites. The latest addition to this palette is graphene, a single atom layer thick carbon allotrope. The most common synthesis strategies used for the preparation of polymer matrix composites are (i) solution mixing; (ii) melt blending and (iii) in-situ polymerisation [85,86].

2.5.1 Preparation of graphene/polymer nano-composite

2.5.1.1 Solution mixing

Solution mixing is the most straight forward process to disperse GO platelets in polymer matrices, provided the solvent is compatible with polymer and filler. This method is very simple that makes processing of the composite easy. The method generally involves mixing the colloidal suspensions of GO or other graphene derivatives in a polymeric matrix by simple stirring or shear mixing. Later, the suspensions must either be heated or appropriate steps must be taken to remove the solvents. Due to the presence of oxygen functionalities, the GO which is amphiphilic in nature is soluble in polar solvents; hence all the polymers that are compatible with polar solvents can be used to disperse GO [87]. Reduced graphene oxides show limited solubility in both organic and inorganic solvents. Therefore, sonication is combined with high speed shear mixing where sonication yields a metastable state of dispersion.

In the past few years, graphene sheets have been incorporated into a wide range of polymer matrix, including epoxy [88], poly vinyl alcohol (PVA) [89,90], poly methyl methacrylate (PMMA) [91], Polystyrene [6], poly aniline (PANI) [92], poly urethane (PU) [93] which are widely prepared by solution mixing method. However, restacking of the platelets is possible for this method as the degree of exfoliation achieved during or prior to dispersion contributes to this re-aggregation of filler. In order to overcome the restacking, functionalization of graphene sheets or use of surfactants are common solutions to achieve better dispersion [94,95].

2.5.1.2 Melt blending

Melt blending/mixing is another approach similar to solution mixing, which is economical and scalable, where polymer melt and dry powder form of filler are subjected to high shear mixing. Unlike solution mixing, this method does not involve the use of solvent. This method employs high temperature and high shear forces to disperse the fillers. However, one of the drawbacks of this method is rolling or shortening of graphene sheets and hence the degree of dispersion is not as expected where exfoliation of graphene sheets occur during processing [96]. Kim et al observed a phase separation in melt blended graphene/polyethylene and graphene/polyurethane composites [93,97]. Though, this method has its drawbacks, there are studies where improvement in properties was observed due to the incorporation of graphene/ graphene based derivatives [98,99].

2.5.1.3 In-situ polymerisation

In this method, the nano-particles are first swollen in a liquid monomer, then appropriate initiator is dispersed which is subsequently polymerised through external source. In the case of two-dimensional fillers, the monomers intercalate into the layered structure which increases the interlayer spacing between the layers. Therefore, composites prepared via this method exhibit better mechanical properties at lower percolation threshold. Thus, a well-dispersed morphology is obtained. It is possible to form covalent bonding of the filler and matrix through chemical reactions. The major drawback in this method is the increase in viscosity during in-situ polymerisation which affects the quality of dispersion at higher filler content.

Graphene oxide/poly methyl methacrylate nano-composite prepared via in-situ polymerisation showed 14% improvement in storage modulus for 0.5wt% loading [100,101]. Polyethylene nano-composite became stiffer and thermally stable when incorporated with graphene nano-sheets prepared by in-situ polymerisation [102]. In-situ polymerisation of styrene in the presence of expanded graphite yielded electrically conducting composite exhibiting an electrical conductivity of 10^{-2} S/cm at a filler loading of 3.0wt% [103].

Researchers have also shown the possibility of in-situ reduction of graphene oxide in the presence of polymers. In this method, GO is reduced at moderate temperatures in the presence of polymers [104]. GO is first dispersed in the monomer solution, to which the reducing agent hydrazine is added and then heated at moderate temperature. This process reduces the GO to form reduced graphene oxide which is later followed by polymerisation step. The main

advantage of this method is that GO can be easily and homogeneously dispersed in polymers [72,73].

2.5.2 Properties of graphene/polymer nano-composite

2.5.2.1 Electrical properties

Graphene, a single layer of honeycomb lattice consisting of carbon atoms, has a unique form factor and exceptional physical properties which can be useful in electronic applications. The charge carrier mobility of graphene is 2-3 orders of magnitude higher than semiconducting silicon [105]. When dispersed in a polymeric matrix, graphene sheets can provide conductive pathways for electron transfer similar to other carbon fillers such as CNTs and CB, thereby making the composites electrically conductive.

Ruoff and his co-workers reported an electrical conductivity value of 0.1 S/m for 0.1vol% of graphene loading in a polystyrene matrix [6]. Later studies were involved in dispersion of graphene sheets in an electrically conductive polymer like poly aniline [106,107]. Reports show that when well-defined graphene flakes are grafted with polypyrrole through in-situ polymerization the obtained electrical conductivities were as high as 27 S/m [108,109].

Although graphene polymer composite exhibits higher electrical conductivity compared to CNT dispersed composites, the electrical percolation threshold is achieved at lower filler loadings for CNT/polymer composites [24,110]. However, the lowest percolation threshold achieved for graphene nano-sheets dispersed in an ultra-high molecular weight polyethylene was 0.07vol% [111].

2.5.2.2 Thermal properties

In comparison to 1D fillers, the 2D fillers are expected to have a larger surface area and hence better stress and heat transfer in 2D (in plane lattice). However, unlike the exponential increase observed in electrical conductivity for polymer nano-composites, such dramatic increase is not found for thermal conductivity [112]. Theoretical and some experimental works show that graphene based thermal interface materials perform better as they have lower Kapitza resistance [113].

Thermal conductivities of GNP/silicone composite prepared by three-roll milling technique improved by 18% for 25.0wt% loading of commercially available GNPs [114]. Comparing the thermal conductivities using different fillers like neat graphite, expanded graphite and graphene nano-platelets in an epoxy matrix, there was a marginal increase in thermal conductivity for

GNPs and this value decreased as the filler content is increased beyond 0.6vol%. This is attributed to the poor dispersion of the filler [115]. Another study based on non-covalent functionalization of graphene sheets dispersed in epoxy reported 800% increase in thermal conductivity for 4.0wt% of filler loading. This is attributed to strong interaction between the matrix and filler, which reduces the interfacial thermal resistance and also homogeneous dispersion due to functionalization [116]. In order to understand the thermal energy transport properties, a better engineered heat transfer property in graphene polymer composites is important. Theoretical studies have shown that thermal energy transport across the interface depends on polymer density, size of graphene flakes and on the covalent bonding between the polymer and graphene [117].

2.5.2.3 Mechanical properties

As listed earlier, monolayer graphene (defect free) is said to have a Young's modulus in the range of 1 TPa. This led scientists to design graphene polymer composites with enhanced mechanical properties. Though researchers have found an improvement in the modulus; the percentage of enhancements varies with filler content, modification of filler, host polymer matrix and interfacial bonding strength. From the current studies on the mechanical properties of graphene/polymer composites, it can be seen that the enhancement in property is achieved at very low filler loadings.

Investigations on the mechanical aspects of GNP/epoxy, pertaining to its fracture toughness and flexural modulus have shown significant improvement with an increase in loading. Further, the mechanical properties are greatly dependent on the lateral flake size of the filler [118]. In another study on graphene epoxy composite at low filler content of 0.1wt%, a noticeable increment of 31% in modulus and 40% in fracture toughness was observed [119]. Apart from epoxy, functionalized graphene sheets were dispersed in poly vinyl chloride to prepare composite films. With 2.0wt% loading of graphene, 58% increase in Young's modulus and 130% increase in tensile strength was observed [120]. Another type of graphene investigated was graphene nano ribbons (unzipped nanotubes) which, when dispersed in poly vinyl alcohol, gave 50% and 58% improvement in modulus and tensile strength, respectively, with 1.0wt% of filler loading [121,122]. Ramanathan et al showed an enhancement of 33% in modulus for 0.01wt% of functionalized graphene sheets dispersed in poly methyl metha acrylate matrix [91]. Studies on graphene dispersed in epoxies showed improvements not only in tensile properties but also in compression after impact strength [123] fatigue life [124], compression

strength [125], flexure strength [126] and also in fracture toughness (discussed in a separate section).

2.5.2.4 Fracture toughness: graphene/epoxy composite

Epoxy polymers that fall under the class of thermoset polymers are used as matrices for fibre reinforced composites and also as adhesives. In view of their cross-linked network structure, these polymers are used in structural engineering applications owing to their low moisture absorption, high modulus and high temperature performance. However, they also come with an undesirable property of brittleness with low fracture resistance because of their structure. Thus, the enhancement in fracture toughness has been a critical issue when it comes to their application and hence engineers have been working on the toughening of epoxies [127,128].

Researchers have come out with a solution of incorporating secondary phase particles in the epoxy matrix in order to increase its toughness. The dispersed secondary phase particles can either be soft fillers (e.g., thermoplastic particles, rubber, and etc.) or rigid fillers (e.g., silica beads or titania or alumina) [129]. Here, the toughening effect of soft particles is significant on the epoxy resin; however, they also reduce the stiffness and the glass transition temperature (T_g). On the other hand, modification using rigid fillers enhances the stiffness and T_g of the epoxy composites and the toughening effect was generally insignificant. To overcome these trade-off relationships, more effective rigid fillers were desired [130-133].

With the emergence of nano-technology, the enhancement of toughness in nano-composites is considerable at lower loadings. These nano-composites are polymers (epoxy in our study) that are reinforced with nano-phase rigid fillers (nano silica, nano clay, carbon nanotubes, carbon black, graphene, and fullerene) [134]. These nano fillers enhance the toughness to a larger extent than micro fillers at very low filler loading due to their high surface area [135-138]. It is seen from the reported literature, that the toughening effect of graphene is significant when compared to nanotubes. Indeed, previous works have shown that the fracture toughness increases by 53% for graphene based epoxy nano-composites [119]. A comparative graph on the normalized fracture toughness of nano-composites based on nano-clay, multi walled carbon nanotubes and graphene as a function of filler content is shown in Fig. 1.

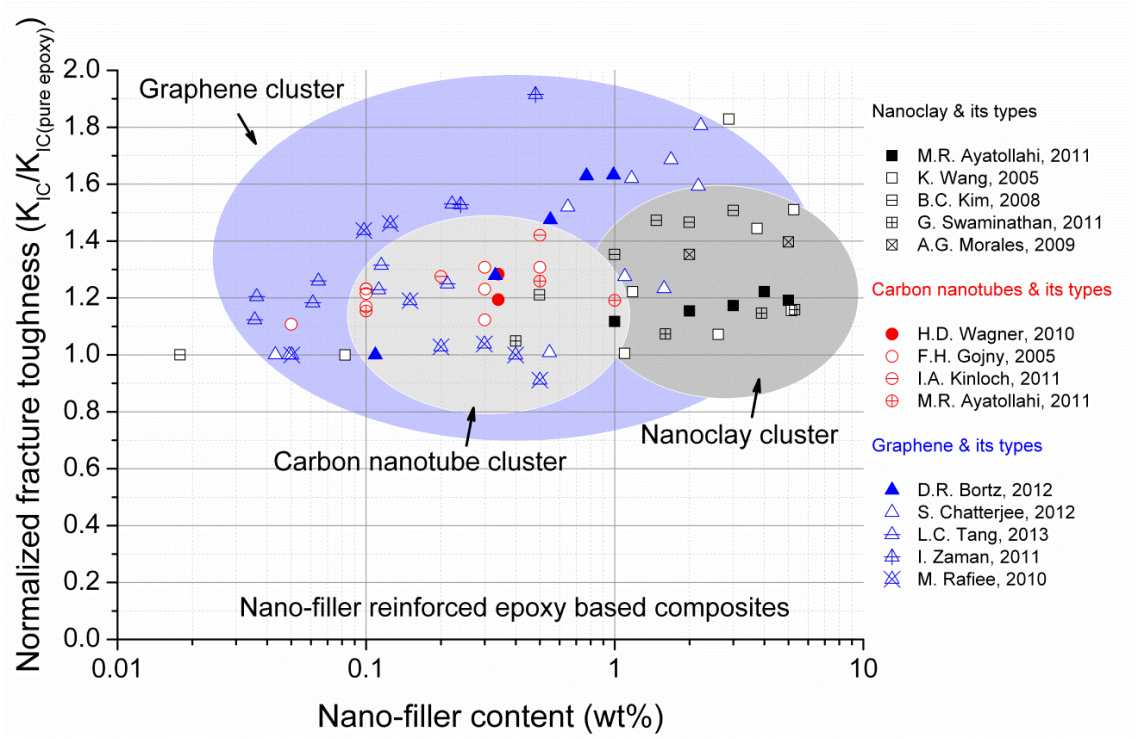

Figure 2.7: Normalised fracture toughness as a function of filler content for different nano-filler reinforced epoxies. References used in the plot [8], [118], [134], [139-148].

It can be seen that nano-clay toughened epoxies also show an increase in K_{IC} but at higher filler contents (1.0-10.0wt%). At the same time, MWCNT reinforced epoxies exhibits higher K_{IC} but at lower filler content (0.1-1.0wt%). Graphene based epoxy composites show better improvement in K_{IC} at lower filler content varying from 0.01-1.0wt%. Though there are literature available on the fracture toughness of graphene based epoxy composites, the potential of toughening effect and toughening mechanism of graphene based epoxy composite have not been well discussed.

3 Experimental procedure

This chapter focuses on the materials used in this work, preparation methods for nano - composites and testing methods adopted to characterize the same.

3.1 Materials

For this study, epoxy system containing Araldite LY556 (resin), Aradur CH917 (hardener) and DY070 (accelerator) from Huntsman (Switzerland) was used as the polymeric matrix. This is a low-viscous, anhydride cured system commonly used in high performance composite parts. For the nano-composite preparation, three different nano-fillers viz., Multi Wall Carbon Nanotubes (MWCNTs), Thermally Reduced Graphene Oxide (TRGO) and Graphite Nano-Platelets (GNPs) were used. The particulars of the as-received fillers from the supplier are listed in Table 3.1.

Table 3.1: Datasheet of as-received MWCNT, TRGO and GNP nano-fillers.

	Nanocyl7000® MWCNT	**TRGO**	**GNP**
Supplier	Nanocyl, Belgium	Freiburg University, Germany	Punto Quantico - Research Lab, Italy
Colour/Appearance	Black powder	Black powder	Greyish black powder
Carbon content	90 %	81-97 %	>98 %
Average flake thickness	-	N/A	12 nm (25 monolayers)
Lateral size	Avg. diameter - 9.5 nm; Avg. length - 1.5 µm	1.4 - 4.6 µm	20 - 50 µm
Specific surface area	250 - 300 m^2/g	650 - 900 m^2/g	60 - 80 m^2/g

3.2 Preparation of the nano-composite

Obtaining a good dispersion of the nano filler in the matrix always remains a challenge to the scientific community. The nano fillers are prone to form agglomerates due to their high specific surface area (SSA) which are difficult to break down during the processing. A variety of methods like sonication, stirring, high speed shear mixing, three-roll milling, ball milling and planetary mixer has been used in the past decade to disperse the nano fillers in the polymeric matrix. The above mentioned methods have their own advantages and draw backs but they are mostly based on the concept of introducing high shear forces in the system.

In this work, a lab-scale three-roll mill (3RM) from EXAKT® 120E (Advanced Technologies GmbH, Germany) is used to disperse the nano fillers in the epoxy matrix. The gap between the feed roll and the apron roll was varied from 120 µm down to 5 µm and the whole suspension was milled seven times in total, in order to achieve uniform dispersion.

In order to study the effect of dispersion on the final property of the nano-composite, apart from the 3RM process, two more dispersion methods were adopted and compared with each other. For this study, only GNP reinforced epoxy nano-composite system was investigated to analyse the effect of dispersion method.

Among the two other dispersion methods, one of them is sonication combined with high speed shear mixing technique (Soni_hsm), where the GNPs were sonicated in solvent (ethyl acetate) for 30 min to exfoliate the fillers. To this solvent/GNP slurry appropriate amount of epoxy was added and then subjected to high speed shear mixing for 1.5 h at 11000 rpm, which was simultaneously heated at 70 °C to remove solvent. For further removal of solvent, overnight heating in the oven at 70 °C was carried out.

The third method adopted is sonication combined with 3RM process (Soni_3RM), where the sonicaiton of GNPs were carried out similar to Soni_hsm process. After the sonication step, the solvent/GNP slurry is heated at 70 °C until the solvent evaporates. The sonicated GNPs are now added to appropriate amount of epoxy and are subjected to the default 3RM process.

The composite suspensions that were obtained after 3RM process (MWCNT/epoxy, TRGO/epoxy and GNP/epoxy); Soni_hsm process (GNP/epoxy) and Soni_3RM process (GNP/epoxy) was then manually mixed with appropriate amounts (100:90:1) of hardener and accelerator for 10 minutes, which was later degassed at 50 °C and then cured in oven for 80

°C - 4 h followed by post curing at 140 °C - 8 h. A detailed flow chart explaining the composite preparation is presented in Fig. 3.1.

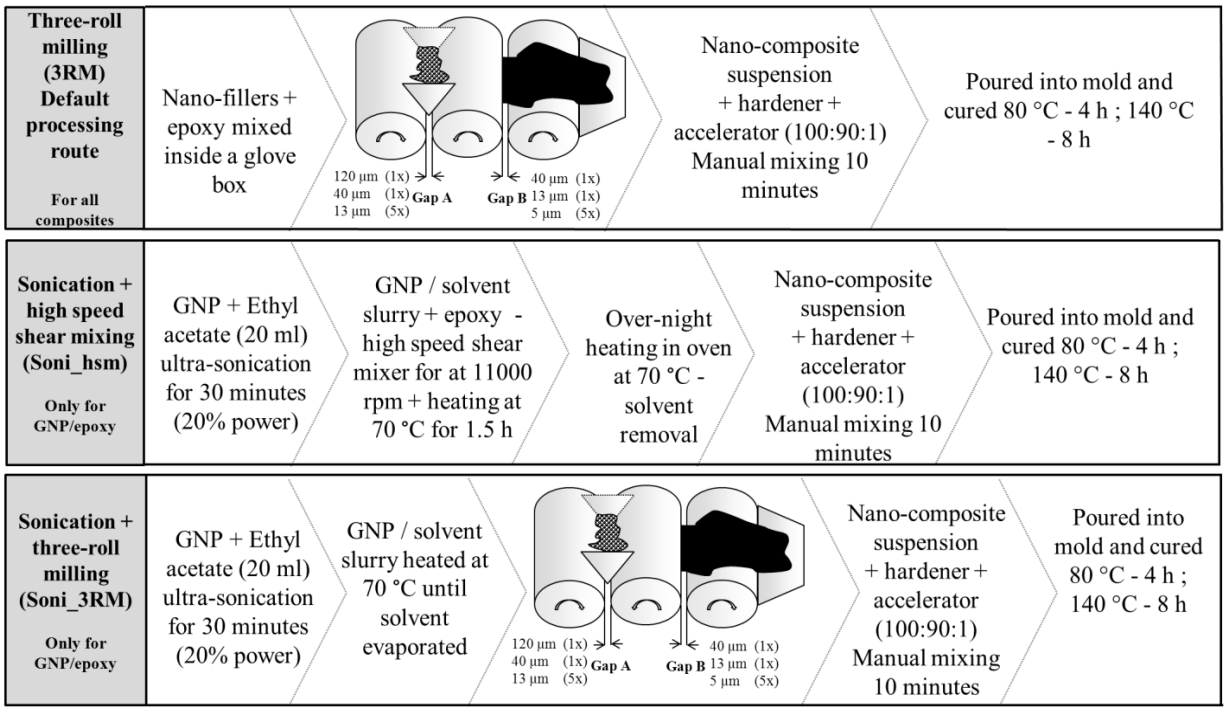

Figure 3.1: A flow chart of the dispersion methods used for preparation of the nano-composite.

For the study that involves bi-filler suspension containing TRGO and MWCNT, individual suspensions (TRGO/epoxy and MWCNT/epoxy) at the required filler wt% were prepared using the normal 3RM process. Then, the suspensions were mixed in 1:1 ratio and were subsequently milled again using 3RM under similar operating conditions.

Unless mentioned, the default dispersion method used in this study is the three-roll milling process. In general, the nomenclature of the nano - composite is (X)wt% (Y)/epoxy_(Z) where, (X) - amount of filler content; (Y) - nano-filler type; (Z) - dispersion method used. It must be noted that the amount of filler used in rheological experiments and light microscopic studies is with respect to LY556 epoxy (i.e., prior to the addition of anhydride and imidazole components), whereas, for the cured composite the weight percentage of the filler quantum is halved due to the addition of hardener and accelerator.

3.3 Sample geometry

Rectangular plates of the cured composite were obtained after complete curing process and the nano-composites were subjected to several characterisation techniques. Depending on the test

method involved, samples were cut out from the rectangular plate and ground to achieve the desired dimensions as per the test standard. A schematic diagram showing the sample geometry for various tests involved is illustrated in Fig. 3.2. In the case of rheological tests, nano-composite suspensions (i.e., prior to mixing of hardener and accelerator) obtained after the 3RM process was used in the test equipment.

All the samples were ground and polished as per dimensions to ensure uniform geometry and the tolerance level was close to 0.15 mm. The samples for scanning electron microscopy were prepared by cutting 500 nm thin slices of the cured composite using an ultra-cut microtome. For a broader view, cryo-fractured* surface of the cured composite was also prepared and investigated. For transmission light microscopic analysis, a tiny drop of as prepared nano-composite suspensions from 3RM process was placed on the glass slide and was then covered with a glass coverslip.

* Cryo-fractured - Samples were soaked in liquid nitrogen and were then broken manually.

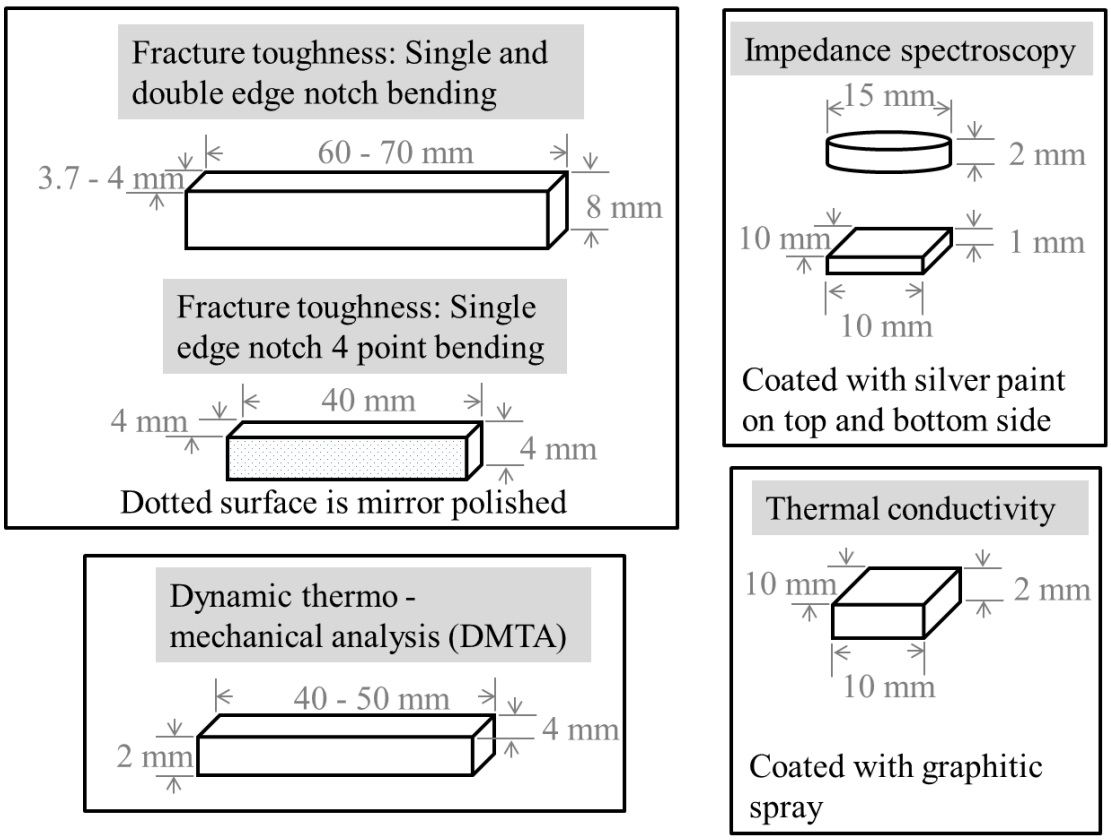

Figure 3.2: Sample geometries for different test methods.

The as-received nano-fillers were also subjected to systematic characterisation studies and hence the powders were compressed to form pellets. The pellets were prepared using Evacuale Pellet die from Perkin Elmer having 13 mm diameter. The whole set-up was connected to a vacuum pump and was placed under a compression molding press. The amount of powder filled in the die and the pressure applied varied for each sample.

3.4 Notch preparation for fracture toughness

Fracture toughness measurements were carried out in both three point bending (3PB) and four point bending (4PB) test set-ups. Single edge notch bending (SENB) tests were done in both 3PB and 4PB test fixtures, whereas, double edge notch bending (DENB) tests were carried out only in 4PB test fixture. For the insertion of notch, a standard procedure used in ASTM standard D5045 was implemented. A raw notch was inserted using a diamond saw blade until half the height of the sample, and this notch was further tapered by sliding a razor blade across the raw notch as given in schematic presented in Fig. 3.3.

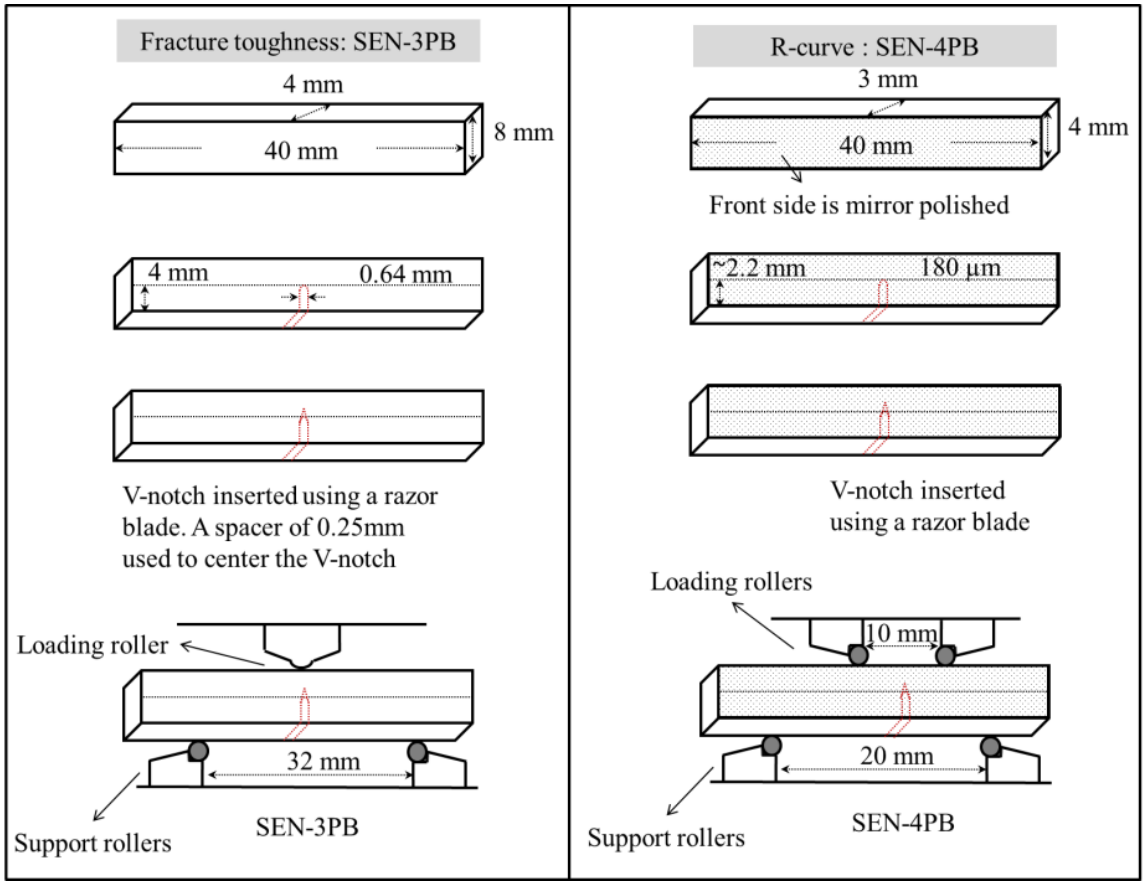

Figure 3.3: Specimen geometry and notch preparation for fracture toughness tests.

As regards testing of samples under SEN-3PB mode, it was not required to have a mirror polished surface and hence only cutting and grinding was sufficient to maintain a uniform dimension across the sample. However, raw notch was inserted using a 0.64 mm thick diamond cut-off wheel which is much thicker than the previous saw blade. The procedure to insert V-notch remains unaltered. To ensure that the inserted V-notch is at the centre of the raw notch,

a spacer of 0.3 mm thick was used for positioning the razor blade. A graphic of the notch insertion with the photograph of the diamond saw stage is shown in Annexure (see Fig. A.1).

In the case of SEN-4PB tests, one of the faces of the sample must be mirror polished in order to observe crack propagation during the test. After cutting the sample in desired geometry, subsequent grinding and polishing was done on an ATM Saphir 350 / Rubin 350 polishing machine. The sample was polished using silicon dioxide grinding paper by gradually changing the mesh size for reducing the roughness of the surface. A finer polish was done using 9 to 1 µm sized diamond suspension on polishing cloth (Struers GmbH, Willich, Germany) to achieve a mirror like polished surface. A raw notch was introduced, using an MCP abrasive saw from EXAKT Advanced Technology GmbH, Norderstedt, Germany which consists of a rotating diamond-studded abrasive cut-off wheel of 180 µm thick followed by a V-notch using razor blade. DEN-4PB samples require insertion of two notches, the spacing between the notches was $1/9^{th}$ of the spacing between the support rollers in the test fixture.

3.5 Experimental set-up

3.5.1 Microscopic analysis

Morphological characterization of the cured nano-composite as-received filler was done using scanning electron microscope (SEM) from LEO 1530 FE-SEM (Carl Zeiss, Germany) in both "in-lens" and "secondary electron" mode. The samples were investigated at low acceleration voltage (1 kV) without any sputtering to avoid masking of nano-fillers or fractographic features. Light microscope (LM) from Leica Polyvar was used in transmission mode to analyse the as prepared nano-composite suspension. Energy dispersive X-ray analysis was employed on the nano-fillers to identify its elemental composition qualitatively.

3.5.2 Spectro-chemical analysis

The as-received fillers were pelletized and were subjected to Raman spectroscopy and X-ray diffraction (XRD) to assess their quality. The diffractograms were recorded using Brucker AXS – D8 Advance X-ray diffractometer from 15 to 65° with a step size of 0.02°, operating with Cu-K_α radiation. The Raman measurements were recorded with a Horiba Jobin Yvon HR800 spectrometer. The spectra were taken using He-Ne laser with a wavelength of 638.2 nm and the spectra was recorded in the range of 100-3000 cm^{-1}.

3.5.3 Electrical studies

The electrical properties of the cured nano-composite were measured by means of impedance spectroscopy using Hewlett-Packard impendence analyser (HP 4284A LCR) with two point contact. Three circular samples of 15 mm diameter × 2 mm for each sample type and filler content, coated with silver paint that acts as electrodes were tested. The frequency range tested from 20 Hz to 1 MHz was set at voltage amplitude of 1 V. For comparison, conductivity values at low frequency (200 Hz) comparable with the DC conductivity were taken.

The powder electrical conductivity of the nano-filler was measured using Veeco FP-100 four point probe instrument. The resistivity and sheet resistance of the pelletised nano-fillers was measured. The set-up contains four thin collinear tungsten wires which are made to contact the sample under test. Current (I) is made to flow between the two outer probes, and voltage (V) is measured between the two inner probes, without drawing any current. Generally for sheet resistance measurements, the size of the sample is not large when compared to inter probe spacing and therefore, a correction factor corresponding to sample dimension must be applied.

3.5.4 Thermal studies

The thermal diffusivity of the cured nano-composite was measured by means of laser flash method, using the LFA-447 Nanoflash apparatus from NETZSCH, Germany at three different temperatures (30 °C, 50 °C and 100 °C). Five measurements at each temperature were made. The samples were prepared in square-shaped forms of 10 mm × 10 mm and a thickness of 2 mm. Before testing, the samples were coated with graphite spray to ensure increased absorbance of flash energy on the front surface and emission of infrared light from the rear.

Thermo-Gravimetric Analysis (TGA) measurements were done using TAQ500 from TA instruments on the as-received fillers under nitrogen and synthetic air atmosphere to estimate impurities and thermal stability of the nano-fillers. The TGA was operated on hi-resolution sensitivity mode with a heating rate of 5 °C/min. The samples were heated first from room temperature to 900 °C under nitrogen atmosphere with a gas flow of 60 ml/min. Then it is cooled down to room temperature under nitrogen. The cooled sample is further heated under synthetic air till 900 °C with the same gas flow rate.

3.5.5 Rheological studies

For measuring the viscosity, strain controlled rheometer (TA ARES®) from TA instruments having parallel plate geometry was used. The plates were of 40 mm in diameter and the gap

between the plates was maintained at 0.5 mm. Three measurements for each composite suspension were carried out in steady mode and the viscosity of the suspension as a function of shear rate was measured.

Combined rheological and electrical measurements were carried out on the freshly prepared suspensions using a modified stress-controlled rheometer (StressTech HR, Rheological Instruments), in order to evaluate the agglomeration behaviour of the composite suspension under shear. It must be noted that the time gap between the measurement and the sample preparation was less than 24 h. This was to ensure that there were no effects on the agglomeration or sedimentation and in turn on the conductivity from the storage time. The measurements were performed in steady mode with parallel plate geometry of 35 mm diameter. The lower glass plate of the rheometer has two rectangular gold electrodes (10 × 5 mm) with 2 mm gap in between. The upper rheometer plate contains a reflective non-conductive coating which aids for optical observations. Optical, electrical and rheological in-situ measurements were possible with this test setup [149]. Shear rate step tests were carried out by shearing at a constant rate for 10 min and by simultaneously measuring the electrical conductivity. The conductivity was measured parallel to the shear direction under 1 V and 100 Hz frequency. The shear rates were changed from 100 s^{-1} to 0.1 s^{-1} [150,151]. Measurements were carried out at 60 °C for better resolution of the data.

3.5.6 Mechanical studies

Investigation of the thermo-mechanical behaviour was performed using a Gabo Eplexor 500 N. For the measurements, a minimum of three rectangular samples of size 40 × 4 × 2 mm were cut from the composite plate and ground. The tests were performed in tensile mode at a frequency of 10 Hz, with a dynamic strain of ± 0.1%, within a temperature range between 20 °C and 200 °C at a heating rate of 3 °C/min.

The fracture toughness (K_{IC}) was evaluated by three point end notch bending (SEN-3PB) test. The SEN-3PB test was carried out according to ASTM D5045 standard using Zwick universal testing machine. A minimum of 5 samples was tested in each system. The cross-head speed was 10 mm/min, and the length of the support span was 32 mm. The load was taken from the force displacement curve and the crack length was measured using microscope after the test on the fracture surface. The fracture toughness was calculated using the following equations (Eqs. 3.1 & 3.2).

$$K_{IC} = \frac{\mathrm{FL}}{B.w^{\frac{3}{2}}}.f(x) \quad \text{Eq. (3.1)}$$

$$f(x) = 3x^{\frac{1}{2}}\left\{\frac{[1.99-x(1-x)(2.15-3.93x+2.7x^2)]}{2(1+2x)(1-x)^{\frac{3}{2}}}\right\} \quad \text{Eq. (3.2)}$$

where F - maximum force; L - span length; B - width of the specimen; a - crack length; w - height of the specimen; x - (a/w); ratio of a and w.

For (K_{IC}) and R-curve measurements, SEN-4PB tests were carried out on an indigenously built test set-up at the Institute of Advanced Ceramics, TUHH. The basis for all measurements was to achieve a stable crack growth under four point- bending and to collect multiple data points of the R-curve for each sample. The measurement set up is explained in detail by Jelitto et al [152]. The experimental procedure includes the use of a computer aided control system which aids in controlling the growth of the crack. All experiments were carried out in a semi-automated mode [153] and the following equation (Eqs. 3.3 & 3.4) was used to calculate the fracture toughness.

$$K_{IC} = \frac{3F\Delta s\sqrt{\alpha}\Gamma(\alpha)}{2bh^{\frac{3}{2}}(1-\alpha)^{\frac{3}{2}}};\ \alpha = \frac{a}{h};\ \Delta s = s_2 - s_1 \quad \text{Eq. (3.3)}$$

$$\Gamma(\alpha) = 1.1215\sqrt{\pi}\,[\frac{5}{8} - \frac{5}{12}\alpha + \frac{1}{8}\alpha^2 + 5\alpha^2(1-\alpha)^6 + \frac{3}{8}e^{-6.1342\left(\frac{\alpha}{1-\alpha}\right)}] \quad \text{Eq. (3.4)}$$

The whole setup was arranged on an extremely rigid steel frame to minimize deformation of the measurement device and thus storage of elastic energy was ensured. The specimen rests on two steel support rollers with a diameter of 5 mm and a distance of 20 mm between the rolls. The notch was centred between these rollers and the polished surface of the specimen faces a light microscope with a fixed magnification of 250×. This allows observation and measurement of the crack development as visible on the surface of the specimen.

A LabVIEW-based computer aided control system was used to permanently record and analyse displacement and force during the measurement procedure. This was based on the fact that a cracked specimen is more compliant than an undamaged one. Hence, the force resulting from a given displacement decreases, even if an undamaged specimen develops crack under a certain displacement which enables to achieve a controlled crack growth. The specimen surface was constantly observed with a digital camera connected to the light microscope in front of the device. The actual crack length was determined with the aid of a scale in one of the oculars in the light microscope which was later used to plot the crack-resistance curve.

4 Results

The content of this chapter focuses on the results obtained from the tests that were done on the cured nano-composite, suspension and the as-received filler. The chapter first reports the results collected from characterisation of the as-received fillers, followed by dispersion of fillers in matrix, electrical, thermal, and mechanical properties of the cured composite.

4.1 Filler characterisation

As mentioned earlier in Chapter 2, the multi-wall carbon nanotubes used are produced by chemical vapour deposition. Grown with the help of a metal catalyst on silicon wafer, the MWCNTs are not aligned but with random orientation. The high surface area and the van der Waals forces between the tubes, leads to strong affinity and hence they tend to form bundles like twisted ropes which are usually called primary agglomerates. The morphology of the MWCNTs in the form of bundles, along with some amorphous carbon and metal catalysts is shown in Fig. 4.1a, both in the as-received powder form and in the pelletized form (Fig. 4.1b).

The other two fillers TRGO and GNP belong to the same class of 2D filler, and the raw material from which they were synthesised is graphite. The problem of forming agglomerates is valid for these fillers also. The morphology of both the fillers, in the as-received and pelletized form is depicted in Figs. 4.1c-f.

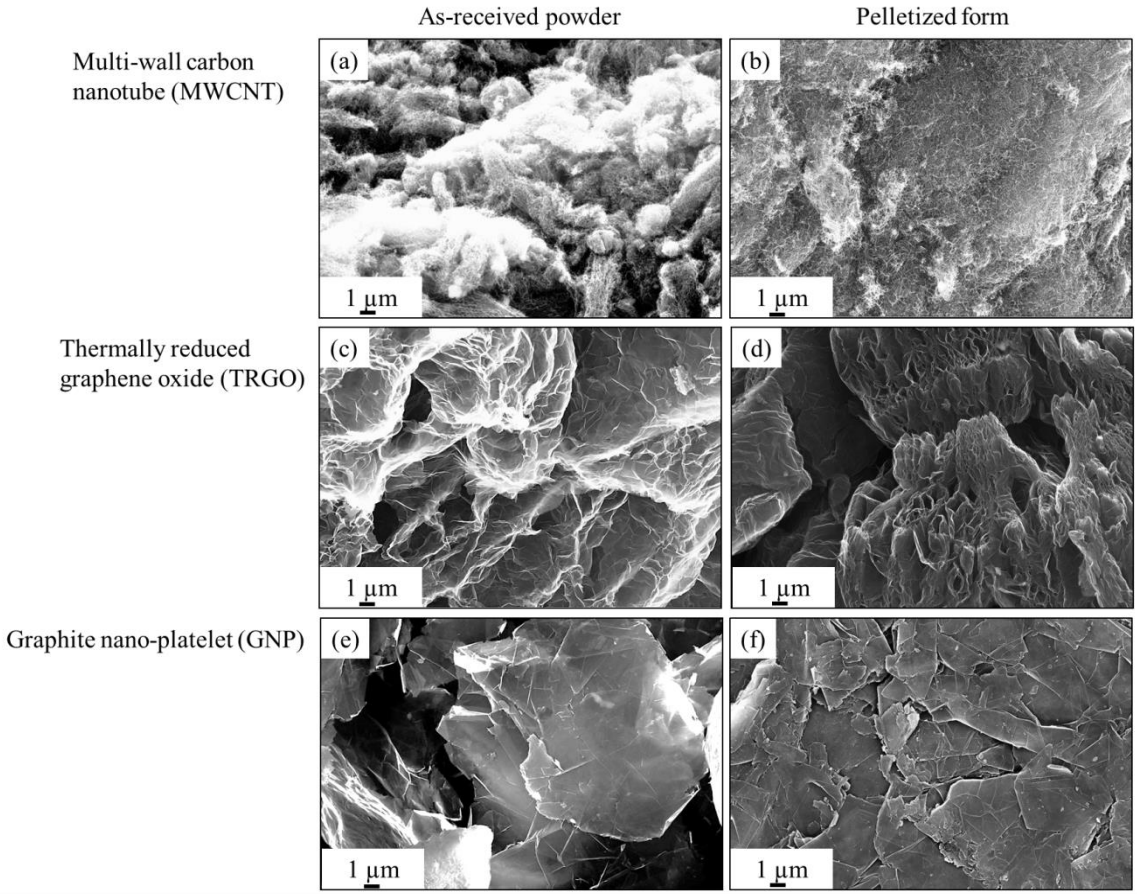

Figure 4.1: Scanning electron micrograph of carbon nano-fillers MWCNT,TRGO and GNP - (a, c and e) as-received powders; (b, d and f) pelletized fillers.

In the above figure (Fig. 4.1), though TRGO and GNP are synthesised from a common raw material, their morphology is entirely different. Both are few layered (number of layers unknown) and have a wrinkled surface which is due to thermal treatment. TRGO has an accordion-like structure whereas GNPs remain as flakes with a less wrinkled morphology.

The TGA tests give the mass loss of the sample as a function of temperature under two different atmospheres as given in Fig. 4.2. The mass loss curve under nitrogen atmosphere gives information about oxide functionalities. The curve under synthetic air atmosphere gives the decomposition temperature of the carbon filler and at the end of the cycle, the remaining weight percentage corresponds to the metal impurities present.

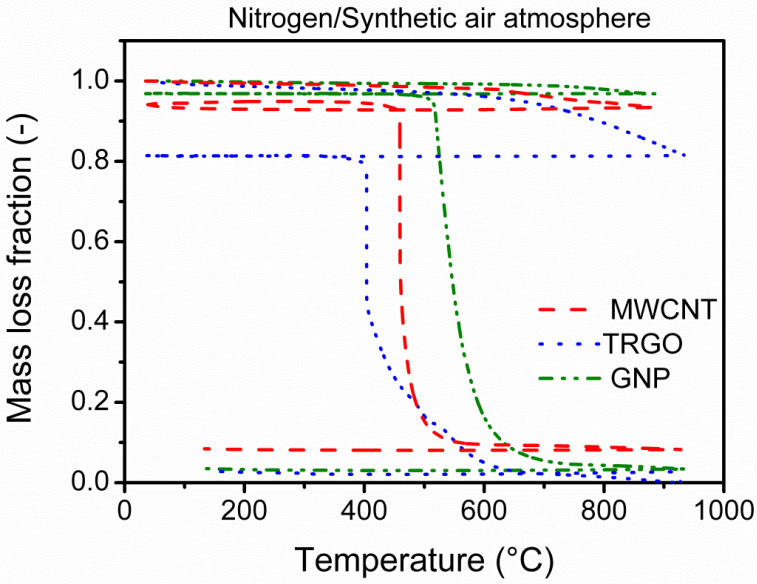

Figure 4.2: TGA mass loss curve for MWCNT, GNP, TRGO fillers under nitrogen and synthetic air atmosphere.

The decomposition temperature at 50% mass loss under synthetic air is 403 °C for TRGO and 460 °C for MWCNT, which is almost 100 °C less than that of GNP which decomposes at 547 °C. Moreover, there is 6% and 4 % mass loss for MWCNT and GNP after nitrogen cycle, and it is 20% for TRGO which is an indication of the presence of oxide functionalities in TRGO.

The quality of graphene sheets was analysed using XRD and Raman spectroscopy; the d-spacing of MWCNTs, TRGO and GNPs as well as the number of graphene layers stacked was calculated from Bragg and Scherer equations (Eqs. 4.1 & 4.2).

Bragg equation: $d_{(0\,0\,2)} = \lambda/2sin\theta$ Eq. (4.1)

Scherrer equation: $D_{(0\,0\,2)} = 1.84\lambda/FWHMcos\theta$ Eq. (4.2)

Number of layers: $N = D_{(0\,0\,2)}/d_{(0\,0\,2)}$ Eq. (4.3)

where,

d - Spacing between the diffracting planes in Å

λ - Wavelength of the target (Cu K_α: 1.5418 Å)

$FWHM$ - Full width at half maximum of the primary peak in degrees

θ - Position of the primary peak in degrees

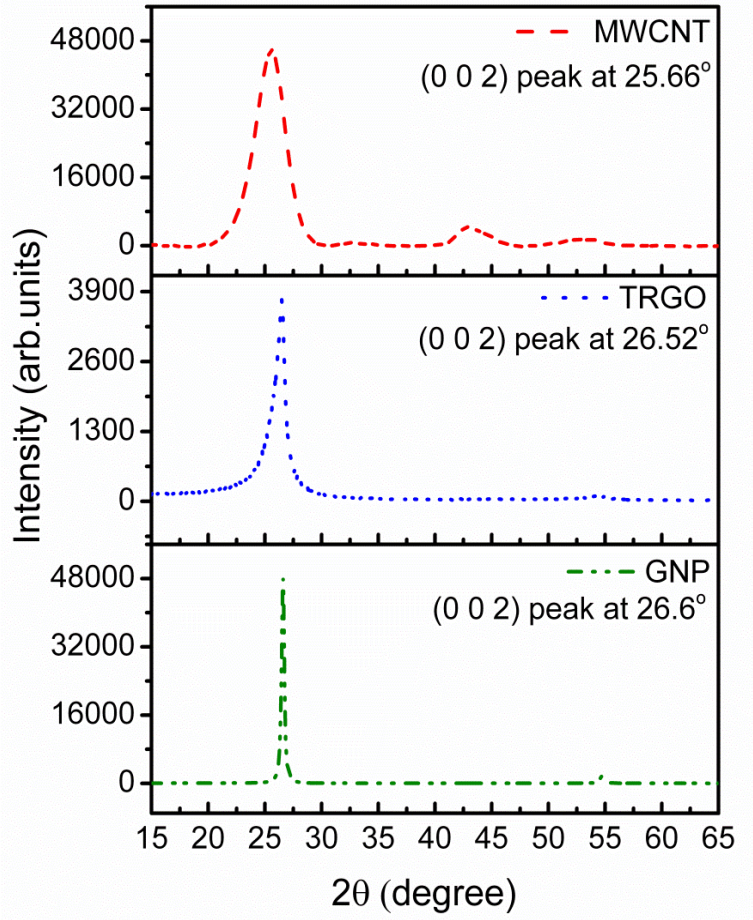

Figure 4.3: X-ray diffractogram of the as-received nano-fillers.

The X-ray diffractogram of MWCNT, TRGO, GNPs shown in Fig. 4.3, has the characteristic (0 0 2) peak positioned at 25.66°, 26.48° and 26.6 respectively; its corresponding d-spacing value is 3.48 Å, 3.36 Å, 3.35 Å which is closer to the graphite d-spacing. The peak at 55° for TRGO and GNP corresponds to the reflections from (0 0 4) planes. The Full Width at Half Maximum (FWHM) was calculated by fitting the curve using Lorentz function and was used in Scherrer equation to calculate the crystallite thickness ($D_{0\,0\,2}$). Dividing the thickness with d-spacing gives a rough estimate about the number of layers, and in the present case was found to be 13 (MWCNT), 38 (TRGO) and 170 (GNP).

The Raman spectrum of a mono-layer graphene has two important peaks viz., G band that appears at 1580 cm^{-1} and the second peak is the 2D band also known as the G' band that appears at 2700 cm^{-1}. It is shown in literature that the 2D band of a monolayer graphene can be fitted with a single Lorentzian peak, whereas a bi-layer is fitted with four such peaks indicating four double resonances. As the number of layers increases, this resonance process increases and converges to that of graphite which can be fitted with only 2 peaks.

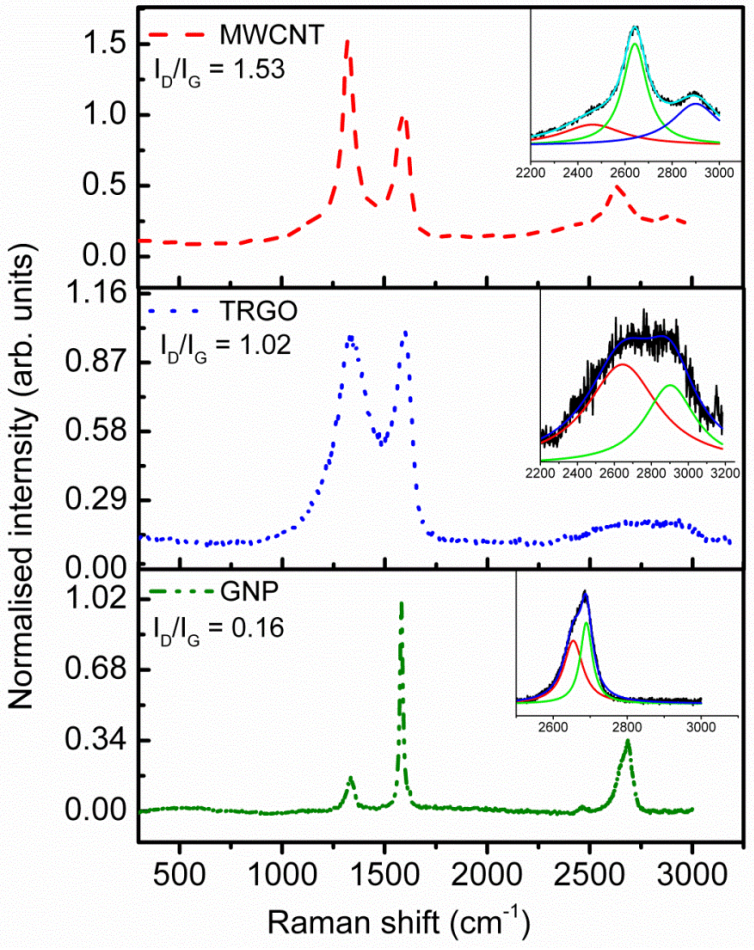

Figure 4.4: Raman spectra of the as-received nano-fillers taken using He-Ne laser.

The Raman spectrum of as-received MWCNTs, TRGO and GNPs shown in Fig. 4.4 was taken using He-Ne laser. It can be clearly seen that the I_D/I_G ratio is smaller (1.06, 0.2) which indicates that there are lattice defects that are smaller for GNPs compared to TRGO. The 2D band was fitted with two Lorentzian peaks, which is already an indication that the number of graphene layers stacked in GNP is more than 10.

It is of interest to find the electrical conductivity of the as-received filler before dispersing in the matrix. Pellets of the as-received nano-fillers were prepared and subjected to four point probe measurements in order to find the sheet resistance of the sample. The density of the powders was measured separately, and the density of the pellet was calculated from the mass and volume of the pellet. The volume fraction and the volume conductivity of the pellet were obtained using the following equations (Eqs. 4.4 & 4.5) and are presented in Fig. 4.5.

$$Volume\ conductivity = {}^{1}/_{Volume\ resistivity}\ \text{(S/m)} \qquad \text{Eq. (4.4)}$$

$Volume\ resistivity\ = Rs.t$ (ohm.m)

$$V_f = \frac{\rho_{th}}{\rho_{exp}}.pf \qquad \text{Eq. (4.5)}$$

where,

Rs - Sheet resistance in ohms.

t- Thickness of the pellet in metre.

ρ_{th} - Theoretical density (mass/area × thickness) of the pellet in g/cc.

ρ_{exp} - Experimental density (density of the powders) in g/cc

pf - Packing fraction (MWCNT - 0.907 [154]; TRGO, GNP - 0.74)

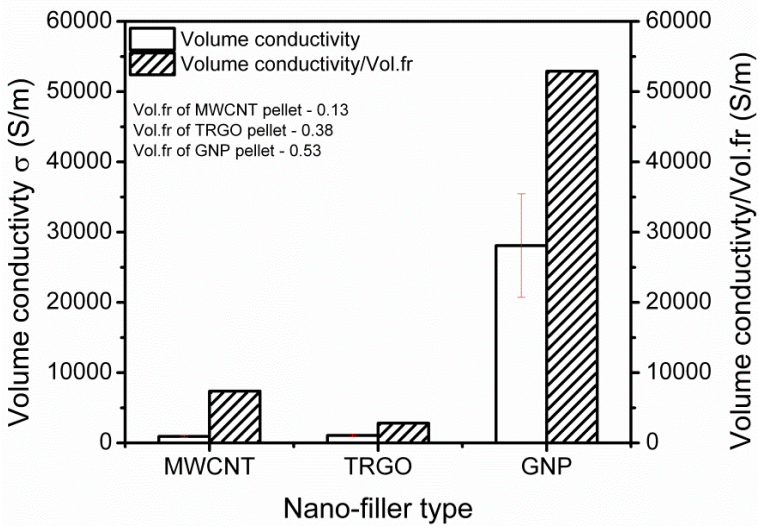

Figure 4.5: Volume conductivity of the pelletized nano-fillers.

The GNP pellet shows highest conductivity similar to that of graphite (the conductivity value assumed is ~30000 S/m). MWCNTs are second highest with 10000 S/m; TRGO is almost one of magnitude less than MWCNT with 1000 S/m. All these test results on the quality of the fillers indicate strong influence of the preparation methods on the properties of the as-received filler. With this basic information obtained from filler characterisation, their dispersion in the epoxy matrix and the properties of the nano-composite obtained will be discussed further.

4.2 Nano-composite characterisation

One of the major difficulties encountered during the preparation of nano-composite is to achieve uniform dispersion of nano-fillers in the epoxy. Superior mechanical properties of the fillers can be obtained only when each individual filler is in contact with the epoxy resin. But the nano-fillers tend to form cluster or aggregates either due to physical interaction or due to van der Waals force between them. Apart from the dispersion method employed, the properties of the intrinsic filler and their aspect ratio also affect the dispersion. For example, the as-produced commercially available MWCNTs are found in the form of twisted bundles as in Fig. 4.1a which are generally called "primary agglomerates", when present in the composite, diminishes the mechanical properties.

In the aspect of mechanical properties, to harvest the full potential of a nano-filler when dispersed in a polymeric matrix, a homogeneous dispersion of the filler in the polymeric matrix and strong interfacial bonding between the filler and the matrix must be achieved. The attainment of homogeneous dispersion of nano-fillers is difficult due to van der Waals interaction between the fillers, which usually lead to formation of aggregates. This poses a main challenge for the development of advanced nano-filler/polymer composites. In the present study, the polymeric matrix is an epoxy based system; hence the nano-filler is first dispersed in a monomer suspension and is then mixed with other components which are then cured. The behaviour of these fillers in viscous medium and the time-temperature dependent behaviour of the suspension are responsible for the formation of an electrically conductive network (dynamic percolation) during curing.

The movement of these nano-fillers in epoxy suspension can be explained using colloidal theory, where inter-particle interaction and particle-matrix interaction play a key role. Prior to dispersion the nano-particles are subjected to attractive forces (i.e., weak van der Waals force) due to low inter particle distance between the particles and high surface to volume ratio of nano-fillers. Beyond a critical inter particle distance columbic electrostatic repulsive forces dominate [155]. When the epoxy matrix containing nano-particles is subjected to dispersion, hydrodynamic force is applied via shear or stirring and the particles are dispersed in the matrix. With increasing shear, the hydrodynamic force increases and the particles are forced to agglomerate. Apart from these effects, the particles are also subjected to Brownian motion and the viscous forces of the epoxy matrix, temperature and time contribute to the final dispersion state of the particles [156,157]. But, in practice it can be seen that the presence of agglomerates

is essential in order to form an electrically conductive network, but the mechanical properties can be enhanced only when the individual nano-particles are dispersed [158].

A sketch that relates the distribution and dispersion of fillers in the matrix to the observed electrical and mechanical property is depicted in Fig. 4.6. As explained briefly above, when the applied shear forces are high enough to break the primary agglomerates then a homogenous distribution of individual particle is obtained which is the ideal desired model for improved mechanical properties. However, due to the effects of particle-particle interaction and by movement of the particles in the resin after dispersion, a re-agglomeration process is inevitable which leads to an agglomerated dispersion state in the matrix. To obtain an electrically conductive system, a percolated network is desired for electron conduction and hence an inhomogenous distribution of particles in the matrix is necessary. Hence, an optimum dispersion is a state where the primary agglomerates of the nano-fillers are broken down and there is sufficient re-agglomeration to form a conductive network such that there is no compromise between electrical and mechanical properties [156,159].

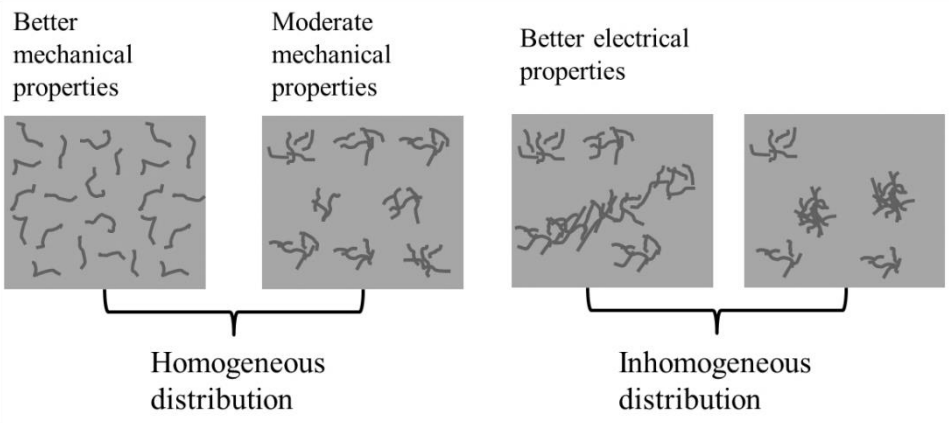

Figure 4.6: Schematic that relates the dispersion state and distribution of nano-fillers to the subequent mechanical and electrical properties of nano-composite.

Among the various dispersion methods available, the most commonly used ones are calendering, ultra-sonication, ball-milling, stirring and extrusion processes. The calender commonly known as the three-roll mill (3RM) is a machine that employs high shear forces using three rotating rollers at very high speed to disperse the nano-fillers in a viscous medium. The innermost roll is called the feed roll where the material is fed and the outermost roll is called the apron roll which is in contact with a razor blade which scraps the composite suspension. One of the advantages in this method is the degree of fineness to which the gap between the rollers can be controlled (down to 5 µm). Also the speed of the rollers can be

varied and hence the material is subjected locally to a very high shear force that can break the bigger agglomerates. This process can be repeated several times until the desired dispersion is achieved. But, one limitation is the breakage of nano-particles when milled for longer times. However, this process is more efficient in breaking down the agglomerates but not in obtaining the individual nano-particle dispersion in the matrix [15].

In ultra-sonication, the ultra-sound energy is applied to swirl the particles in a solution. This energy is applied either through a sonication bath or through a sonication probe where power can be varied. The applied ultrasonic waves basically peel off the nano-particles from its aggregates. To apply this method for dispersion, the solution must be extremely less viscous, and hence a low viscous volatile solvent such as acetone, ethanol can be used. These solvents are later removed by heating, and the suspension is later subjected to mechanical stirring or calendering [160].

In ball-milling, the material is ground to fine powders by grinding them in the ball-mill. In the case of nano-particles, it is done using the presence of a chemical to enhance their dispersion ability [161,162]. Extrusion is employed when the particles need to be dispersed in high viscous polymer melts [163].

4.2.1 Dispersion quality: Different dispersion method

As mentioned earlier, the default dispersion method adopted in this study is 3RM process, where the nano-fillers are sheared along with the resin at very high shear rates. The dispersion quality was assessed after every cycle in the three-roll mill and this step was carried out to visualise the effect of applied shear rate on the nano-filler agglomerates. The composite suspension was placed on a glass slide and viewed under transmission mode in light microscope as in Fig. 4.7; the weight percentage is with respect to the epoxy resin.

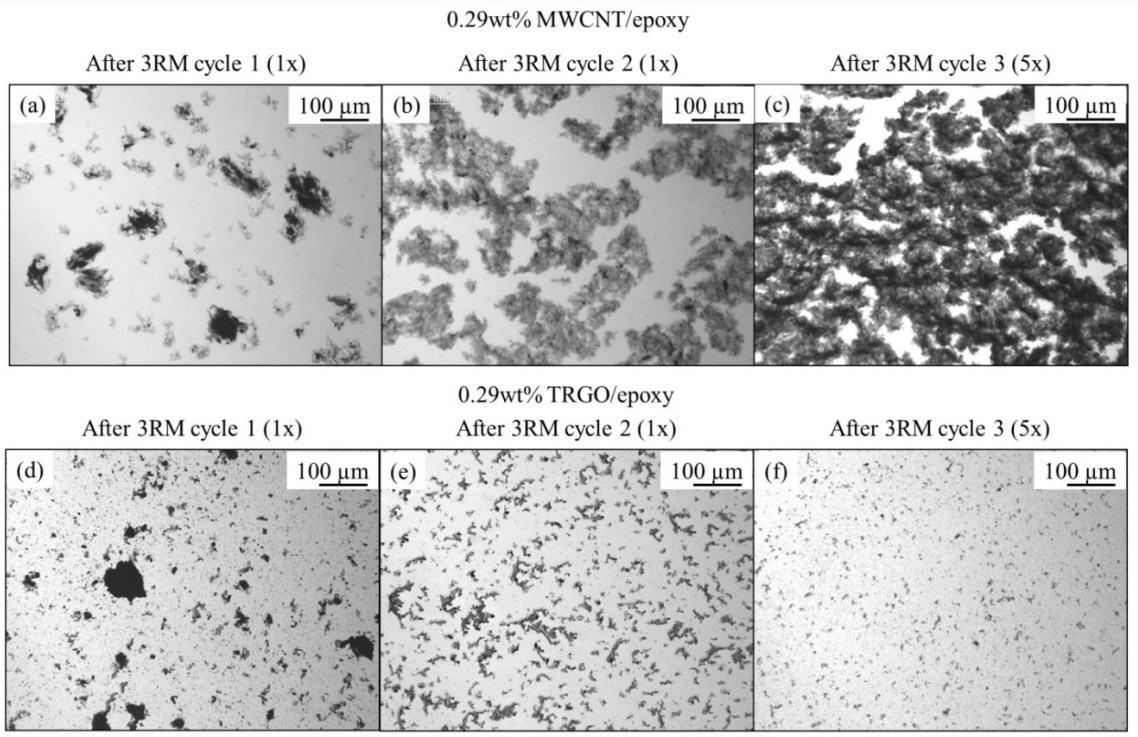

Figure 4.7: Transmission light microscopic images of (a-c) 0.29wt% MWCNT/epoxy after different dispersion cycle in 3RM; (d-f) the same for 0.29wt% TRGO/epoxy respectively.

The differences after each dispersion cycle and also between two different types of fillers (MWCNT and TRGO) can be seen in Figs. 4.7c and 4.7f. Since GNP and TRGO belong to the same class of filler family, the dispersion was almost similar to that of TRGO/epoxy. After the first cycle (shear rate - 31000 s^{-1}), the size of the agglomerates is bigger and it is difficult to distinguish between the primary and secondary agglomerates (Figs. 4.7a and 4.7d). As the shear rate is increased (shear rate - 96000 s^{-1}), the primary agglomerates are broken down and a uniform dispersion is reached and some of the nano-fillers/agglomerates even re-agglomerate to form a network structure. But after the final dispersion step (shear rate - 250000 s^{-1}) a network structure in the case of MWCNT/epoxy is clearly visible (Fig. 4.7c), whereas, TRGO/epoxy is a fine dispersion (Fig. 4.7f) which is mainly due to the filler geometry. However, these images are not representative dispersion state of the filler in the final cured composite, as temperature influence during curing must also be considered.

The morphology of the as-prepared suspensions using the other two dispersion methods (Soni_hsm and Soni_3RM) along with 3RM was also investigated. For ease of comparison, a representative sample from the GNP/epoxy system is chosen; the weight percentage is with respect to epoxy resin.

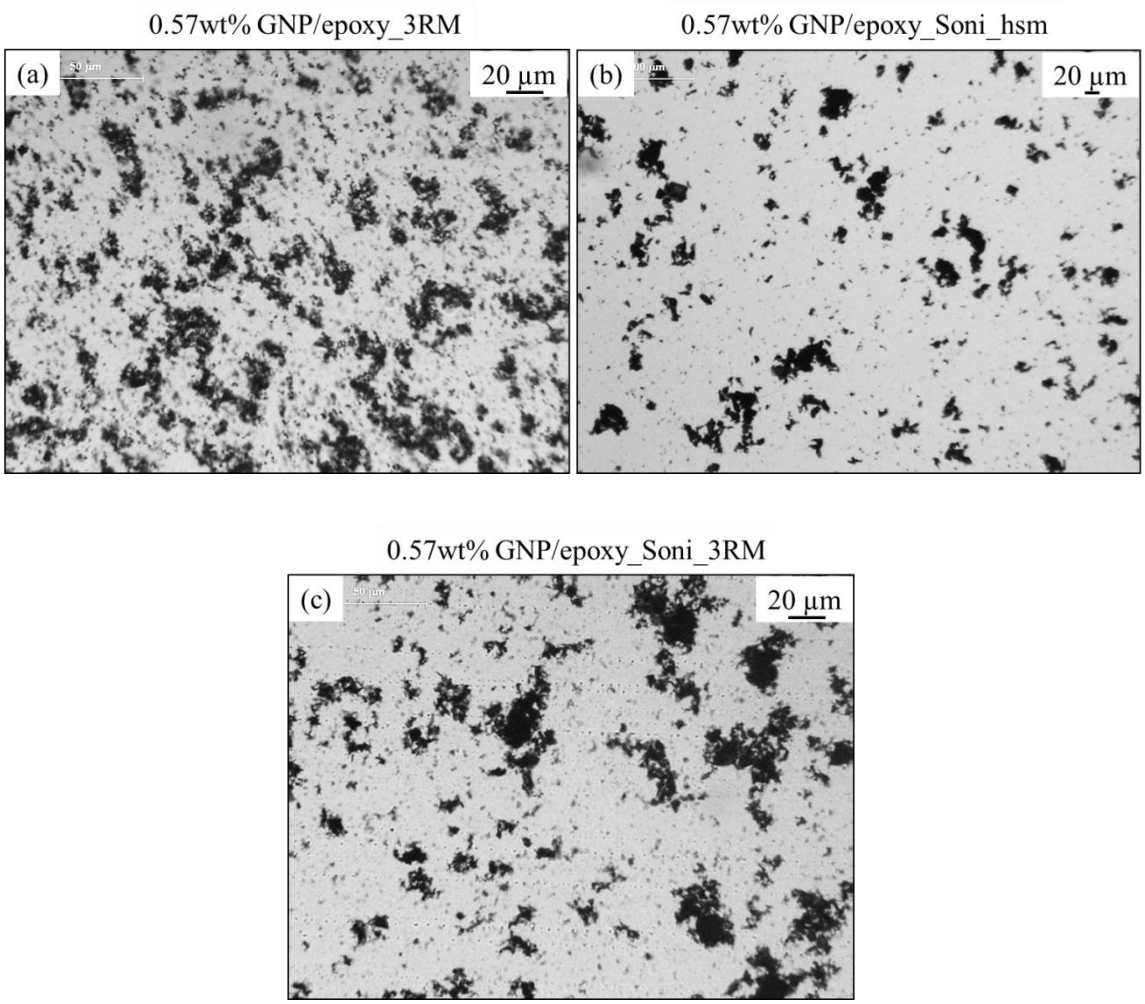

Figure 4.8: Transmission light microscopic images of 0.57wt% GNP/epoxy prepared by different dispersion methods (a) 3RM; (b) Soni_hsm and (c) Soni_3RM.

The suspension prepared using 3RM (Fig. 4.8a) exhibits formation of a network structure. On the other hand, in the suspension from Soni_hsm (Fig. 4.8b) no such network structure is visible. However, there are visible flakes which are agglomerated. The ultra-sonication combined with 3RM process (Fig. 4.8c) has both flake agglomerates and a small amount of networks formed. The effect of these processing routes on the electrical conductivity and on mechanical property will be discussed in the following section.

Optical micrographs of the bi-filler suspensions (TRGO_MWCNT/epoxy) were also viewed under transmission mode as shown in Fig. 4.9. It can be seen that the bi-filler composite suspension has a different morphology when compared with mono-filler suspension (MWNCT/epoxy); the weight percentage is with respect to resin.

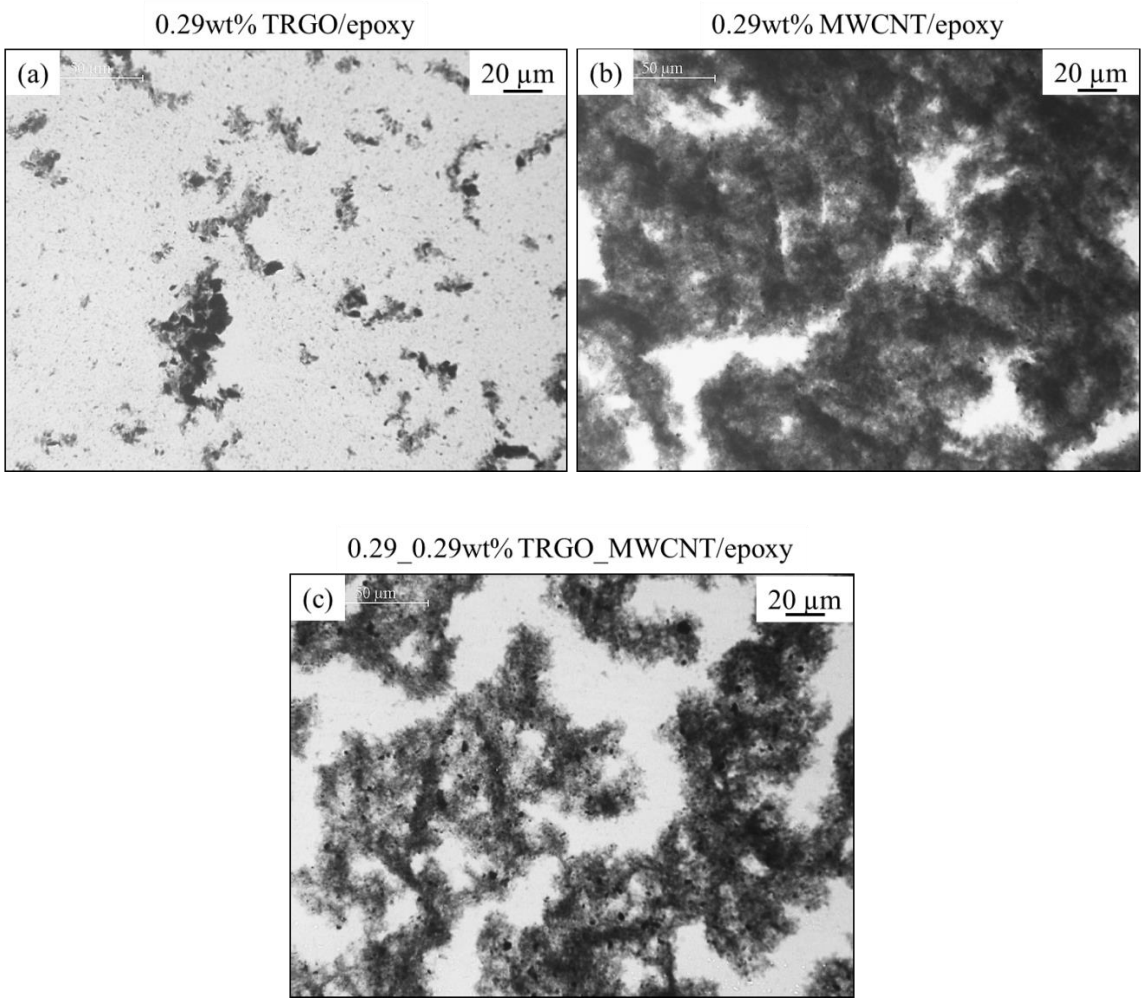

Figure 4.9: Transmission optical micrograph of mono-filler and bi-filler systems (a) 0.29wt% TRGO/epoxy; (b) 0.29wt% MWCNT/epoxy and (c) 0.29_0.29wt% TRGO_MWCNT/epoxy.

MWCNT/epoxy shows dense network morphology (Fig. 4.9b), whereas the bi-filler suspension shows a lesser dense network structure (Fig. 4.9c). This effect of TRGO addition to MWCNT is later studied in detail using electro-rheological measurements.

4.2.2 Microscopic analysis of cured composite

The morphology of the cured nano-composite was examined using scanning electron microscope. The distribution of filler was observed on the cryo-fractured surface of a 500 nm thin slices of the cured composite. The micrographs were taken in "in-lens" mode, where the secondary electron detector is placed above the objective lens of the microscope [164]. This mode works well at low kV and short working distance and therefore, the nano-fillers are easily visible as observed in Fig. 4.10.

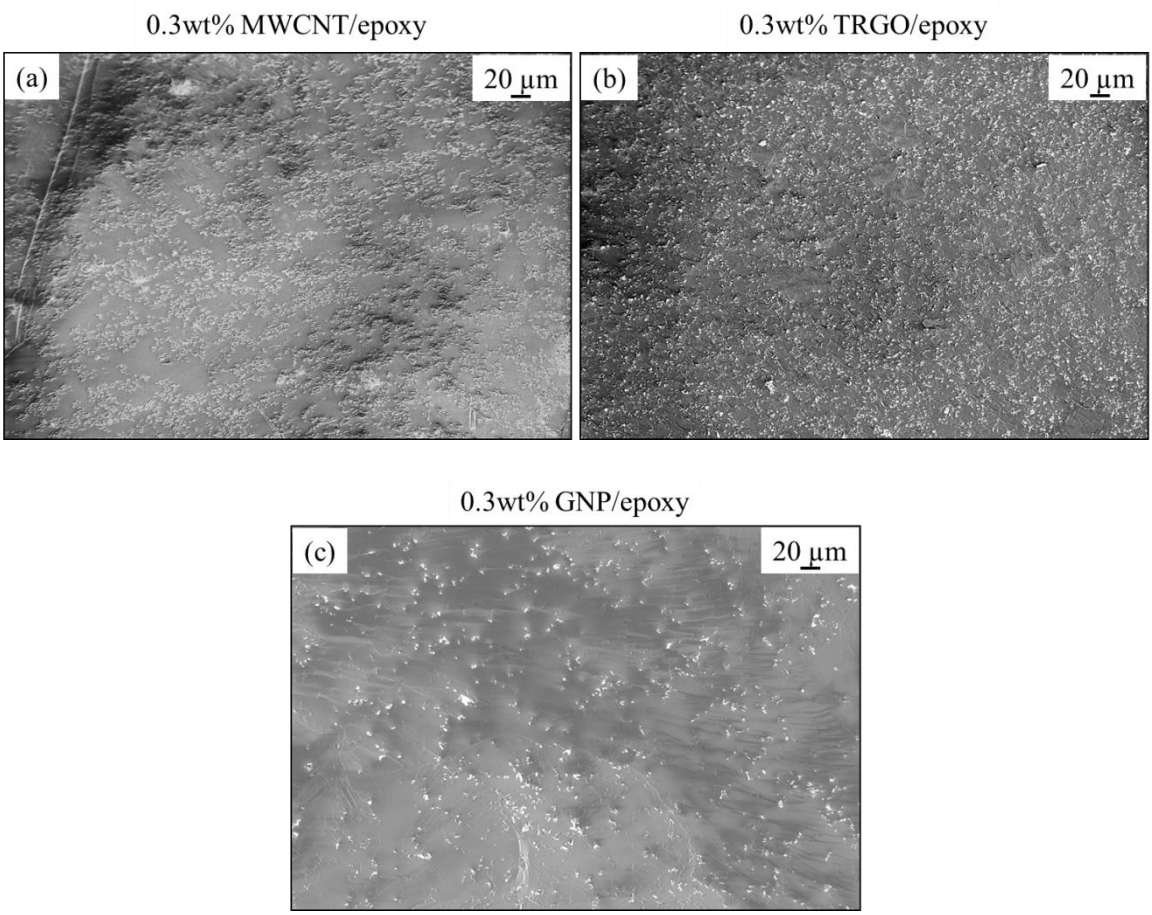

Figure 4.10: Scanning electron micrograph in "in-lens" mode of cryo-fractured cured composites containing (a) 0.3wt% MWCNT/epoxy; (b) 0.3wt% TRGO/epoxy and (c) 0.3wt% GNP/epoxy, showing the distribution of fillers in matrix.

The above micrographs (Fig. 4.10) exhibit a fairly uniform distribution of fillers using the three-roll mill process. To avoid excessive charging, the bulk sample is coated with silver paint and is placed on a carbon tape. The epoxy resin is positively charged, and to neutralise this, nano-fillers acquire a negative potential. The negative potential favours emission of secondary electrons and hence the nano-fillers appear bright [165]. Considering TRGO/epoxy and GNP/epoxy for the same amount of filler content TRGO seems to have a well dispersed state when compared to that of GNP/epoxy. While processing, the initial shearing breaks down the primary agglomerates into finer ones and upon addition of hardener small aggregates start to form. When the suspension is cured at high temperature, due to the effects of temperature these small aggregates combine to form a macroscopic network throughout the resin [166]. However, it is difficult to distinguish the primary and secondary agglomerates from the above micrographs. Hence, electron micrographs in “in-lens” mode were taken for thin slices of the composite at various weight fractions of the filler as in Fig. 4.11.

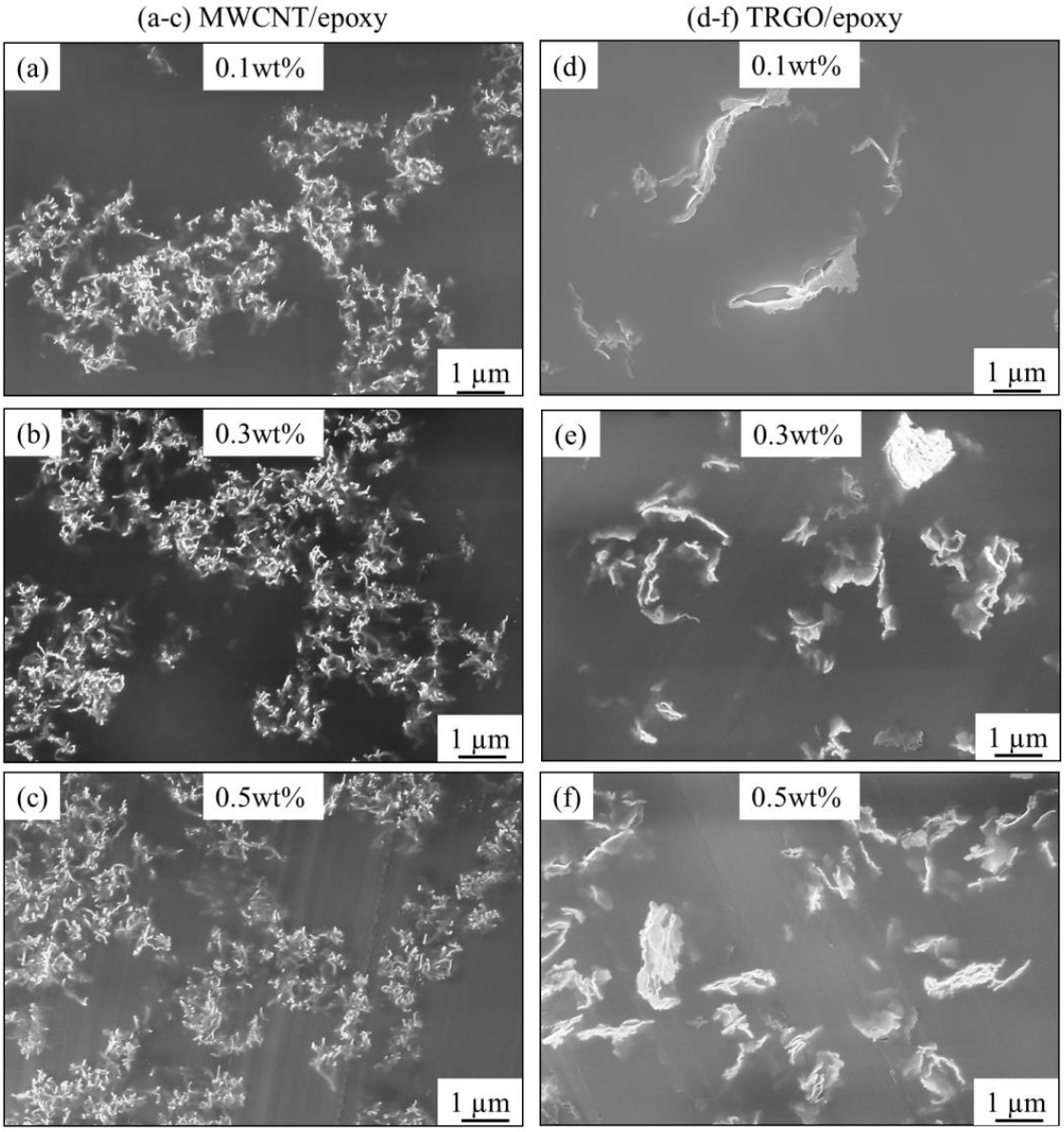

Figure 4.11: Scanning electron micrographs of thin slices (500nm thick on Si wafer) of cured composite in "in-lens" mode (a-c) 0.1-0.5wt% of MWCNT/epoxy and (d-f) 0.1-0.5wt% TRGO/epoxy.

The visualisation of the percolated networks formed in the cured composite can be well recognised in the above micrographs. For MWCNT/epoxy, it could be seen that the network of MWCNTs also connects the neighbouring agglomerates which helps in electrical conduction through this 3D network. For TRGO/epoxy and GNP/epoxy the morphology remains similar, with increased primary agglomerates as the filler content increases. However, unlike MWCNTs, the 2D fillers do not show prominent network formation in between the

agglomerates. The dispersion of fillers in the epoxy matrix remains fairly uniform down to microscopic level.

4.3 Electrical conductivity

Polymers are generally good insulators due to the lack of free charge carriers. But when reinforced with conducting particles like carbon nano-fillers, there is a transition from the insulating behaviour to a conductive polymer nano-composite [167]. To explain this conduction mechanism, percolation theory is widely applied in the nano-composite. Percolation is a standard model applied for dis-ordered systems. According to this theory, at low filler concentrations, as there are no conducting paths, the conducting particles are either separated or they are present in the form of small clusters, and hence the electrical property is dominated by the matrix [168]. As the concentration increases, at one point the clusters start to percolate and below this concentration the composite remains as an insulator [169]. This concentration is called the percolation threshold and hence the DC conductivity of the composite is governed by the following equation (Eq. 4.6).

$$\sigma \propto (\varphi - \varphi_c)^t \qquad \text{Eq. (4.6)}$$

where, σ - conductivity of the sample, φ_c - percolation threshold and t - critical index.

Above the percolation threshold, the structure is so dense with multiple conducting paths, and the conductivity value reaches saturation due to lesser influence of the links between the conducting particles. Based on the above arguments, the electrical percolation curve is represented in the form of an S-curve as in Fig. 4.12. This percolation threshold is strongly influenced by (i) the geometry and aspect ratio of the filler [170], (ii) poor wetting between the resin and the filler and (iii) dispersion of the filler itself [166], [171,172].

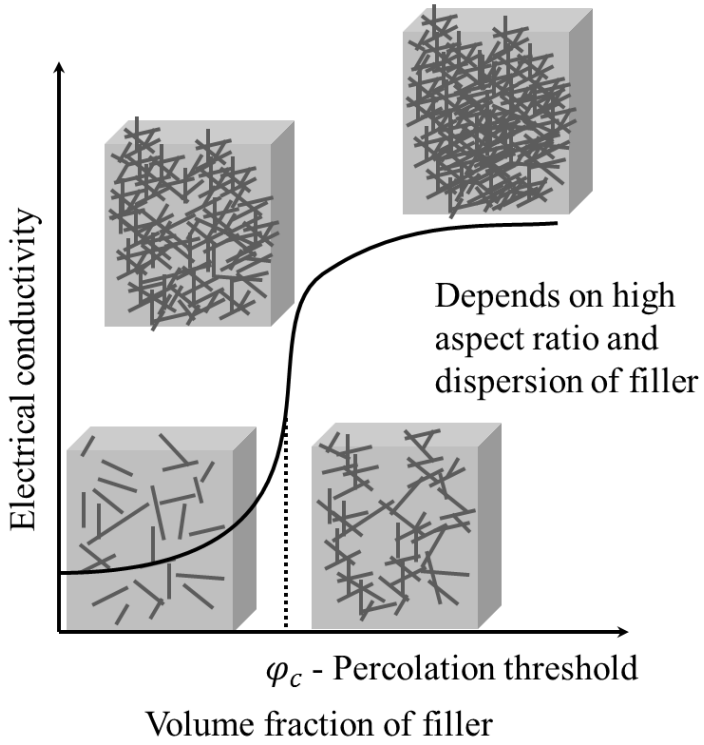

Figure 4.12: Schematic representation of filler dispersion by varying the filler loading and its corresponding electrical conductivity.

The conduction mechanism in these nano-composites is mainly due to (i) intrinsic conductivity of the fillers, (ii) conductance due to direct contact between the fillers and (iii) conductance due to electron tunnelling between the fillers [14], [173-175].

The above mentioned geometrical model is well suited for thermo-plastics, whereas for thermosets the resin are liquids with lower viscosity and hence colloidal theory which considers the interaction of particles, structure and dynamics of agglomeration must be considered. Schueler et al., investigated a carbon black epoxy system where experimental results showed existence of a potential barrier which is formed due to the electrostatic columbic repulsion of particles. The particle obtained the electrostatic charges up on dispersion in the resin. It is possible to overcome this barrier through external forces such as dispersive or thermal or by increasing the ionic concentration. Apart from particle-particle interaction, due to the low viscous nature of resin, dispersed particles tend to migrate through the medium like colloids and can stick to each other to form agglomerates while colliding with each other. This is purely based on the dynamics of the polymer matrix used which accounts for the re-agglomeration process after dispersing the particles in resin [155].

4.3.1 Electrical percolation curves of cured nano-composite

Epoxies are generally insulating in nature but, when incorporated with conductive particles (carbon nano-fillers in our study), they tend to form a three - dimensional network throughout the component. Upon increasing the filler content, these networks connect with each other forming a conductive path and are known as percolation (φ). When percolation threshold (φ_c) is reached, the electrical resistance drops by several orders of magnitude, and the composites beyond this filler content are conductive in nature [176]. This percolation threshold is widely affected by factors like the filler type, the dispersion state and the shear rate applied during the preparation of the composite. The following Fig. 4.13 shows the percolation threshold curve for MWCNT/epoxy, TRGO/epoxy and GNP/epoxy measured at 200 Hz using an impedance analyser.

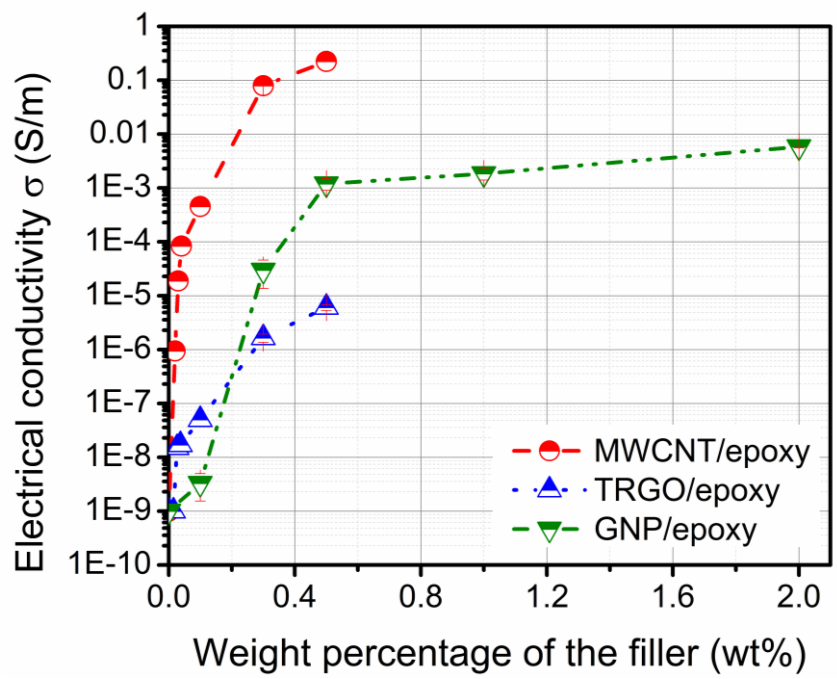

Figure 4.13: Electrical percolation curves for MWCNT/epoxy, TRGO/epoxy and GNP/epoxy.

The most striking result from Fig. 4.13 is that the electrical percolation threshold (φ_c) for MWCNT/epoxy is lower (φ_c = 0.03wt%) than TRGO/epoxy and GNP/epoxy systems. For GNP/epoxy the φ_c is at 0.5wt%, whereas TRGO/epoxy does not exhibit any sharp increase in the conductivity. MWCNT/epoxy composite reaches the maximum conductivity (σ) of 0.2 S/m at 0.5wt% followed by GNP/epoxy with σ of 5.8 x 10^{-3} S/m at 2.0wt%, and TRGO/epoxy has the minimum conductivity of 6 x 10^{-6} S/m at 0.5wt%. Clearly, the minimum optimal amount of MWCNT for percolation threshold does not require a homogenous dispersion but an

adequate dispersion, sufficient enough to form a conduction pattern along the matrix. This is possible with MWCNTs in epoxy at even lower loadings due to the high dispersive surface energy which produces spontaneous re-agglomeration. This difference in the percolation threshold for different fillers can be due to the difference in the geometry of the filler. With one class of filler (2D) GNP/epoxy performs better in terms of electrical conductivity than TRGO/epoxy which may be attributed to lower intrinsic conductivity of TRGO filler and also the ability of it to disperse well as it is partly functionalised which should also influence the re-agglomeration process. Higher filler content samples for MWCNT/epoxy and TRGO/epoxy could not be prepared owing to increase in viscosity of the suspension which makes processing and the re-agglomeration more difficult.

4.3.2 Effect of dispersion method on electrical conductivity of GNP/epoxy

The nano-fillers have high aspect ratios which gives them large surface area for interaction with the matrix. Commercially available nano-fillers are already in the form of bundles and agglomerates because of electrostatic interaction between the particles and due to van der Waals forces. All the above aspects result in inherent difficulties for dispersion of these nano-fillers. By varying the dispersion technique, the physical property of the final composite is significantly affected. For graphene literature, ultra-sonication of the filler in a solvent aids in further exfoliation of graphene sheets giving rise to better dispersion. Since the dispersion method involved in the present study is three roll-milling it was compared with the other techniques reported in literature. The following electrical percolation curve (Fig. 4.14) of GNP/epoxy was obtained for the samples prepared using three different dispersion methods as explained in Chapter 3 Section 3.2.

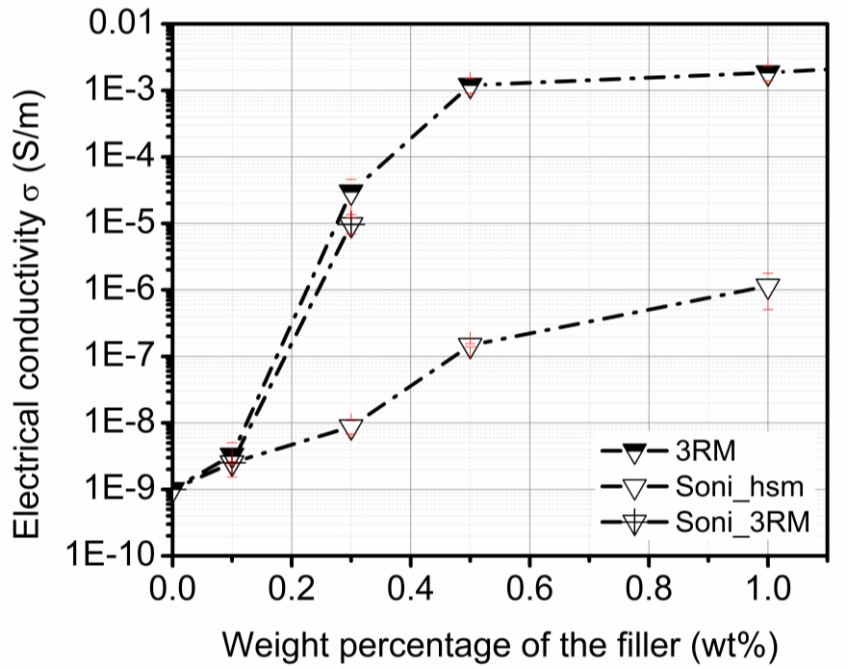

Figure 4.14: Electrical percolation curve for GNP/epoxy system prepared via different dispersion methods.

It is apparent from Fig. 4.14 that 3RM process has the highest conductivity of 2 x 10^{-3} S/m at 1.0wt% whereas GNP/epoxy_Soni_hsm has an electrical conductivity of 1 x 10^{-6} S/m at same filler content. It must be noted that the sonication combined with high speed shear mixing process involves the use of solvent ethyl acetate. Though the amount of solvent present in the suspension is less than 2% (checked using TGA measurements), the addition of solvent has its effects on the epoxy used. Clearly, 3RM process has at least 3 orders of magnitude higher conductivity than the other process involved. The Soni_3RM process yield composites with a conductivity value close to that of the samples prepared by 3RM process.

4.3.3 Effect of addition of TRGO on the electrical conductivity of MWCNT/epoxy

The most striking observation to emerge from Fig. 4.13 is that MWCNT/epoxy nano-composites show better performance in terms of electrical conductivity. Recent research findings exhibited synergetic effect in electrical conductivity when two carbon nano-fillers (MWNCT and CB) were combined [177]. Therefore, electrical properties of a bi-filler epoxy based composite containing MWCNTs and TRGO, were studied. The investigation was focussed mainly on the effect of addition of TRGO on the percolation behaviour of MWCNT/epoxy composites and to understand the filler-filler interactions.

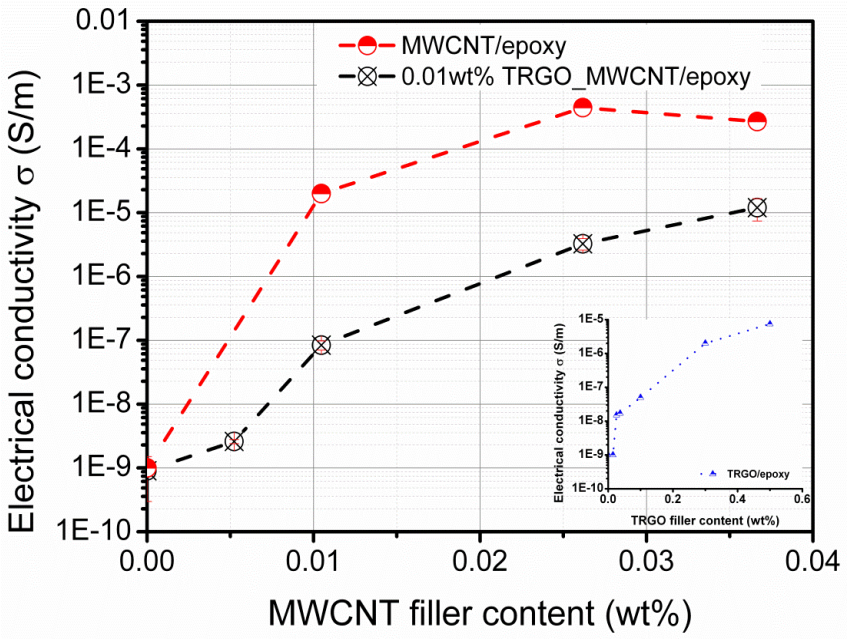

Figure 4.15: Comparison of the electrical conductivity between bi-filler 0.01wt% TRGO_MWCNT/epoxy and mono-filler MWCNT/epoxy cured composite. Insert shows the electrical percolation curve for mono-filler TRGO/epoxy composite.

In Fig. 4.15 the electrical conductivity of 0.01wt% TRGO_MWCNT/epoxy composites as a function of MWCNT weight percentage is shown. Comparing it with the inset (TRGO/epoxy electrical percolation curve), it can be concluded that TRGO/epoxy composites are less conductive than MWCNT/epoxy composites. When the two fillers are combined, the bi-filler composites neither exhibit synergy nor obey the rule of mixtures; instead, an opposite of the synergetic effect is observed. On comparing the conductivity of the bi-filler (TRGO_MWCNT/ epoxy) cured composite to that of MWCNT/epoxy cured composite, there seems to be a decrease in conductivity of the composite due to the addition of TRGO. As can be seen above, in the case of cured MWCNT/epoxy composites there is a steep increase in electrical conductivity whereas in the case of TRGO_MWCNT/epoxy composites there is no significant change.

The decrease in conductivity of the bi-filler cured composite is about two orders of magnitude for lower concentration of filler content (0.01 _0.01wt% TRGO_MWCNT/epoxy) and is about one order of magnitude for higher filler content (0.01_0.035wt% TRGO_MWCNT/epoxy). Thus, the addition of TRGO affects the conductivity of MWCNT/epoxy cured composite more at lower concentrations of MWCNT. It is therefore evident that as the filler content increases, agglomeration of tubes due to high concentration dominates the electrical transport behaviour. However, this does not depend much on the type of filler added, but rather only upon increase

of conductive fillers coming into contact. When a steep increase in electrical conductivity is observed for the cured MWCNT/epoxy composites, a less significant change in conductivity is found in the TRGO_MWCNT epoxy composites. The above measurement was also carried out for higher concentration of filler, which is 0.3_0.3wt% TRGO_MWCNT/epoxy and a similar observation of decreased electrical conductivity for bi-filler composite was observed (see Annexure Fig. A.2). Since the rheological percolation threshold value for MWCNT/epoxy is 0.3wt% (measured from previous studies [178]), samples with higher filler content were tested. The electrical conductivity of 0.3_0.3wt% TRGO_MWCNT/epoxy cured composite is 3×10^{-3} S/m which is one order of magnitude lesser than the mono-filler 0.3wt% MWCNT/epoxy cured composite (7.8×10^{-2} S/m).

4.4 Rheological measurements

The physical properties of the nano-composite are strongly dependent on the dispersion of the filler and the processing condition. Better dispersion quality usually results in increased viscosity and, in turn, higher viscosity generally makes processing and manufacturing more complicated. The rheology of the material is concerned with the flow and deformation of the material experienced on applying force. The deformation and the flow behaviour of material can either be purely elastic (governed by Hooke's law) or purely viscous (governed by Newton's law). In practice, polymers possess a combination of both these behaviours and hence are viscoelastic in nature. When the apparent viscosity is a function of shear rate such behaviour is termed as non-Newtonian.

For a particle suspension, the rheology is dependent on the volume fraction of the particle, particle shape, interaction between the particles and spatial arrangements between the particles. The rheological property of the suspension is used to examine the changes in the dispersion state. It is also observed that the increase in viscosity for MWCNT reinforced polymer is much higher than CB reinforced polymer. It is also reported in literature that the applied shear forces can either build or destroy conductive pathways. Hence a combined electro-rheological study helps to understand the network formation and filler-filler interaction in a particle suspension [179-182].

4.4.1 Steady shear rate sweep measurements

The change in viscosity as a function of shear rate is plotted for the dispersion methods used, where 3RM process is used to prepare the nano-composite for MWCNT/epoxy and

TRGO/epoxy systems. A steady rate of shear flow measurement can directly be used to characterize the dispersion state because the viscosity of the mixture is strictly related to the spatial and orientation distribution of nano-fillers in the matrix. Since TRGO/epoxy and GNP/epoxy belong to same class of filler, GNP/epoxy system was not investigated. The suspension after final milling in the three-roll mill is collected and the viscosity is measured for the three different nano-composite systems as presented in Fig. 4.16.

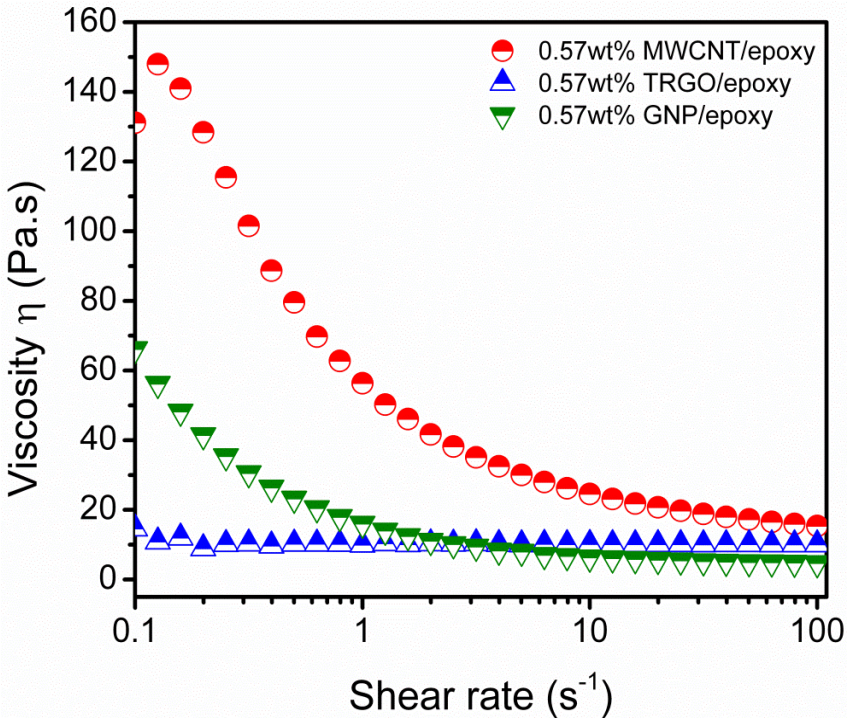

Figure 4.16: Viscosity of different nano-composite suspensions as a function of shear rate.

The viscosity gradually decreases when the shear rate is increased resulting in shear thinning. This is due to destruction of agglomerates at higher shear rates. This phenomenon is more significant in the case of MWCNT/epoxy than TRGO/epoxy. For TRGO/epoxy the viscosity does not change from the Newtonian regime of pure epoxy. This change in the viscosity for MWCNT/epoxy from Newtonian to shear thinning is due to particle-particle interaction, polymer-particle interaction, and their rod like geometry which allows them to readily form networks. On the other hand, the planar structure of TRGO and the functionalised groups present in the filler do not allow them to form a network structure and hence their viscosity is lower than MWCNT/epoxy. Also, the viscosity for MWCNT/ epoxy increases as the gap between the rollers is decreased (see Annexure Fig. A.3). This is an evidence for better dispersion of fillers in the matrix which leads to an increase in viscosity of the system.

4.4.2 Steady shear rate sweep measurements: Effect of different processing technique

After optimising the dispersion state in the 3RM process, GNP/epoxy suspensions were prepared using three different processing methods to investigate the dispersion ability. The viscosity of GNP/epoxy suspensions with 0.57wt% of filler as a function of shear rate is plotted in Fig. 4.17.

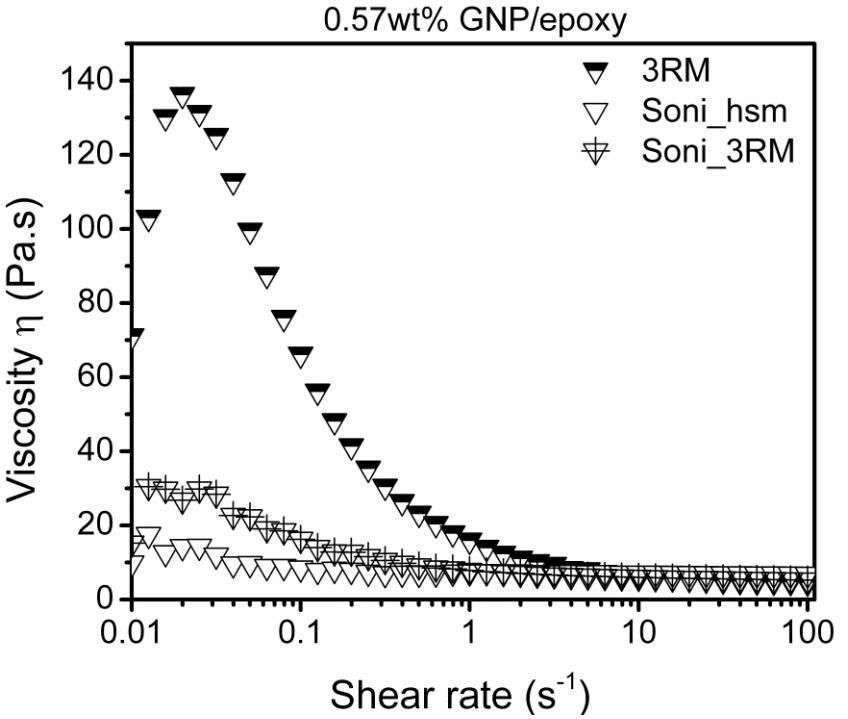

Figure 4.17: Viscosity as a function of shear rate for 0.57wt% GNP/epoxy composite suspension prepared via different dispersion methods measured under steady state.

The above results show that milling induces higher shear forces compared to the other two dispersion methods leading to a finer dispersion. The higher viscosity observed for milled system is due to agglomeration and network formation. The low viscosity observed for sonication coupled with high speed shear mixing is due to the presence of bigger agglomerates that are already visible in the light microscopic images of the suspension (Fig. 4.8). A direct relationship of this can also be made with electrical conductivity results where the samples prepared from Soni_hsm have lower conductivity. This investigation suggests that the milling process that induces high shear force, aids in breaking down the bigger agglomerates of the raw material [183].

4.4.3 Combined electro-rheological studies of TRGO_MWCNT/epoxy (shear rate step test)

The electrical conductivity for different weight percentages of MWCNT in epoxy suspension as function of shear rate is shown in (Fig. 4.18). The electrical conductivity for both mono-filler (MWCNT/epoxy) suspensions and bi-filler (TRGO_MWCNT/epoxy) suspensions are plotted in the same graph for ease of comparison. It must be noted here that rheological measurements were performed on composite suspensions prior to the addition of hardener and accelerator. Hence the weight percentage of the filler content mentioned in this section is with respect to epoxy resin alone. Also, the time between the measurement and sample preparation was less than 24 h. This, ensured that there were no effects of time induced agglomeration or sedimentation of nano-fillers on the electrical conductivity.

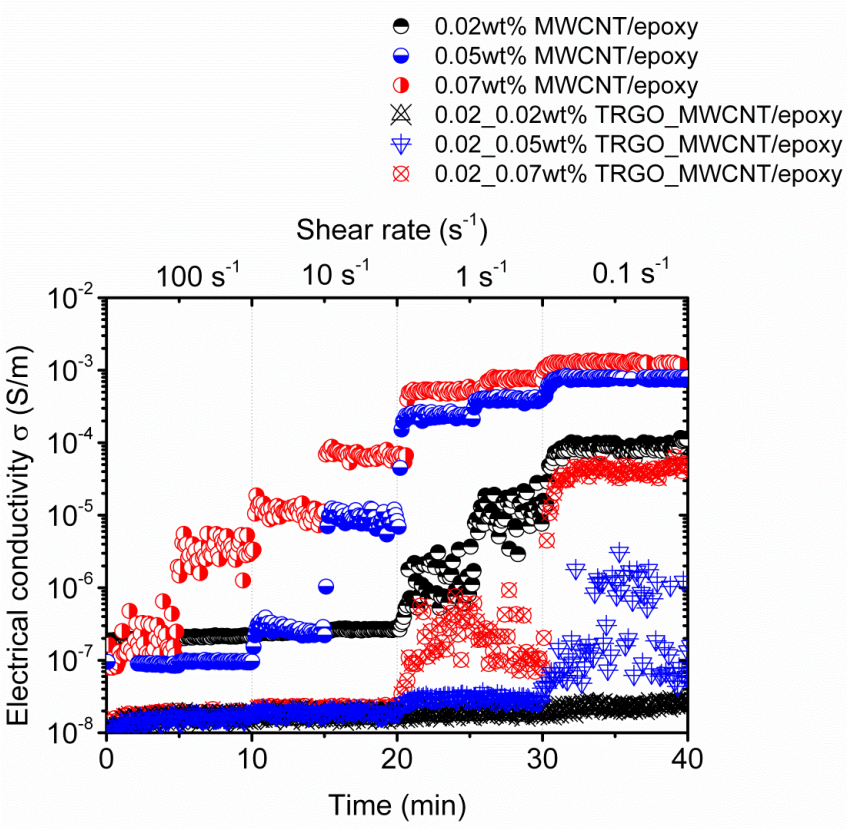

Figure 4.18: Electrical conductivity at different shear rates for the MWCNT/epoxy and TRGO_MWCNT/epoxy suspensions at lower filler concentration.

It is visible from the above graphs, (Fig. 4.18) that the electrical conductivity increases as the shear rate is decreased for both bi-filler and mono-filler suspensions. At higher shear rates (e.g. 100 s^{-1}) the filler particles cannot agglomerate, as the energy input by shearing is enough to separate the particles from each other. When the shear rate is decreased, the filler particles are

expected to build up agglomerates and their contact, giving rise to an electrically conductive network. However, the electrical conductivity of TRGO_MWCNT/epoxy suspensions does not increase at low shear rates unlike mono-filler MWCNT/epoxy suspensions.

Unlike MWCNT suspensions, the bi-filler (TRGO_MWCNT/ epoxy) suspensions seem to have a less pronounced tendency to form agglomerates under shear. The first agglomerates of MWCNT start to connect already at 0.02wt% MWCNT, whereas for bi-filler suspension (0.02_0.07wt% TRGO_MWCNT/epoxy) the first agglomerates form only at 0.07wt% of MWCNT. The suspension containing 0.02_0.05wt% TRGO_MWCNT/epoxy also shows the formation of conducting agglomerates at 0.1 s^{-1} shear rate, but these agglomerates are not stable under shear. Only at 0.02_0.07wt% TRGO_MWCNT/epoxy, stable agglomerates can be formed at a shear rate of 0.1 s^{-1}. At this percentage of the nanotubes (0.07wt%), the electrical conductivity of the mono-filler epoxy suspension is at least two orders of magnitude higher than the corresponding suspension containing TRGO and MWCNT. A similar trend is also observed at 0.57_0.57wt% TRGO_MWCNT/ epoxy suspensions (see Annexure Fig. A.4), which indicates that the effect of TRGO on MWCNT/epoxy suspension is same irrespective of the filler content. Adding high content of TRGO also seems to reduce the electrical conductivity of MWCNT/epoxy system. An in situ optical microscopy analysis of the filler structure formed under shearing at lower concentration is shown in Fig. 4.19.

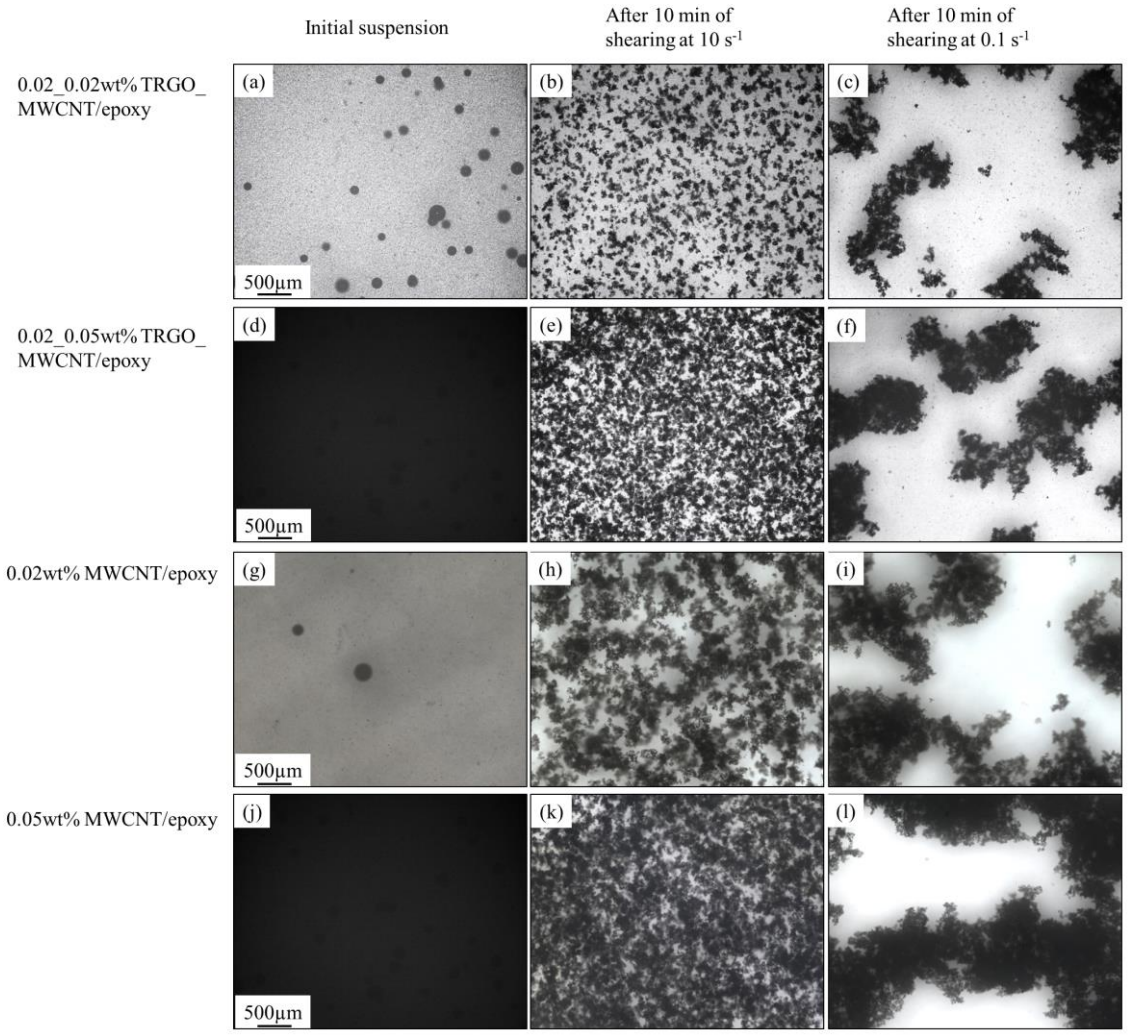

Figure 4.19: Optical micrographs of (a–c) 0.02_0.02wt% TRGO_MWCNT/epoxy; (d-f) 0.02_0.05wt% TRGO_MWCNT/epoxy; (g-i) 0.02wt% MWCNT/epoxy and (j-l) 0.05wt% MWCNT/epoxy.

It is evident from the optical micrographs (Fig. 4.19) that the size of the agglomerates of MWCNT/epoxy suspension is bigger than that of the TRGO_MWCNT/epoxy suspension. In fact, the suspension at 0.02wt% MWCNT forms already connected agglomerates (Fig. 4.19i) at 0.1 s^{-1}, whereas, the corresponding one containing TRGO does not show any connected network (Fig. 4.19c). This is in line with the insulating behaviour of the suspension all over the range of applied shear rates. A clearly visible agglomerated network can be observed for the 0.05wt% MWCNT/epoxy suspension (Figs. 4.19k and 4.19l), while a less connected structure is present in the corresponding suspension containing TRGO and MWCNT (Figs. 4.19e and 4.19f). The shear induced agglomeration behaviour of the suspension containing only 0.02wt% TRGO/epoxy was investigated as well, and no network formation during shear was appreciated both by electrical measurements and morphological observations. (Findings are in Annexure

Figs. A.5 and A.6). The electrical conductivity measured for bi-filler suspension of 0.02_0.07wt% TRGO_MWCNT/epoxy suspension is mainly due to the presence of MWCNTs at high content, which is sufficient enough to form connected network of agglomerates. The filler agglomeration observed in TRGO_MWCNT/epoxy suspension is mostly due to the tendency of MWCNTs to form percolated network structure. Graphene oxide flakes confine the MWCNT in finite and restricted regions within the resin, hindering their agglomeration and consequent contact and thereby reducing the electrical conductivity. These first results on the study of the ‘‘shear induced agglomeration behaviour’’ of TRGO_MWCNT suspensions show that addition of TRGO lowers the conductivity of MWCNT/ epoxy suspension by hindering the formation of shear induced percolated network.

4.5 Thermal conductivity of GNP/epoxy nano-composite

The thermal conductivity of the GNP/epoxy samples as function of weight percentage of GNPs at three different temperatures were measured and are shown in Fig. 4.20. The samples were tested 5 times at each temperature and the standard deviation was <1% and hence not represented in the figure. As expected, thermal conductivity increases with increase in temperature, which is a common trend exhibited by epoxy resins below their T_g. As seen from Fig. 4.20, thermal conductivity increases by 6% for 1.0wt% and is doubled to 14% for 2.0wt% filler loading at 30 °C, although there is a drop in thermal conductivity for 0.3wt%. This increase of 14% at 2.0wt% is very much in accordance with the values that are reported in literature [184].

The decrease in thermal conductivity occurs at 0.3wt% (which is also the electrical percolation threshold) and a steep increase of thermal conductivity is observed between 0.3wt% and 0.5wt%. This initial drop and subsequent increase is mainly because of two effects which influence the heat flow in the system. Addition of filler in the matrix also creates an interfacial layer in which the phonon scattering reduces the heat flow and this effect dominates when the filler content is 0.3wt%. Beyond 0.3wt%, addition of fillers increases the volume of filler which has high thermal conductivity and hence the overall conductivity of the nano-composite increases. Unlike the electrical conductivity no percolation curve was observed for thermal conductivity. In the case of electrical conductivity, the clusters formed by the electrically conductive fillers alone contribute to the overall conductivity and there is no matrix contribution. But, thermal conductivity is a concept based on phonons and both filler and matrix contribute to the heat flow. Since the difference in thermal conductivity of the filler and matrix

is very high, the presence of large interfacial thermal resistance leads to lack of percolation curve in thermal conductivity.

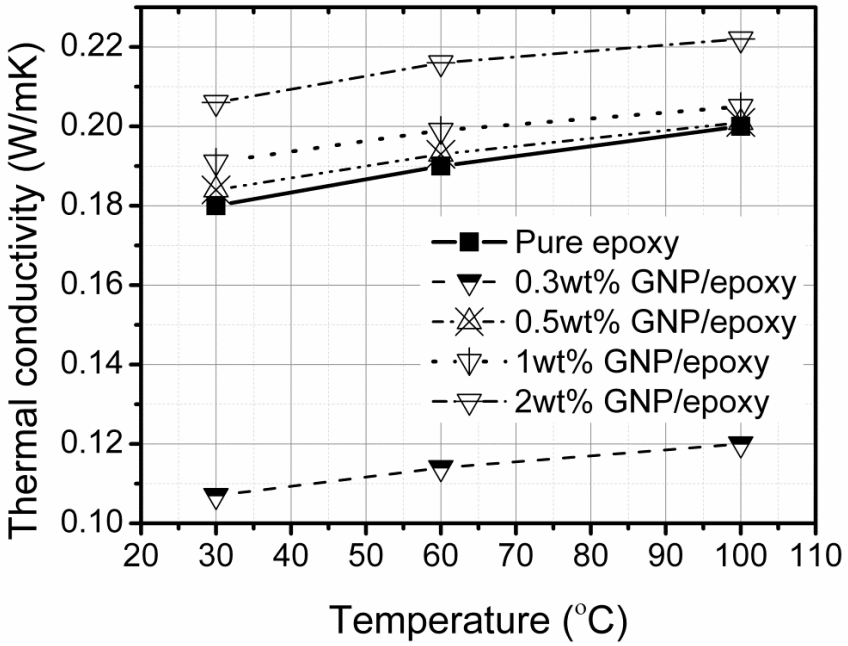

Figure 4.20: Thermal conductivity of GNP/epoxy nano-composite as a function of weight percentage of filler.

Since the effective heat propagation is due to acoustic phonons, a well-dispersed network of GNPs in the matrix at higher filler loadings not only reduces the mean free path of heat carriers but also contributes to increased thermal conductivity with filler content. However, several factors such as aspect ratio of the filler, intrinsic crystallinity of the graphitic layers, dispersion of GNPs, bonding between GNPs and epoxy and interfacial thermal resistance between the filler and matrix affects the thermal conductivity of the nano-composite [185]. To obtain a further enhancement in the thermal conductivity, either the dispersion method needs to be modified or the filler content must be increased. Increasing the filler has its toll on the viscosity of the resin and makes the processing difficult. On the other hand, changing the dispersion method with the use of solvent alters the resin but other properties like electrical conductivity decreases. Without compromising the resin properties and other physical properties of the nano-composite, the other solution is to combine CNTs and GNPs. The current focus of research is on the hybrid systems where both CNTs and GNPs are combined to form a 3D-network, (CNTs bridge the GNPs) and an efficient phonon scatter occurs and a synergetic effect is observed for through plane conductivity [186-188].

4.6 Dynamic thermo-mechanical analysis: Storage modulus and T_g

Dynamic mechanical thermal analysis (DMTA) has been shown as a tool to investigate the viscoelastic response of polymers and composites [189,190]. Useful information on chain mobility of epoxy and deterioration of its thermo-mechanical properties is obtained from the loss tangent (tan δ) curve. DMTA is also employed to detect the interphase effect on the thermal properties of the nano-composites, as it is a convincing approach to provide comprehensive knowledge on the interaction between the filler and matrix [191,192].

4.6.1 Storage modulus and T_g as a function of temperature for MWCNT/epoxy, TRGO/epoxy and GNP/epoxy

Temperature dependencies of storage modulus and loss factor of samples of the neat epoxy and its nano-composites filled with different contents of carbon nano-fillers are shown in Figs. 4.21 and 4.22. Thermo-mechanical characteristics such as storage modulus in glassy and rubbery state, height of tan δ peak and T_g are measured (see Annexure for tabulated values Table A.1). Standard deviations of the measured characteristics are in the range of 1-2% for the glassy storage modulus, 2-5% for the rubbery storage modulus, and 1-2% for the tan δ peak. Differences in T_g of duplicate samples did not exceed 2 K. Rather good reproducibility of the data is obviously related to a fairly good quality of dispersion of the fillers in the epoxy matrix achieved by using three-roll milling process [8].

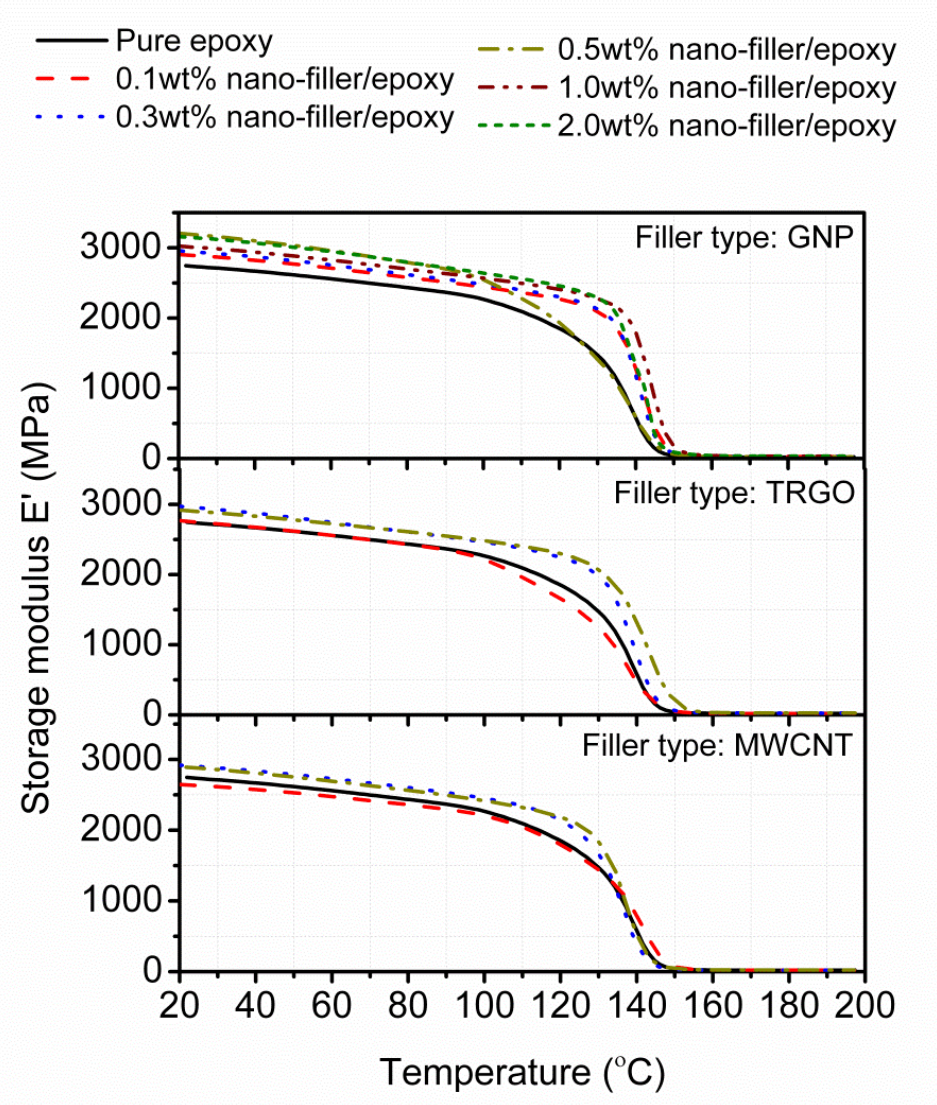

Figure 4.21: Storage modulus curve as a function of temperature for different nano-composite systems.

Addition of nano-fillers clearly altered the thermo-mechanical response of the epoxy resin by shifting the viscoelastic region to higher temperature. As expected, the variations of T_g of different samples are rather small and did not exceed 4 °C, which is related to the thermoset nature of the epoxy and its high degree of cross-linking density. The storage modulus (E') can be again subdivided into two classes viz., glassy modulus (E'_g) which is nothing but E' at room temperature and rubbery modulus (E'_r) which is taken at a temperature of 180 °C (approx. 30 °C after the T_g).

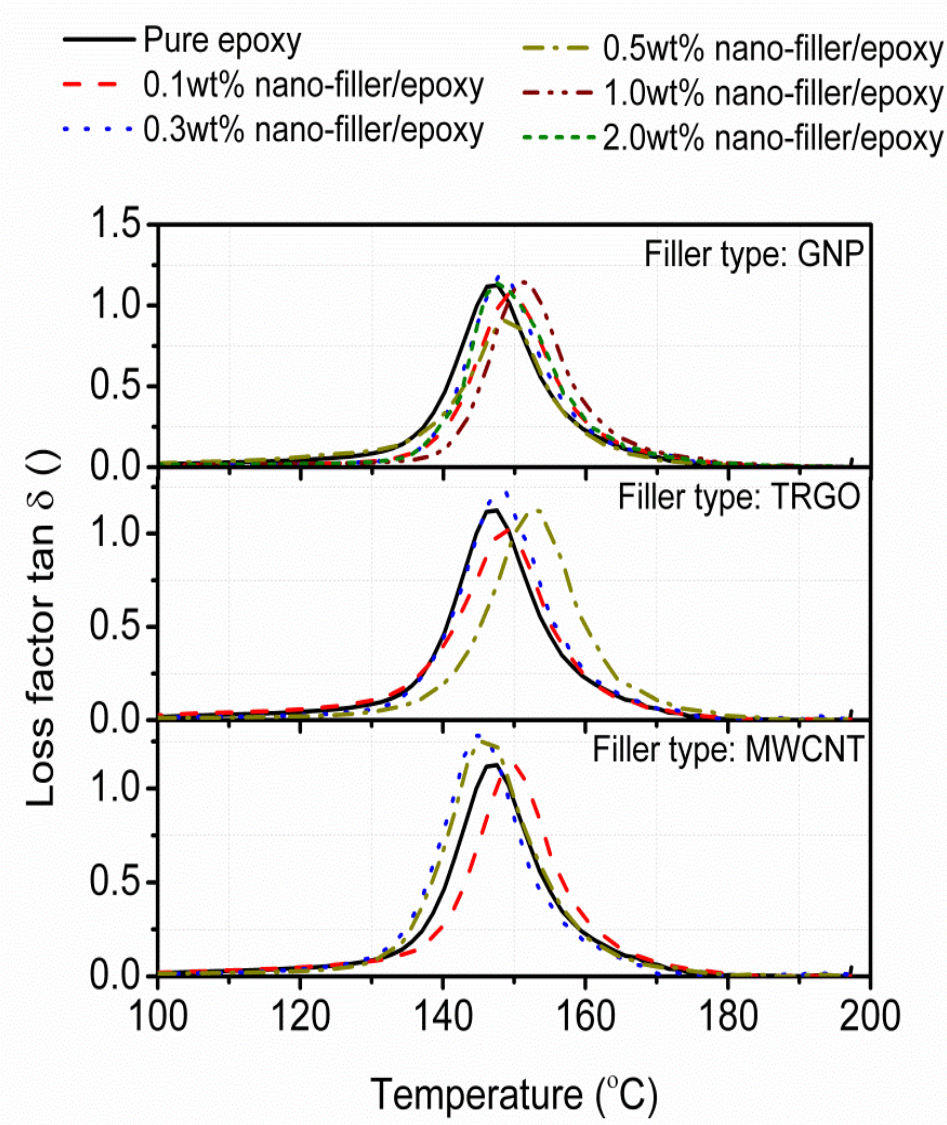

Figure 4.22: Loss factor as a function of temperature for three different nano-composite systems.

Both the moduli of pure epoxy have increased with the addition of 0.3wt% of carbon nano-fillers as in Fig. 4.21. There is a horizontal shift to high temperature range near the glass transition region and this shift in E'_r is 46% for GNP/epoxy, 29% for TRGO/epoxy and 3% for MWCNT. This is an indication of a strong interaction between the 2D filler and the epoxy matrix which arises from the geometric effects and high surface area of the filler. In the case of 0.5wt% GNP/epoxy and 0.1wt% TRGO/epoxy, an anomalous behaviour is observed where E'_g increases by 16% and 0.3% respectively. But, the viscoelastic region is shortened. Several samples where tested and all gave the same result. There was also no trace of any incomplete curing in the composite from differential scanning calorimetric measurements. Obviously, in nano-composites containing 0.1wt% of carbon nano-fillers, the particles are distributed

relatively far from each other and surrounded by an unconnected interphase with bulk matrix, which gives lower contribution into the overall thermo-mechanical response. Incorporating higher amounts of nanoparticles did not yield any noticeable additional improvement in the dynamic properties and the nano-composites filled with 0.3wt% and 0.5wt% of TRGO and MWCNTs showed similar thermo-mechanical behaviour. This can be related to a fact that for both nano-composite systems, a rheological percolation of the interphase polymer is achieved at 0.3wt% loading content. Such an interphase zone is formed around each particle and is characterized by altered mobility of the polymer chains.

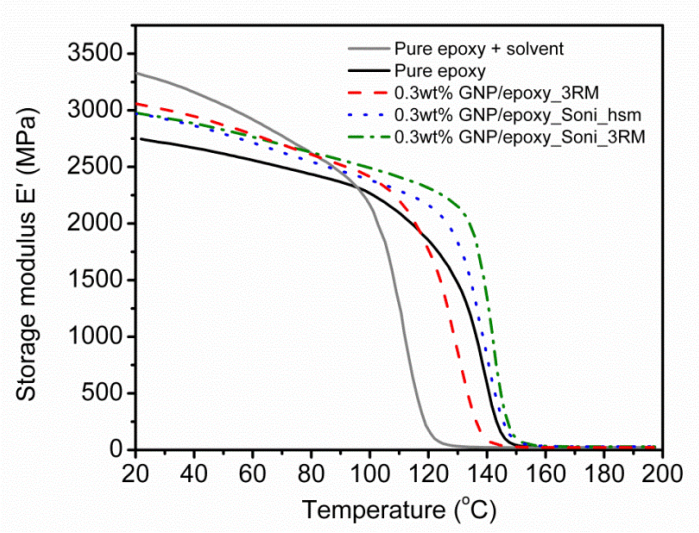

Figure 4.23: Storage modulus of 0.3wt% GNP/epoxy systems using three different dispersion methods.

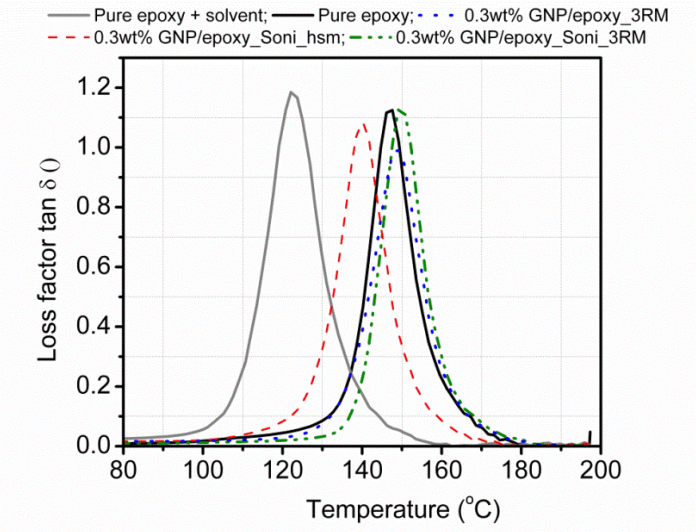

Figure 4.24: Loss factor curve for 0.3wt% GNP/epoxy systems via different processing methods.

The effect of dispersion method on the dynamic thermal response of 0.3wt% GNP/epoxy is shown in Figs. 4.23 and 4.24. The references used in this study are both pure epoxy and pure epoxy with solvent, as the sonication along with high speed shear mixing method involves the use of solvent. The first observation is that there is drastic change in pure epoxy with solvent and pure epoxy, where the T_g reduces by 20 °C and the modulus increases by 21%. The solvent was removed through heating as explained in Chapter 3 Section 3.2 and some remnant solvent (<8% - TGA measurements) is present in pure epoxy. This remnant solvent has affected the degree of cross-linking density which is reflected in the lower T_g. The solvent present in the epoxy resin acts as an anti-plasticiser, where it decreases the T_g but increases the storage modulus [193]. For nano-composites, the amount of remnant solvent present is <2%. The 3RM process outperforms the other two methods with higher E'_r and T_g.

In general, graphene/epoxy composites show a higher rubbery modulus, and lower loss factor than neat resin. The higher rubbery modulus is correlated with stronger interactions between nano-filler and epoxy matrix while the lower tan δ peak and higher T_g indicate a higher crosslinking density and a lower mobility of polymer chains. Interestingly, the lowest loss factor peak intensity and the highest glassy and rubbery modulus are measured in composite manufactured by Soni_hsm method, meaning that there is a stronger bonding and more efficient load transfer at the GNP–epoxy interface than in composites manufactured by 3RM. This could indicate that the interface with the polymer network is more efficient and stronger with thick initial GNPs than with thinner GNPs.

4.7 Fracture toughness and R-curve

Many of the properties of thermosetting polymers, including brittleness arise from their highly cross-linked structure. The toughness substantially relies on plastic flow processes capable of dissipating energy within the crack tip region. Toughness of plastics is measured in terms of critical stress intensity factor (K_{IC}) and the critical strain energy release rate (G_{IC}) at crack initiation is measured by standard test methods. There are two main testing geometries viz., single edge notch bending and compact tension. Both these test methods involve loading of notched specimen that is pre-cracked either in tension or three point bending. The validity of this test depends on the crack length, shape and size and also on the geometry of the specimen. The physical significance of this value K_{IC} is to characterise the resistance of material to fracture in a neutral environment.

For the R-curve measurements, four point bending tests (4PB) were performed on rectangular beams unlike the three-point bending (3PB) tests which were done to calculate the K_{IC}. The difference in three and four point bending is that in 3PB there is a peak stress at mid-point and reduced stress elsewhere. On the other hand, the peak stress in a 4PB test is over an extended region and hence any defect or flaw in the specimen can be highlighted through these tests. Also, the material under test does not fail due to maximum stress concentration unlike 3PB tests.

According to A.J. Kinloch et al., the crack propagation in epoxies is expected to be unstable. In fact there are three theoretical possibilities for crack propagation in epoxies [194]: (i) a stable brittle propagation characterized by a continuous crack growth and a smooth fracture surface; (ii) an unstable brittle mode, also called stick/slip mode and (iii) a stable brittle propagation featured by a continuous crack extension with ductile tearing processes. The R-curve is based on the fact that K_{IC} increases with growing size of the crack in elastic-plastic materials. This curve is mainly used to examine the process of slow stable crack growth and unstable fracture. But this is largely dependent on the specimen geometry [195].

4.7.1 Fracture toughness measurements (SEN-3PB)

The fracture toughness of the nano-composites measured by three point bending test is plotted as a function of weight percentage of the filler for each filler type and is shown in Fig. 4.25. It is evident from the plot that as the filler content increases the K_{IC} also increases for low filler content (0-0.5wt%). For higher weight fraction of GNP (more than 0.5wt %), a decreasing trend was observed. It is reported in literature that the fracture toughness of the nano-composite start to decrease beyond certain weight fraction as the nano-fillers agglomerate. The current result also supports this fact. It is reported in literature that mechanical properties of the nano-composite start to decrease beyond certain weight fraction as the nano-fillers agglomerate.

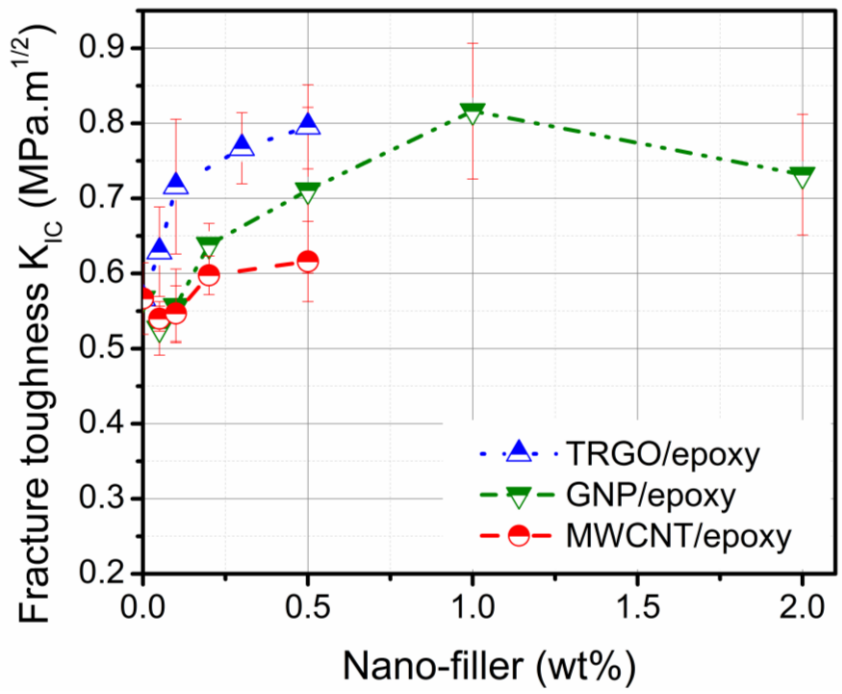

Figure 4.25: Fracture toughness by (SEN-3PB test) as a function of weight percentage of filler for MWCNT, TRGO and GNP reinforced epoxy nano-composite.

As observed in the plot, the toughening effect of TRGO was most significant among TRGO, GNP and MWCNT for the same filler content. The maximum increase in fracture toughness for MWCNT/epoxy composite is only 8% at 0.5wt% of filler content. In the case of 2D filler reinforced composite, for GNP/epoxy this increase was 24% which is three times higher when compared to MWCNT reinforced epoxy and for TRGO /epoxy the increase was 40%. It is observed that for GNP/epoxy above 1.0wt%, the fracture toughness value starts to decrease. The fracture toughness values along with standard deviation for all sample tests are tabulated (see Annexure Table A.2). Since the TRGO/epoxy and GNP/epoxy shows greater improvement than MWCNT/epoxy, detailed fracture analysis is carried out on TRGO/epoxy and MWCNT/epoxy only.

4.7.2 R-curve behaviour (SEN-4PB)

The four point bending experiments revealed that it is possible, though very difficult, to achieve stable crack growth in epoxy (SEN-4PB) specimens using the measurement setup and procedure as described in section 3.2. While it was not possible to stop the crack propagation during its first extension, it was at least possible to stop crack extensions prior to a final fracture in more than one half of the specimens. This stabilization of cracks in epoxies, after a first unstable extension jump, meets exactly the observations reported for pre-cracked compact

tension specimens by Xiao et al. [196] and suggests a stick/slip propagation process. The K_{IC} of the specimen is plotted as a function of crack extension as in Fig. 4.26, where there is a jump in crack extension, and an uncontrolled crack is developed as the specimen is loaded. As mentioned above, it is possible to stabilise the crack after this first extension.

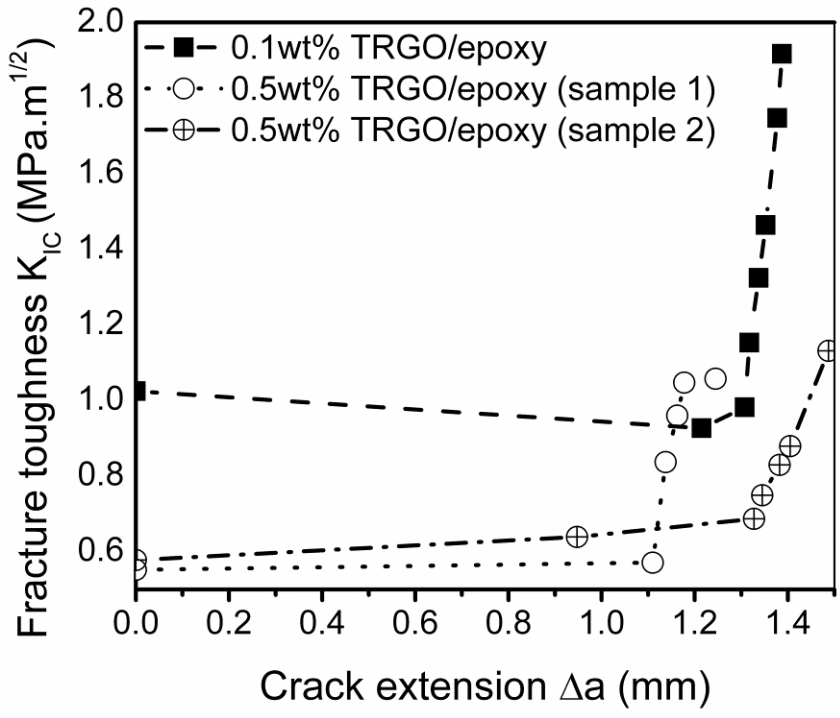

Figure 4.26: R-curve for 0.1wt% and 0.5wt% of TRGO/epoxy exhibiting an increasing trend.

The results show that the fracture toughness of TRGO/epoxy nano-composite displays rising R-curve behaviour. Both the samples with 0.1wt% and 0.5wt% show this effect and this differs from the R-curve observed for pure epoxy and MWCNT/epoxy nano-composite. First value in the curve represents the K_{IC} that corresponds to the formation of first uncontrolled crack formation. This value of K_{IC} is different from the values obtained from the SEN-3PB tests but lies with the standard deviation. This is associated with the radius of the notch root inserted using the razor blade. The higher values from SEN-4PB are due to a slightly blunt crack tip. However, the K_{IC} of the nano-composites is reported based on the SEN-3PB tests. The SEN-4PB tests were done only to drive a stable crack in the material and to understand the toughening mechanism of TRGO filler.

After the first crack extension, the toughness value rises with a steep initial slope, but this rise is in the interval of microns as the sample is relatively weak due to the presence of a longer notch. The curve starts to stabilise almost at the edge of the sample. However, and due to

geometric constraints the test could not be continued and hence only one point was measured in the plateau region. The values in the R-curve for the same weight percentage of TRGO (0.5wt %) varies slightly with crack extension and the values increase from 0.5-0.7 MPa·m$^{1/2}$ up to 1.02 MPa·m$^{1/2}$. However the rising trend is observed irrespective of the weight percentage of the filler.

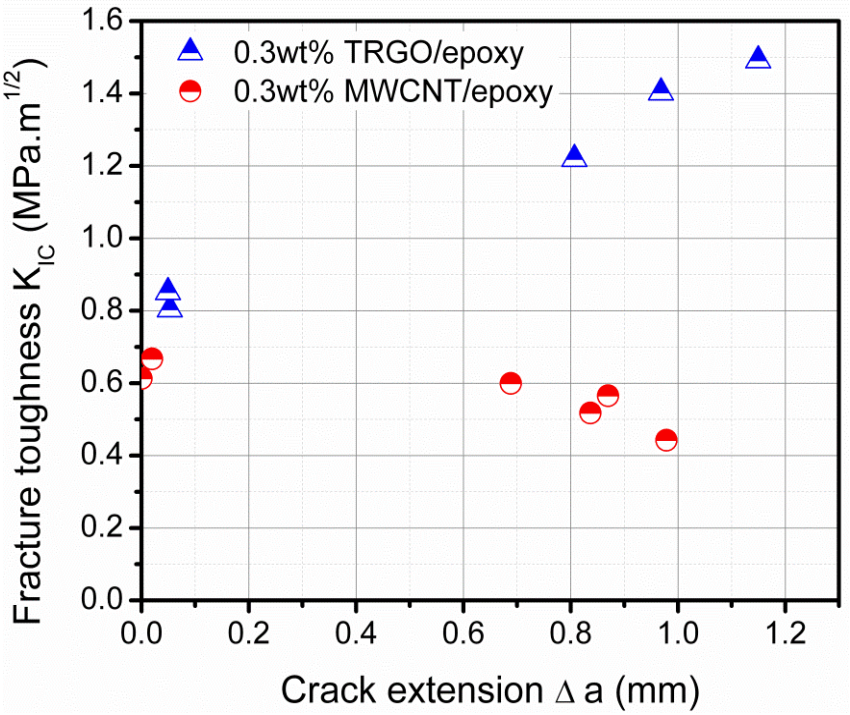

Figure 4.27: Comparing the crack resistance curve for 0.3wt% of TRGO/epoxy and MWCNT/epoxy nano-composite [197].

The MWCNT/epoxy composite seems to exhibit a fairly constant R-curve as depicted in Fig. 4.27. The slightly decreasing tendency of the fracture toughness for increasing crack lengths is not fully understood yet. It is assumed that this behaviour is not material specific but more likely caused by interference of the geometry function and the measurement setup and hence further efforts should be made in future to clear this question. For this work, it is also assumed that the fracture toughness is constant over the crack extension and that its value is approximately in the range of 0.6 to 0.65 MPa·m$^{1/2}$ which is slightly above the fracture toughness of pure epoxy as stated by the manufacturer (0.56 to 0.6 MPa·m$^{1/2}$ [84]) and verified with the epoxy used in the present study (approximately 0.57 MPa·m$^{1/2}$).

5 Discussions

This study aims to assess the potential of using graphene as filler in epoxy composites. At the first instance, the as-received filler was analysed and was found that the intrinsic properties of the filler strongly depend on the preparation methods adopted for the production of graphene.

Earlier studies have noted the importance of the electrical conductivity of graphene in polymer composites. In this study, TRGO/epoxy nano-composite was prepared and compared to the MWCNT/epoxy in terms of electrical conductivity. The TRGO/epoxy showed better mechanical performance and the MWCNT/epoxy outperformed in electrical conductivity.

This led to the study of using bi-filler wherein the TRGO is added to the MWCNT/epoxy nano-composite, and was found that the electrical conductivity of bi-filler composite eventually decreased in contrast to [177,178], where MWCNT and CB were used as fillers.

Based on the results of this study, it was concluded that either the dispersion method or the filler (TRGO) itself affects the property. Hence studies on another type of graphene (GNP) dispersed in epoxy were conducted and compared to TRGO/epoxy. The final work also focussed on different dispersion methods for GNP/epoxy and its influence on the final properties.

5.1 Filler characterisation

The as-received fillers are subjected to a series of spectro-chemical, thermal and electrical tests from which the degree of crystallinity, number of graphitic layers present in MWCNT, TRGO and GNP could be predicted.

In this study Raman spectroscopy technique is used to give an insight on the defects in the structure of the nano-fillers. It is based on inelastic scattering of light which is associated with emission and absorption of phonons. Since the basis of all the three fillers is mono-layer graphene, a discussion based on graphene would cover the above three materials. For sp^2 carbon materials only a few phonons exhibit Raman active modes. The G band and G' band in Raman spectra denotes the first order and second order symmetry in the electronic band structure and is usually related to the graphitic structure. The D band which is not present in monolayer graphene is ideally a defect activated Raman peak. This intensity ratio of D and G peak (I_D/I_G ratio) in Raman spectrum yields information about the crystal structure of the material.

The $I_{G'}/I_G$ ratio in graphene related structure can be used to determine the number of layers in a few layer graphene sample. Because of its dependence on the number of layers, the Raman G' band has been used to characterize the number of layers in few layer graphene samples and the stacking order between these layers. For example, the Raman spectra of highly oriented pyrolytic graphite (HOPG), that has random interlayer stacking, has a very broad G' peak with a shoulder . On the other hand, a bi-layer graphene can be resolved into four peaks which is due to electronic band structural change as a result of layer stacking [198-200].

The Raman spectra of the as-received fillers as presented in Fig. 4.3 Section 4, Chapter 4 shows that the MWCNTs have some defects in the structure. But among the graphene based fillers, TRGO has more defect intensity than GNP. The Raman spectrum of GNP powder almost matches with that of natural graphite. The increase in defect density for TRGO can also arise because of its partial functionalization which occurred during the preparation of TRGO. Systematic Raman and X-ray diffraction (XRD) studies were performed in the 1970's, by Tuinstra and Koenig on several graphitic samples [201]. Results showed the existence of an inverse relationship between the crystallite sizes measured from XRD with I_D/I_G ratio obtained from Raman spectrum [202,203]. Later, Knight and White summarised the results and arrived at an empirical formula that relates the crystalline width to the I_D/I_G ratio [204] as shown in equation (Eq. 5.1):

Knight and White's empirical relation:

$$L_a = \frac{4.4}{I_D/I_G} \text{ in nm} \qquad \text{Eq. (5.1)}$$

where, L_a - crystalline width and I_D/I_G - intensity ratio of D band to G band from Raman spectrum.

On the other hand, XRD is one powerful tool where the inter layer spacing is calculated using the Bragg equation (refer Eqs. 4.1 & 4.2) and the crystallite size or crystalline thickness from the Scherrer equation as presented in Section 4.1, Chapter 4. From the X-ray diffractogram of MWCNT, TRGO and GNP, the crystalline thickness was calculated using the Scherrer equation. The diffractrogram was also used to calculate the crystallinity index (or degree of graphitisation) of the nano-fillers. During the graphitizing process, a less pre-ordered carbon is converted into a three-dimensionally ordered graphite structure. The defects in the carbon nano-fillers are the interruption the sp^2-structure of the graphite lattice, which are responsible

for interruption of the delocalised π-electrons that contribute to filler conductivity. It is therefore important to know the graphitisation degree to obtain information on the electrical conductivity of these nano-fillers.

Degree of graphitisation formula:

$$g = \frac{C_{area}}{F_{area}} \times 100 \text{ in percentage} \quad \text{Eq. (5.2)}$$

where, C_{area} is the area under crystalline peak after background removal and F_{area} is the area of the as obtained diffractogram (i.e., before background removal). The crystallinity index was found to be 34% (MWCNTs), 54% (TRGO) and 92% (GNPs) which explains the higher decomposition temperature observed for GNPs. From the different spectro-chemical experiments the observations made are tabulated below (Table 5.1).

Table 5.1: Consolidated parameters obtained from filler characterisation.

Parameters	**Elements**	**Crystalline width La (nm) and ID/IG ratio**	**Crystalline thickness Lc (nm)**	**Crystallinity index (%) and number of layers**	**Decomposition temperature (°C)**	**Volume conductivity (S/m)**
Experiments	Energy dispersive spectrum	Raman spectrum	XRD spectrum	XRD spectrum	TGA analysis	Four probe electrical conductivity
MWCNT	C, O, Al, Mg, Mn, Co	2.88 and 1.53	4.68	34 and 13	460	927
TRGO	C, O, S, Na, Si, Cl, Cu, Ca, K, Fe, F, Al	1.49 and 1.02	12.94	59 and 38	403	1067
GNP	C, O, K, Na, Si, Al, S, Cr, Ca, Fe	10.73 and 0.16	58.13	92 and 170	547	28079

Comparing within the data presented in Table 5.1 for TRGO and GNP fillers, it can be concluded that GNPs have higher degree of crystallisation, low I_D/I_G ratio which results in high thermal stability and electrical conductivity of this filler. Hence, it is reasonable to conclude that the GNP/epoxy nano-composite exhibited higher electrical conductivity compared to

TRGO/epoxy nano-composite. Though elemental analysis was not used to quantify the elements present in the fillers, qualitative information was obtained from the spectrum which revealed higher oxygen content in TRGO filler than in GNP filler (spectrum shown in Annexure Fig. A.7). This in turn is reflected in the Raman spectrum where higher I_D/I_G ratio was observed. This is due to partial functionalization and structural defects formed during the synthesis of TRGO filler.

After preliminary analysis of the fillers, they were dispersed in epoxy to yield nano-composite which was later subjected to mechanical and electrical tests. The electrical conductivity results (refer Chapter 4 Section 4.3.1 Fig. 4.13) indicate that MWCNT/epoxy composite shows better conductivity and lower percolation threshold followed by TRGO/epoxy.

Earlier studies have shown that partial replacement of MWCNT by carbon black (CB) - spherical nano-particles enabled production of highly conducting epoxy/MWCNT/CB. It was presumed that the CB shortcuts some parts of MWCNT network and thereby increases the electrical conductivity with lower loadings of MWCNT [177]. Hence, it is of interest to combine the two fillers (TRGO and MWCNT) to look for synergetic effects in terms of electrical properties.

5.2 Bi-filler nano-composite TRGO_MWCNT/epoxy

It is evident from the study through combined electro-rheological measurements and through electrical conductivity of cured composite that the addition of TRGO reduces the electrical conductivity of MWCNT/epoxy composite (Section 4.3.1 and 4.4.2). These findings further support the idea that the reduction in electrical conductivity of bi-filler composite occurs irrespective of shear induced or temperature induced agglomeration in the composite. To better understand this finding, scanning electron micrographs were taken on the slices that were obtained from cured composite containing 0.035wt% MWCNT/epoxy and 0.01_0.035wt% TRGO_MWCNT/epoxy. These slices are 500 nm thick and were placed on Si wafer and the micrographs were taken in “in-lens” mode to see the agglomerates of fillers which are shown in Fig. 5.1.

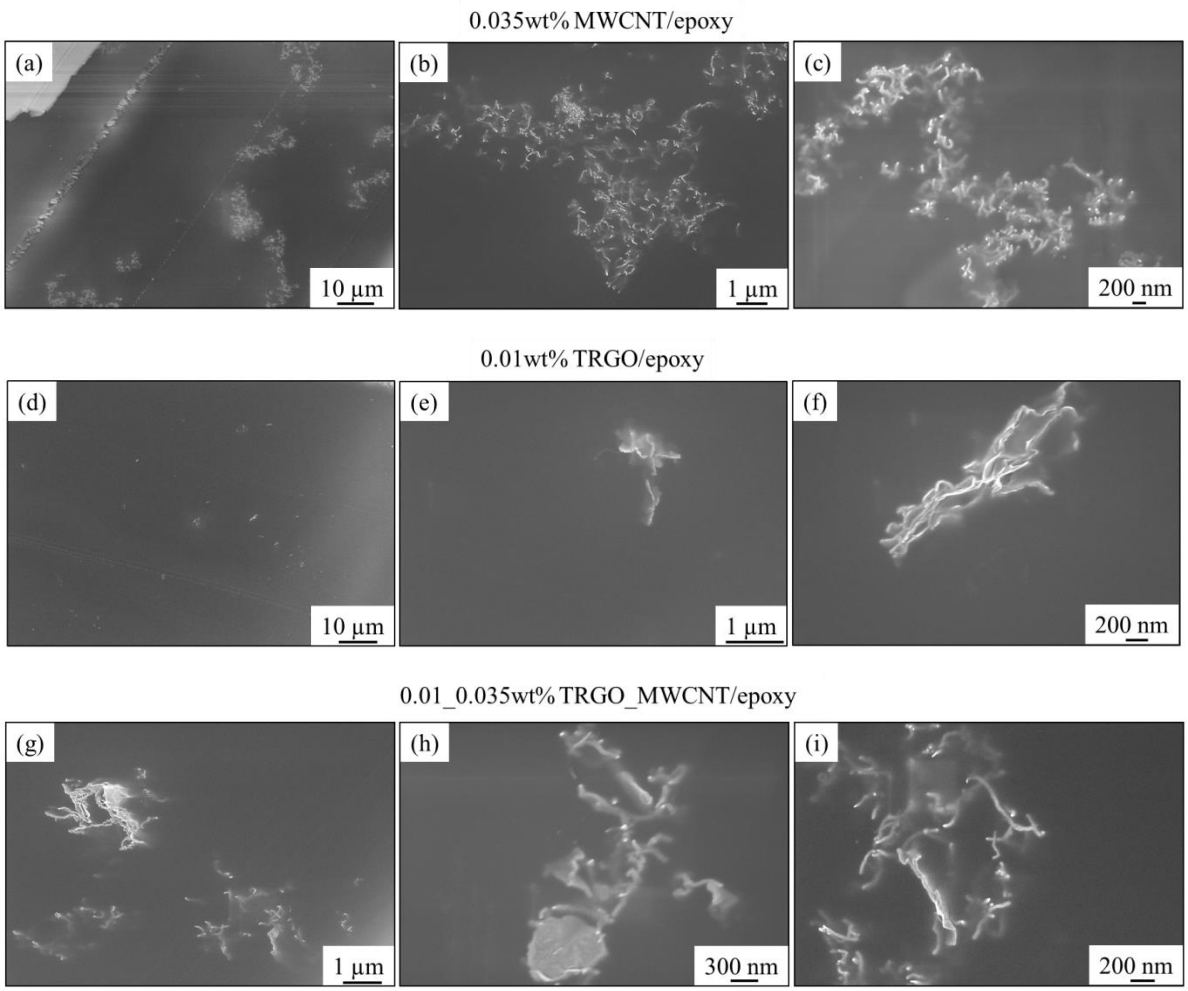

Figure 5.1: Scanning electron micrographs of 500 nm thin slices of composite deposited on Si substrate. (a-c) SEM of mono-filler 0.035wt% MWCNT/epoxy; (d-f) SEM of mono-filler 0.01wt% TRGO/epoxy; (g-i) SEM of bi-filler 0.01_0.035wt% TRGO_MWCNT/epoxy.

The distribution of MWCNT agglomerate and dense MWCNT agglomerates can be seen in Fig. 5.1a and the formation of percolated conducting network by connecting two MWCNT agglomerates are additionally confirmed in Figs. 5.1b and 5.1c. When TRGO is added to the MWCNT/epoxy system, the distribution of MWCNT agglomerates is affected to a great extent. First, the agglomerates are sparsely distributed and appear to be less dense when compared to mono-filler MWCNT/epoxy composite. The question is where do the rest of the CNTs disappear? Figs. 5.1g-i shows an agglomerate of TRGO with MWCNT (0.01_0.035wt% TRGO_MWCNT/epoxy). Closer examinations of these figures show some MWCNT in the vicinity of the TRGO sheets and the agglomerate of TRGO is more three dimensional. More micrographs as in Figs. 5.1h and 5.1i show the hindrance of CNT network by a TRGO sheet both parallel and in perpendicular to the CNT network. This morphology of the TRGO_MWCNT bi-filler composite explains the lower conductivity when compared to mono-

filler MWCNT/epoxy composite. The TRGO sheets attract the carbon nanotubes and thereby hinder the formation of percolated conductive networks. The MWCNT within or on the TRGO can either get entangled within these walls or can get disentangled. The remaining MWCNTs that are not affected by the presence of TRGO sheets form percolated networks giving rise to increased electrical conductivity. However, MWCNTs that are trapped by TRGO sheets do not contribute to the conductive path; hence a higher amount of tubes is needed to reach appreciable levels of conduction. Scanning electron micrographs of 0.01wt% TRGO/epoxy (Figs. 5.1d-f), show the agglomeration of TRGO sheets in epoxy. From the images, it is observed that the depth of agglomerates of TRGO sheets is lesser when compared to TRGO_MWCNT agglomerate in epoxy. This may be due to the presence of MWCNT agglomerates in-between the TRGO sheets.

5.2.1 Proposed theory for reduced conductivity of bi-filler nano-composite

Based on this hypothesis a morphological model is proposed to explain the experimental results as shown in the schematic in Fig. 5.2.

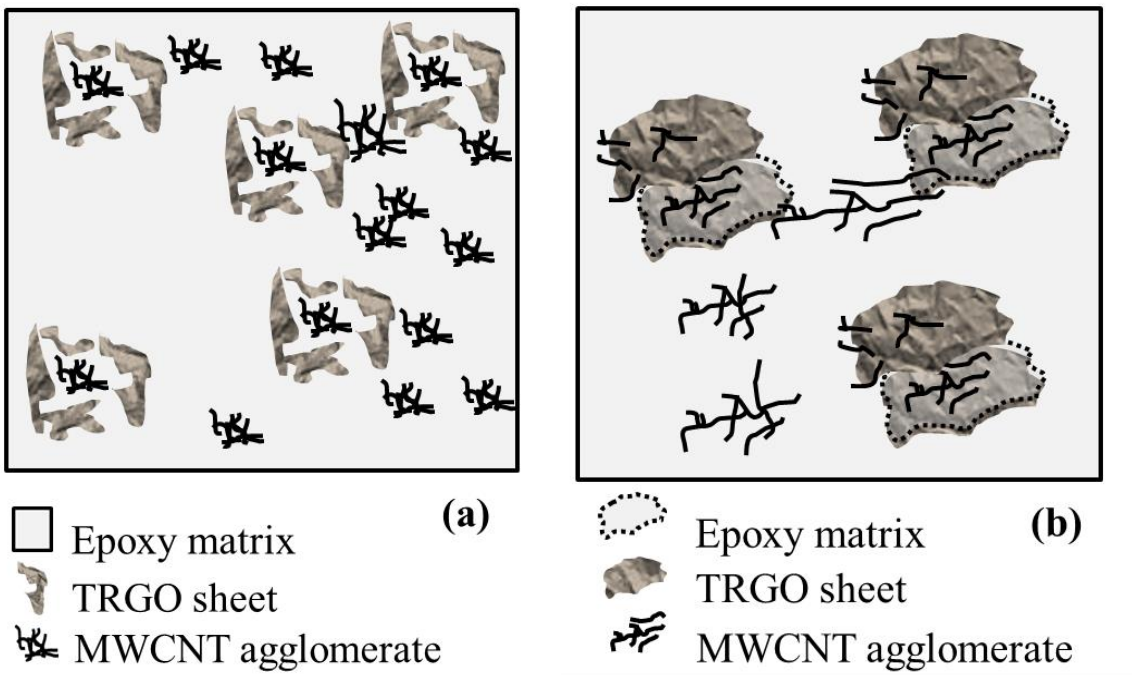

Figure 5.2: Morphological model for TRGO_MWCNT/epoxy cured composite; (a) cross-sectional view and (b) top-view respectively.

The schematic shows both the cross-sectional view (Fig. 5.2a) of this TRGO_MWCNT agglomeration and its top view (Fig. 5.2b). The SEM of pristine TRGO sheets (refer Chapter 4 Section 4.1, Figs. 4.1c and 4.1d) show a much wrinkled surface. This is due to thermal

reduction and exfoliation of sheets by the release of gases. The cross-sectional view of the TRGO sheets has an accordion like structure and the gap between the sheets is found to be more than 1 μm. This gap is sufficient enough for MWCNT to accommodate themselves in. This morphology was very clearly seen at higher concentration of bi-filler composites (0.3_0.3wt% TRGO_MWCNT/epoxy) when the cryo-fractured surface was investigated for filler distribution as shown in Fig. 5.3. The cryo-fractured surface of high concentration bi-filler composite exhibits morphology where the MWCNT agglomerates are trapped by TRGO sheets/agglomerates (Fig. 5.3a). Also, the MWCNTs are in the vicinity of the TRGO sheets. This again is an indication of strong filler–filler interplay through π–π interaction between MWCNTs and TRGO sheets. Another interesting morphological feature observed on the cryo-fractured surface is the pinning/trapping of MWCNTs on/between the TRGO sheets (Fig. 5.3b). Thus, the wavy topography of the sheets also aids to pin the MWCNTs to their surface [205]. Also the TRGO sheets have around 12.0wt% of oxide functionalities as determined from the elemental analysis.

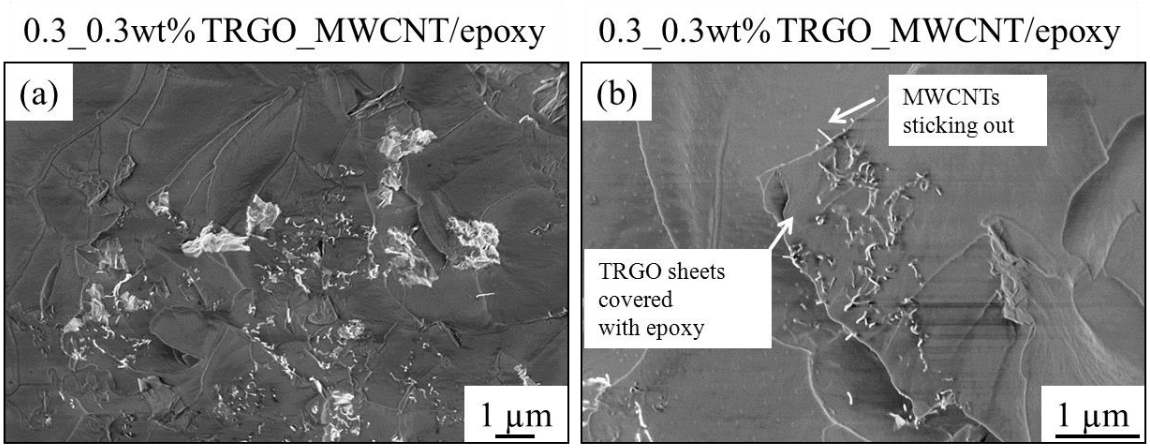

Figure 5.3: Scanning electron micrographs in-lens mode of cryo-fractured surface of bi-filler 0.3_0.3wt% TRGO_MWCNT/epoxy cured composite; (a) MWCNT agglomerates are surrounded by TRGO agglomerates and (b) MWCNTs pinned onto the TRGO sheets respectively.

Recent literatures are available about GO acting as a dispersing agent for MWCNT [206]. Hence, it can be speculated that the oxygen functionalities play a vital role in attracting the MWCNTs to their surface. The oxygen functionalities are decorating the edges of the graphene sheets and also form oxide rich regions like nano-islands on the basal plane. These oxide rich nano-islands are hydrophilic in nature and the regions in the graphene basal plane that are free of oxide groups are hydrophobic in nature.

The MWCNTs are attracted through π–π interaction by those areas in the GO sheets where there are no oxygen groups in the basal plane [207]. Hence the path of electron mobility on the TRGO sheet is already restricted because of oxygen functionalities on the basal plane. In addition, the MWCNTs are attracted by the π conjugated nano-islands. All these effects make the whole aggregate an insulator; it acts as a barrier for electron transport [206]. Adding to this, the specific surface area of the sheets is 413 m^2/g. This is greater than or equal to the specific surface area of MWCNTs and hence the influence of van der Waals force exerted by the sheets on MWCNTs is much higher. The attraction of carbon particles by the TRGO sheets was observed not only with MWCNTs but also for carbon black particles (see Annexure Fig. A.8). The presence of functional groups makes the TRGO partially polar which makes it well dispersed in the matrix and their tendency to agglomerate is low. While mixing with MWCNTs, the sheets act as a barrier reducing the mobility of CNT in the matrix. The π–π interaction between the TRGO_MWCNT is not the only contributing factor for the observed behaviour. The viscosity of the resin along with dispersive shear forces could also contribute to this TRGO_MWCNT interaction.

The lower electrical conductivity exhibited by TRGO, TRGO/epoxy composite and TRGO_MWCNT/epoxy composite is mainly due to the presence of structural defects and functional groups on the surface and edges of the sheet. To overcome this, either graphene filler with lesser defects and functionalities must be used or the dispersion method needs to be modified. Therefore, another type of graphene filler prepared by different preparation method containing less oxide functionalities - GNPs was used.

5.3 Mechanical, thermal and electrical characterisation of GNP/epoxy composite

GNP/epoxy nano-composite was prepared using different dispersion methods such as 3RM, Soni_hsm and Soni_3RM technique and a fairly uniform dispersion of the filler was achieved using the above methods. The degree of dispersion and the spatial distribution of GNPs in epoxy matrix prepared by different methods can be understood from the cryo-fractured surfaces of the cured composite and are shown in Fig. 5.4. The higher surface roughness of GNP/epoxy (3RM) samples shows better dispersion of GNPs than those from Soni_hsm.

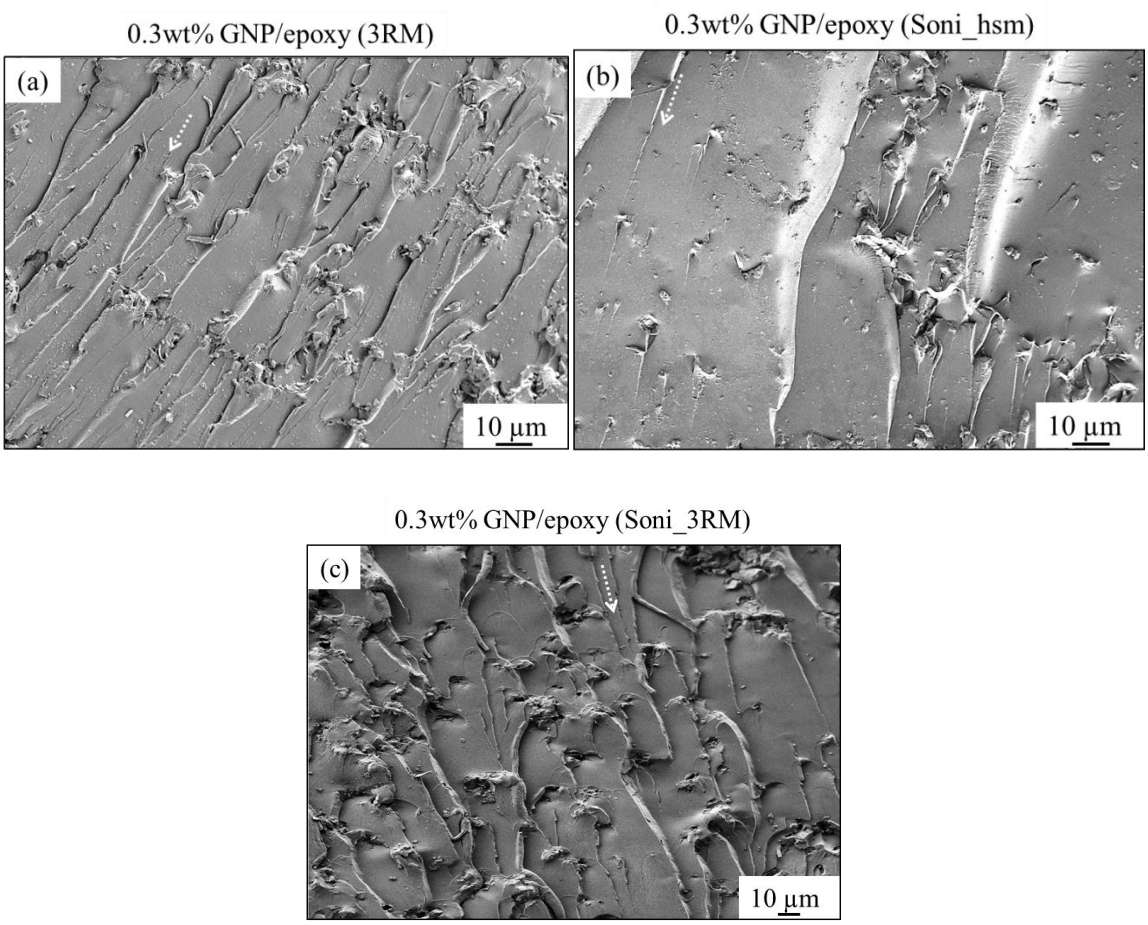

Figure 5.4: Cryo-fractured SEM images of 0.3wt% GNP/epoxy prepared by (a) 3RM technique; (b) Soni_hsm technique and (c) Soni_3RM technique respectively. Dotted lines indicate the crack propagation direction.

It is observed that the GNP/epoxy nano-composite prepared using 3RM technique showed almost 3 orders of magnitude higher electrical conductivity than those prepared via Soni_hsm process (refer Chapter 4 Section 4.3.2 Fig. 4.14). Hence, in view of the effectiveness of the 3RM technique over the other two dispersion methods, as explained above, further characterization of the GNP/epoxy nano-composite in terms of mechanical and thermal properties was carried out on the samples prepared through 3RM technique only.

In the case of electrical conductivity, a minimum amount of GNPs for a percolation threshold is required rather than a homogenous dispersion, so that a valid conduction pattern is created along the matrix. Though the electrical conductivity of GNP/epoxy (3RM) composite reaches 5.8×10^{-3} S/m at 2.0wt%, the percolation threshold is 0.3wt% which is much higher when compared to carbon nanotube epoxy composite. This is possible in epoxy at very low loadings because of extremely high dispersive surface energy of nanoparticles which produce a spontaneous re-agglomeration.

Thermal conductivity of the nano-composite did not increase more than 14% for 2.0wt% of filler. Effective mechanical reinforcement was achieved for 0.5wt% with 17% increase in glassy storage modulus and beyond this filler content not much increase in modulus was observed. A considerable increase in fracture toughness of 43% was obtained for 1.0wt% filler loading. Fig. 5.5 shows a consolidated graph, where the properties (fracture toughness, thermal conductivity and electrical conductivity) of the GNP/epoxy nano-composite prepared via 3RM technique is plotted against the filler loading.

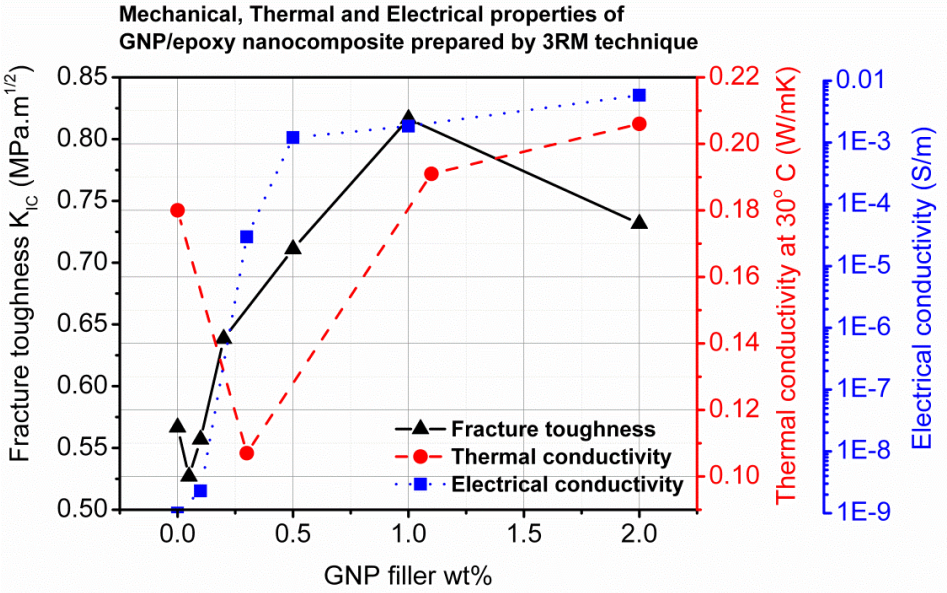

Figure 5.5: Mechanical, thermal and electrical properties of GNP/epoxy composite prepared via 3RM technique as a function of filler content.

The plot reveals that the percolation curve achieved for electrical conductivity is absent for thermal conductivity and the percentage of increase in thermal conductivity is very marginal. It could be observed that, there is a drop in the thermal conductivity at 0.3wt% which is related to heat flow in the system caused by interfacial thermal resistance between the filler and matrix (refer Chapter 4 Section 4.5). Both electrical and thermal conductivity have shown an increasing trend with filler content beyond 1.0wt% of filler. But, the mechanical property (i.e., fracture toughness) starts to drop after 1.0wt%. This plot shows that for GNP/epoxy system prepared by 3RM process 1.0wt% filler loading gives the best results in terms of electrical, mechanical and thermal properties.

Although thermal conductivity and fracture toughness of GNP/epoxy system was studied only for the composite prepared by 3RM technique, a comprehensive analysis was carried out for

the other two dispersion methods on electrical conductivity and thermo-mechanical properties for GNP/epoxy (refer Chapter 4 Section 4.6.1 and 4.3.2).

The study was designed to understand the influence of using graphene based fillers in epoxy matrix on the final properties of nano-composite. TRGO/epoxy and GNP/epoxy nano-composites showed better performance in mechanical tests than MWCNT/epoxy; while a vice versa behaviour was observed in electrical tests as reported in Chapter 4 Section 4.3.1. Under mechanical characterisation, the influence of filler on the epoxy was studied for three properties - storage modulus, glass transition temperature and fracture toughness.

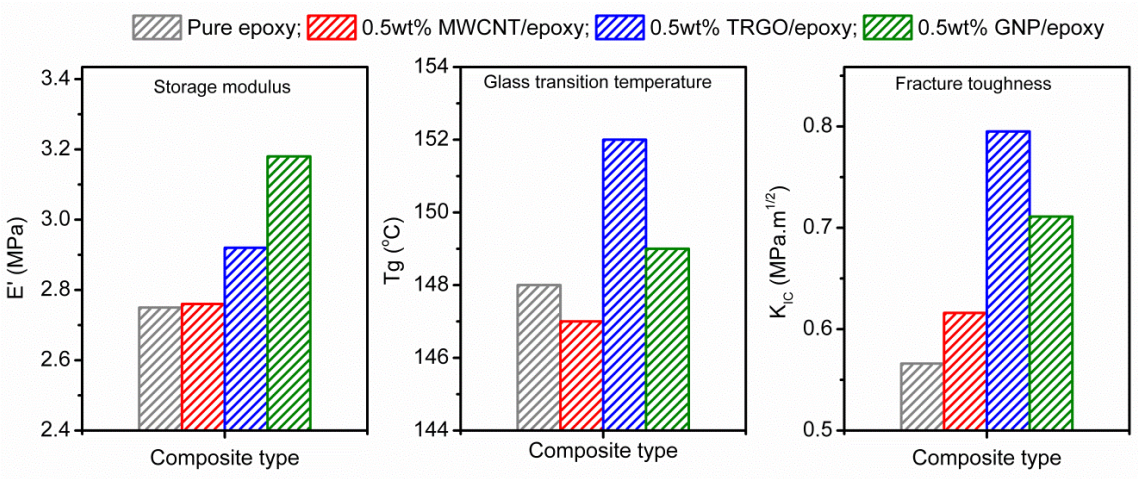

Figure 5.6: Effect of filler type on storage modulus, glass transition temperature and fracture toughness on epoxy based nano-composites.

In the above Fig. 5.6, it can be seen that the potential of graphene based fillers can be realised in terms of mechanical properties. The percentage of enhancement in properties with respect to pure epoxy is 40% in the case of fracture toughness, followed by 15% for storage modulus and 3% for T_g. Since a significant improvement in toughness was observed, the toughening effect of TRGO and GNP fillers on epoxy matrix was investigated in depth through fractographic studies.

5.4 Fractographic analysis

5.4.1 Fracture surface observation through SEM after (SEN-3PB) tests

Fig. 5.7 shows the SEM micrographs of the fracture surface of pure epoxy, and the epoxy resin toughened with 0.1wt% nano-filler. The dotted lines indicate the crack propagation direction from top to bottom. The fracture surface of pure epoxy (Fig. 5.7a) was very smooth. The flow pattern observed at higher magnification is well known as the typical fracture surface of epoxy

resin, and the local crack propagation direction can be estimated by following the pattern [208,209]. The fracture surface of 0.1wt% MWCNT/epoxy (Fig. 5.7b) was also smooth. However, the fracture surface is slightly rougher than that of pure epoxy owing to the existence of MWCNTs as shown in high magnification inset. The failure mechanism for MWCNT/epoxy is a well discussed topic in literature and it is governed by crack bridging, de-bonding and pull-out of nanotubes, which in turn contributes to higher toughness for the present composite [210-212]. On the other hand, the fracture surfaces of GNP/epoxy and TRGO/epoxy (compare Figs. 5.7c and 5.7d respectively) were much rougher than that of neat epoxy and 0.1wt% MWCNT/epoxy. Furthermore, the fracture surface of GNP/epoxy and TRGO/epoxy consists of several small facets at different height levels. Narrow bands were observed at the boundary of these fracture surfaces, and these bands run parallel to the crack growth direction.

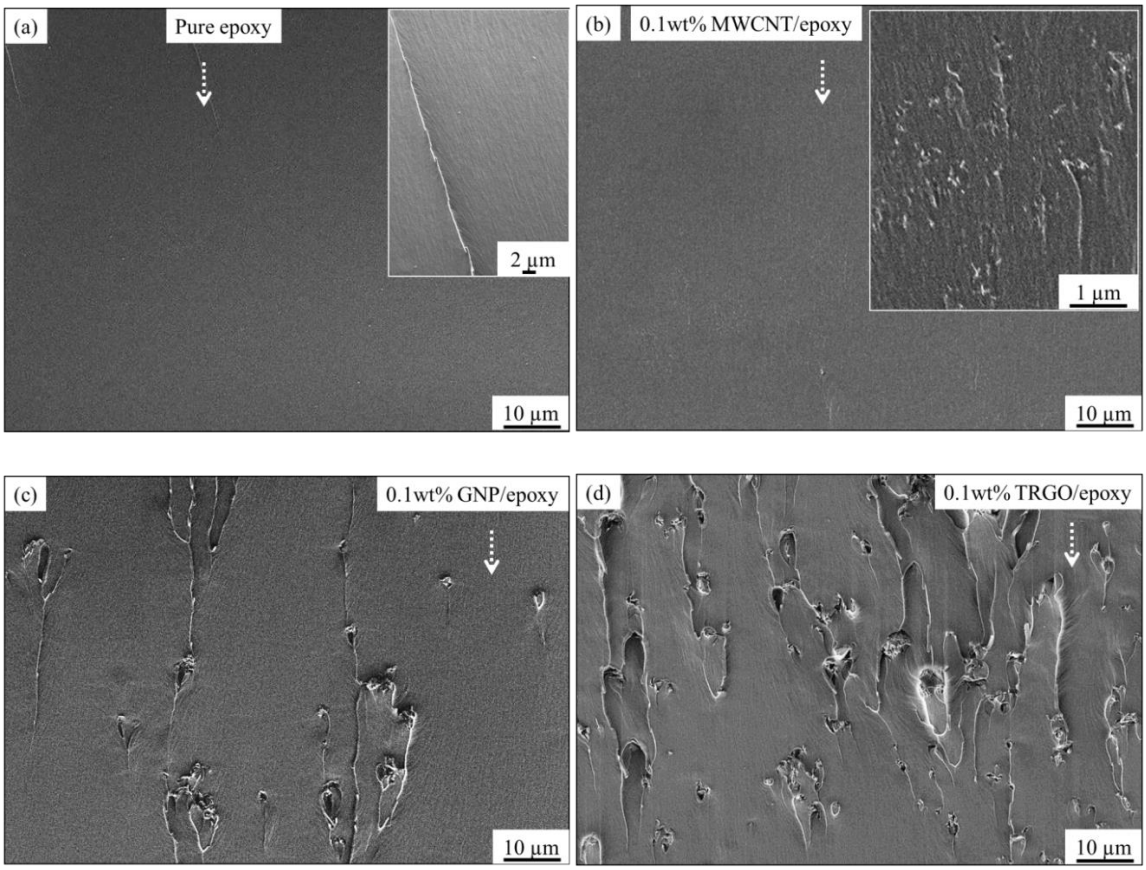

Figure 5.7: Representative fracture surfaces of 0.1wt% nano-filler/epoxy after SEN-3PB test, (a) pure epoxy, (b) MWCNT/epoxy, (c) GNP/epoxy and (d) TRGO/epoxy. Insets in (a) and (b) show higher magnification micrographs.

The flow pattern of epoxy resin in the fracture surface of TRGO/epoxy and GNP/epoxy is seen to flow around the agglomerates. Similar fracture surface was also observed by other research groups [147,148], [213,214]. Each of these facets (i.e., small fracture surfaces) was initiated

probably from the existence of TRGO and GNP sheets or agglomerates, where the main crack front bifurcates into different small fracture surfaces at different height levels by TRGO and GNP. The fracture surface of TRGO/epoxy is relatively similar to that of GNP/epoxy; however, the number of those small fracture surfaces of GNP/epoxy was lesser than that of TRGO/epoxy. This shows the better dispersion ability of TRGO sheets than GNP as they are functionalized with oxide groups. These oxide groups can be epoxy, hydroxyl or carboxylic acid groups and thereby form covalent bonds with the epoxy matrix which enhances the filler matrix interaction. Also, as shown in Fig. 5.1 (refer Chapter 4 Section 4.1), the thickness of as-received TRGO was smaller than that of as-received GNP. This difference of particle thickness probably accounts for increased surface roughness in TRGO/epoxy than in GNP/epoxy.

5.4.2 Failure mechanism in GNP and TRGO/epoxy after (SEN-3PB) tests

In order to understand the failure behaviour of GNP/epoxy and TRGO/epoxy in detail, the fracture surfaces were studied using SEM through both SE2 detector and in-lens detector on both sides of the fracture surfaces after SEN-3PB tests as shown in Fig. 5.8. From the observations, most fracture behaviour in graphene epoxy composites were categorised into three failure modes, (a) crack pinning by filler, (b) separation between the graphitic layers, and (c) shear failure due to difference in height on fracture surfaces. In the following paragraph each failure mode is explained with representative SEM images.

The adjacent fracture surfaces are named as side A and side B for convenience. The images of side A and side B are generally symmetric, and for ease of comparison, the images of side B are reflected upside down. The pattern on the fracture surface of GNP/epoxy on side A (Fig. 5.8a) was quite similar to that of side B (Fig. 5.8b). However, the relationship of the concave-convex shapes are opposite between side A and side B. There is one convex part on the fracture surface of side A, and therefore a concave part on side B, so that A fits into side B. The flow pattern in front of the concave-convex part is straight and parallel to crack growth direction. On the other hand, the pattern near the GNP is curved and wraps around the GNP. There is a narrow band behind the GNP, and the flow pattern behind the GNP was symmetric to this band.

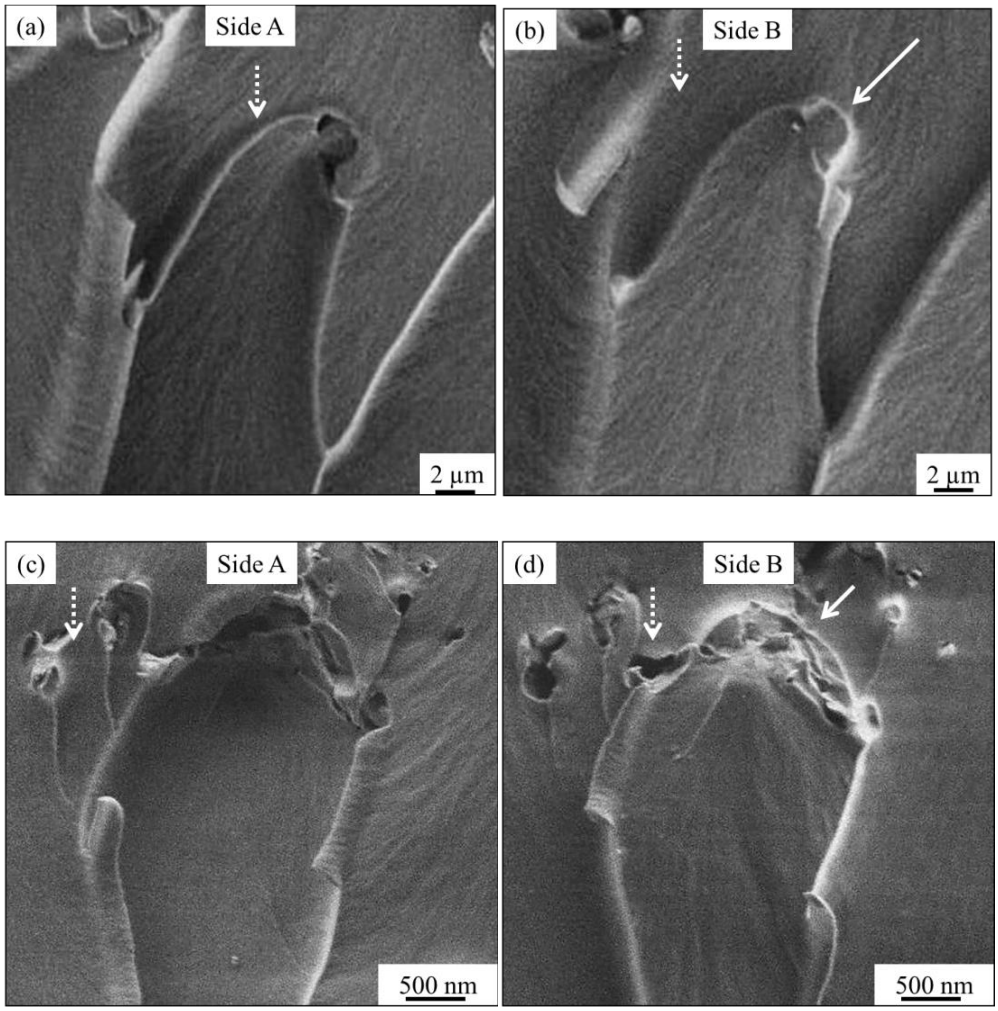

Figure 5.8: Examples of crack pinning failure (a), (b) GNP/epoxy and (c), (d) TRGO/epoxy on both the fracture sides. Dotted lines indicate crack propagation direction.

Based on the above observations, it is seen that the crack propagation is influenced by the crack that initiates and grows near the GNP. Also the crack growth was inhibited and the crack was separated in both sides of GNP i.e., the crack is initially pinned to the GNP/TRGO and bifurcates the particle, but continues to propagate in the "shadow" of the particle. Afterwards, both cracks grow around the GNP, and these cracks connect again later, with the delayed central crack. Here, the height level of one crack plane was not always the same as that of adjacent cracks. Thus, the fracture surface along the boundary of these cracks is not parallel towards the global fracture surface and the narrow band deformation area behind the GNP/TRGO can be observed. This explains the overall view of the fracture surface, where the crack goes around the GNP/TRGO and later connects but with a different height. There are two major failure modes that occur in TRGO/epoxy and GNP/epoxy; one is crack-pinning at the vicinity of GNP/TRGO particles, as described above on the example of GNP and the other is

separation in-between the TRGO/GNP sheets. In Figs. 5.8b and 5.8d, there is a sector indicated by a white arrow, whose height is different from that of the main crack face. The flow pattern on the main crack in front of the particles was parallel to the global crack growth direction, and the pattern near the particles is slightly curved and wraps around the GNP. It is therefore evident that there is a change in the flow pattern of the epoxy resin in the sector and near the sector. Thus, as the cracks continue to propagate, parts of the crack are pinned by the particles and the rest continued to propagate, giving room for the left behind part of the crack to catch up later. However, that can happen at different height levels on the fracture plane. Therefore the characteristic ramps are seen as lines in the direction of crack propagation mainly in Fig. 5.8, but generally in all SEM pictures.

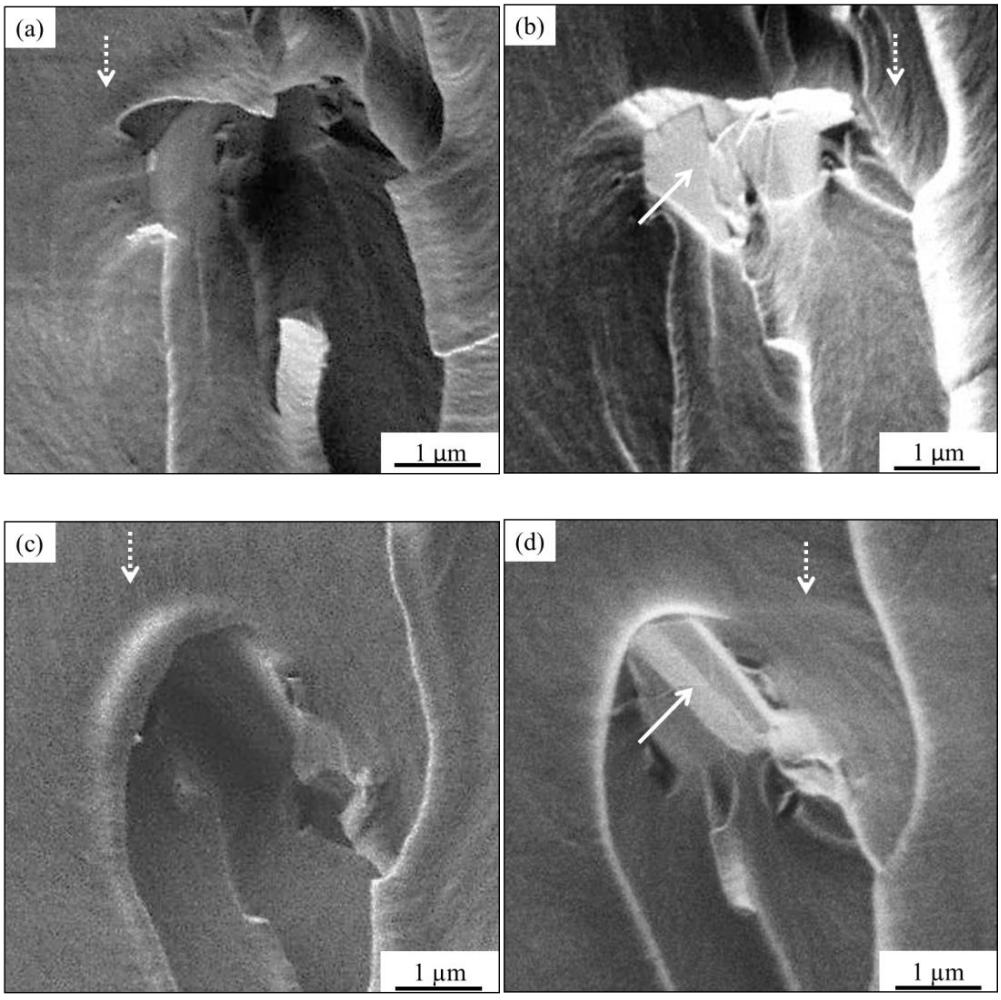

Figure 5.9: Examples of failure by separation in between the GNPs on both fracture sides (a), (b) and TRGO (c), (d) where the white arrows indicate the delaminated surface of nano-filler.

The second failure mode is the separation between GNP/TRGO sheets which is representatively shown in Fig. 5.9. Both the opposite pairs of the fracture surface are shown in

Figs. 5.9a and 5.9b for GNP/epoxy and Figs. 5.9c and 5.9d for TRGO/epoxy. In the image, the arrows indicate the separation between TRGO/GNP sheets. In the flat surface, no flow patterns that are typical for the fracture surface of epoxy resin are observed. This fact indicates that this face is not the fracture surface of epoxy resin but the surface of TRGO/GNP. This is one of the toughening mechanisms of TRGO/epoxy and GNP/epoxy and is clearly visible in those sheets that are oriented in a direction perpendicular to the crack propagation direction.

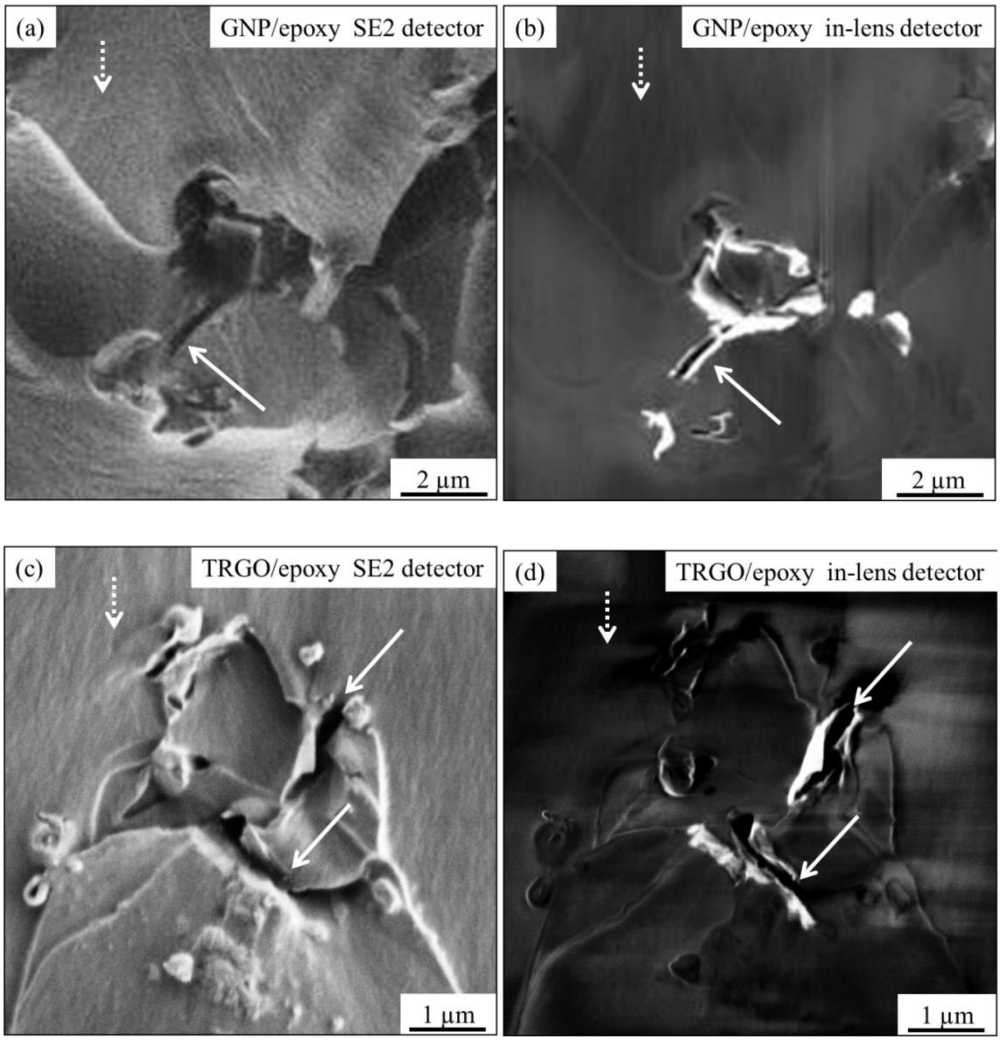

Figure 5.10: Examples of GNP/TRGO separation in between the graphitic layers: (a) GNP /epoxy and (c) TRGO/epoxy through SE2 detector; (b) GNP/epoxy and (d) TRGO/epoxy through in-lens detector (arrows indicate the nano-filler layers oriented perpendicular to crack front).

In Fig. 5.10, examples of GNP/epoxy and TRGO/epoxy using both SE2 and in-lens mode are shown. In-lens mode enables to visualize the nano-fillers which appear in white in Figs. 5.10c and 5.10d. However, electron transparency of these nano-fillers depends on the number of layers present. In both the TRGO/epoxy and GNP/epoxy nano-composites, the white arrows

indicate exfoliation in-between the graphitic layers. It can be seen that the nano-fillers are oriented perpendicular to the crack propagation direction which shows the separation in-between the graphite sheets.

Based on the two failure modes observed from the fracture surfaces, a schematic representation of the crack propagation mechanism is shown in Fig. 5.11.

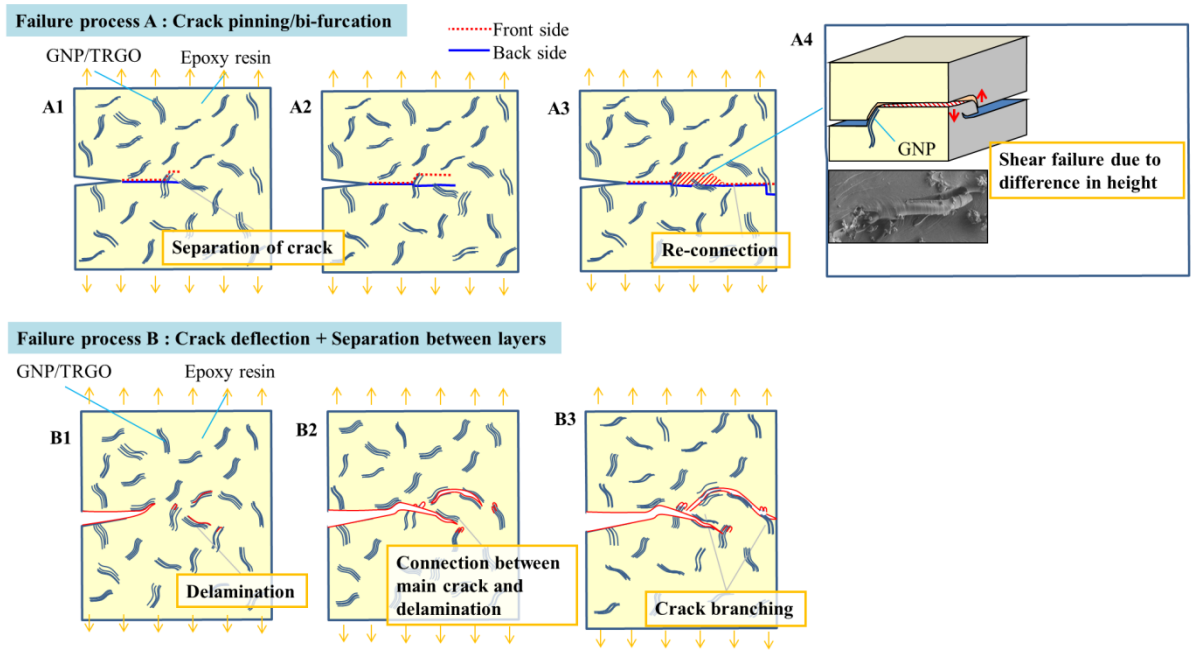

Figure 5.11: Schematic of the observed crack propagation mechanism in TRGO/GNP epoxy composite.

While considering the failure mode (A) - crack pinning, the schematic shows that as the crack propagates into the composite, it encounters one of the agglomerates of nano-filler (GNP/TRGO) oriented perpendicular to the crack direction. At this point, the crack face has to bifurcate and one part goes around the sheet and another beneath the particle (A1). This continues to grow with difference in height between the two separated crack faces (A2) and then joins after some distance (A3) leaving behind a narrow band formation. In the SEM image (A4), we see one such narrow band formation at the right corner. Here, the flow pattern on the narrow band deformation area is aligned to perpendicular direction. This implies that the cracks grew from the outside of the narrow band deformation area to the inside of the narrow band deformation area. Further, it is observed from the failure mode (B) that crack deflection and/or separation between the sheets occur (see Fig. 5.12). In other words, the crack runs along the surface (B1) that is along the TRGO or GNP/epoxy interface. A similar phenomenon has also been reported in literature through modelling studies [215]. In certain places, depending on

orientation of the nano particle relative to the crack face, separation between the graphitic layers emerges (B2). Since the force between the sheets is a secondary force (van der Waals) [216,217], the separation of sheets is facilitated with easy crack propagation. This separation occurs simultaneously at several particles and, in a few instances; the main crack propagates through this particle (B3). Apart from this, the deflected crack and the main crack propagate in different planes resulting in crack branching (B4).

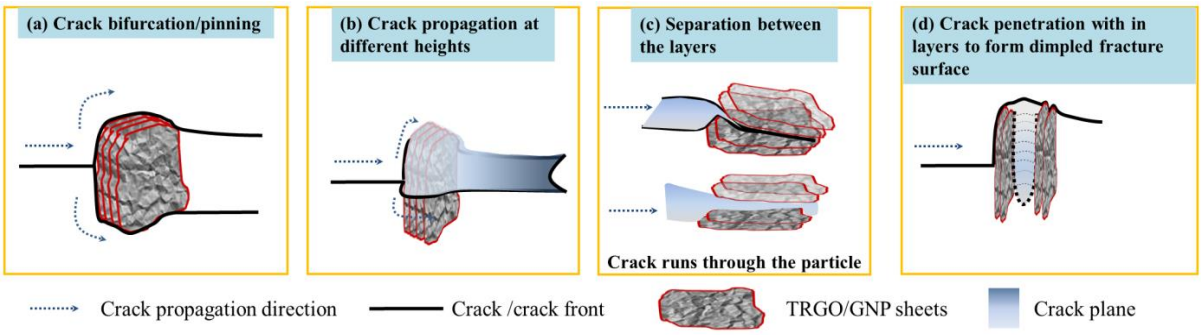

Figure 5.12: Schematic on the interaction of crack front with GNP/TRGO particles.

The above mentioned schematic (Fig. 5.12) shows the interaction of a crack/crack front when it encounters the edges or surface of TRGO/GNP sheets. When the crack front meets the surface of the graphene sheets it can either get deflected or it bifurcates and goes around the particle (Fig. 5.12a). When the crack gets deflected, there is a height difference between the deflected crack front and the original crack front (Fig. 5.12b). This makes the crack to take a torturous path and accounts for the rough surfaces observed under electron microscope. Another failure mechanism occurs when the crack meets the edges of the graphene sheets. The crack continues to propagate in between the graphene sheets and finally passes through by separating the layers (Fig. 5.12c). This is possible because of the layered structure and the ease of shearing between the graphene layers. A combination of crack deflection and separation between the graphene layers can also occur. A crack front that is deflected by the surface of TRGO/GNP particle oriented under an angle in the range of 90° and goes around it where it meets the edges of the particle. At this juncture, it is possible for the crack to run the particles creating a dimpled fracture surface (Fig. 5.12d).

While observing the fracture toughness of GNP/epoxy, as a function of the weight percentage of the filler (refer Chapter 4 Section 4.7.1 Fig. 4.25), it is clear that after 1.0wt% of filler, the K_{IC} values start to drop for 2.0wt% of filler. The fracture surfaces of GNP/epoxy and

TRGO/epoxy at different weight percentage were viewed under scanning electron microscope to explain this drop in K_{IC} as in Fig. 5.13.

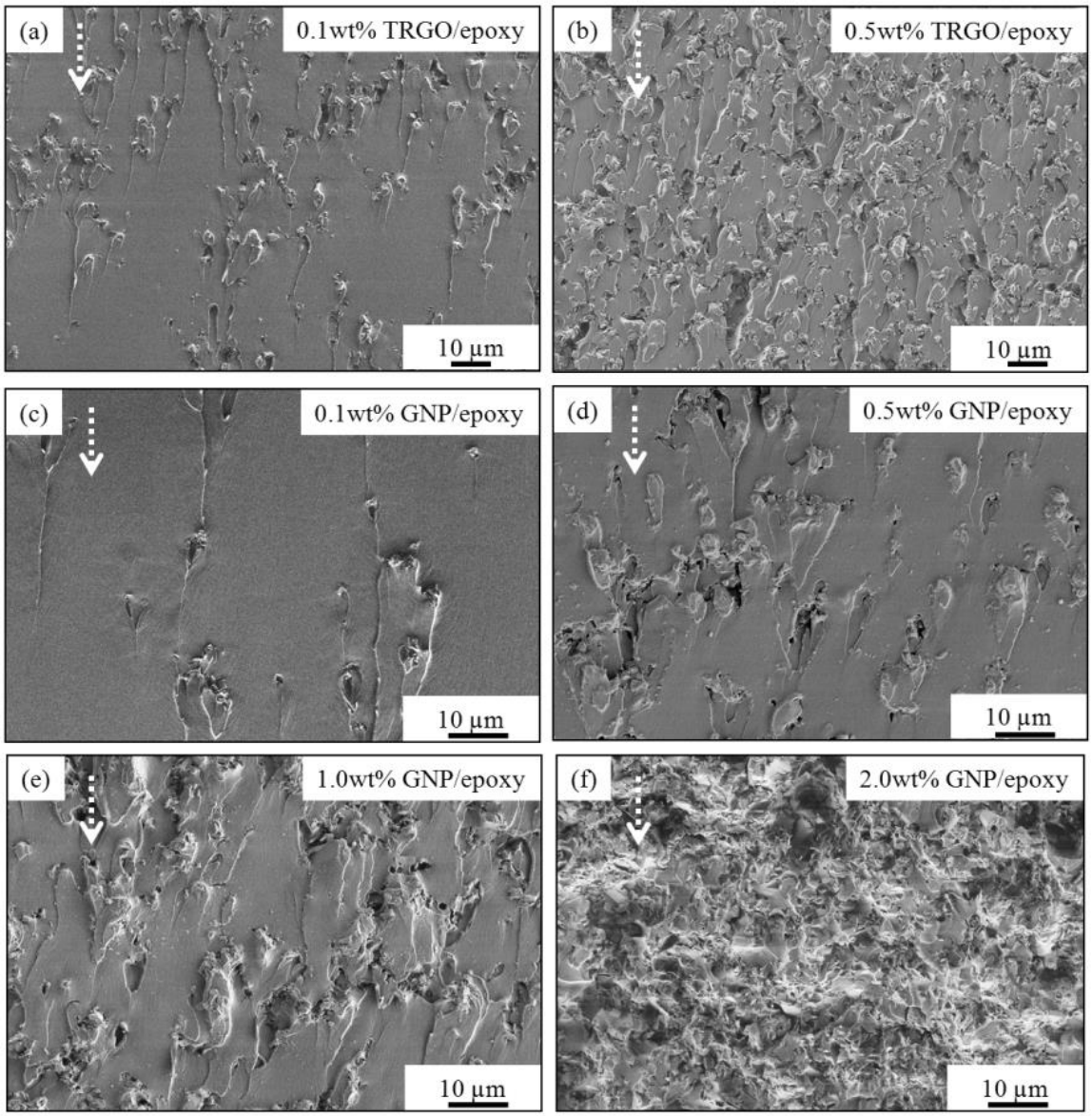

Figure 5.13: Scanning electron micrograph of fracture surface of GNP/epoxy (a) 0.1wt%; (b) 0.3wt%; (c) 0.5wt%; (g) 1.0wt%; (h) 2.0wt%; and of TRGO/epoxy (d) 0.1wt%; (e) 0.3wt% and (f) 0.5wt% respectively (dotted arrows indicate crack propagation direction).

Comparing the Figs. 5.13c-f, it is observed that the surface roughness increases with increase in filler content for both GNP/epoxy (Figs. 5.13c-f) and TRGO/epoxy (Figs. 5.13a and 5.13b). A decrease in surface roughness can also be found for GNP/epoxy for the same weight percentages when compared to TRGO/epoxy (Figs. 5.13a and 5.13c; 5.13b and 5.13d). The higher surface roughness exhibited by TRGO/epoxy when compared to GNP/epoxy, explains the increased K_{IC} values observed for this system. This increase in surface roughness may arise

due to better dispersion ability of TRGO filler as they are partly functionalised due to the presence of a fewer number of layers (refer Table 5.1) and because of their wrinkled morphology (refer Chapter 4 Section 4.1 Fig. 4.1c). Observations at higher magnification support the fact of mechanical interlocking due to wrinkled morphology and separation between the TRGO sheets occurring at multiple places that are formed ahead of the crack front Fig. 5.13d.

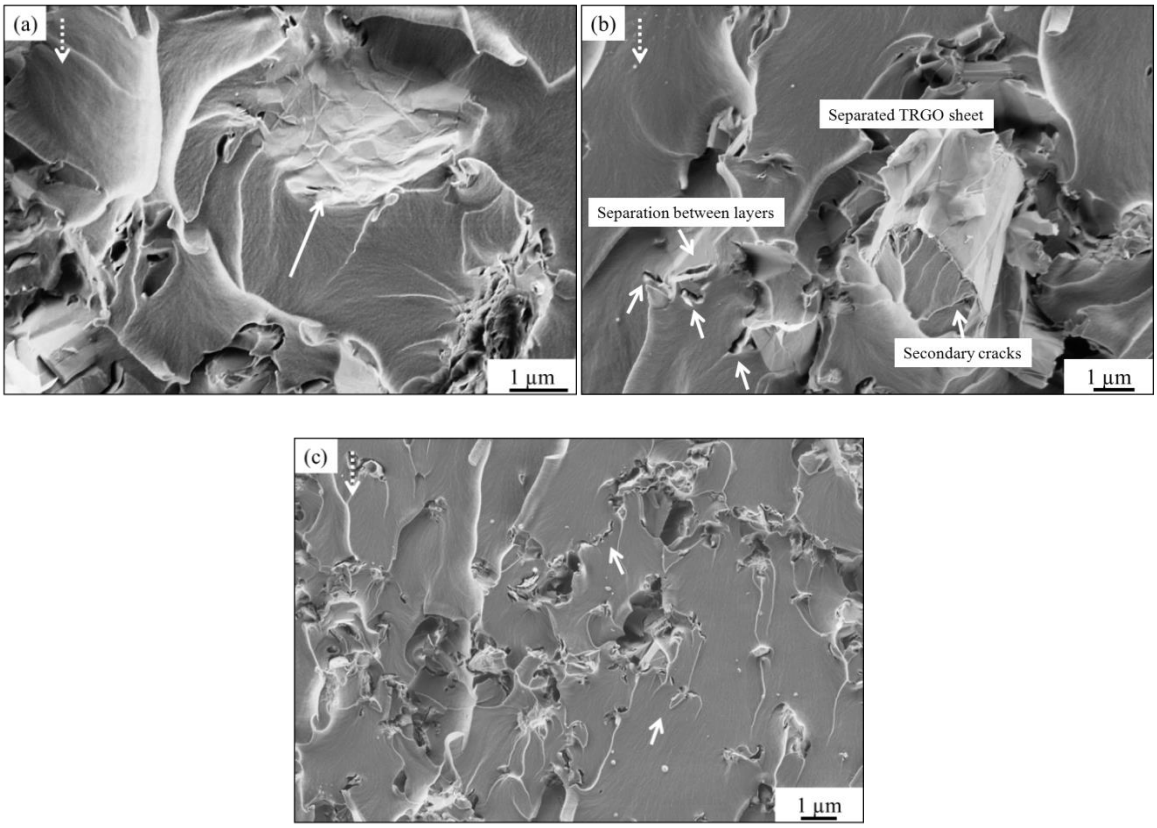

Figure 5.14: Scanning electron micrographs of fracture surface of TRGO/epoxy (a) shows wrinkled morphology of filler; (b) secondary cracks emerging beneath the TRGO sheet and (c) formation of multiple cracks respectively. Dotted lines indicate crack propagation direction.

The white arrow in Fig. 5.14a points to one of the TRGO sheets in the epoxy matrix which has a wrinkled morphology that aids in mechanical interlocking between the filler and the matrix. In Fig. 5.14b, secondary cracks emanating from beneath the TRGO sheet could be seen along with some layer separation between the TRGO sheets (indicated by white arrows). The TRGO sheet in this case is oriented in such a way that the edges of the sheet meet the crack front. The crack has propagation in between the sheets and emerges on the other side with secondary cracks. Another example of the above discussed mechanism is observed in Fig. 5.14c where

multiple cracks are formed ahead of the main crack due to separation in between the TRGO sheets (indicated by white arrow).

However from the K_{IC} vs. filler weight percentage plot, drop in fracture toughness for GNP/epoxy is vividly seen. Owing to processing difficulties of TRGO/epoxy, higher weight percentage samples could not be prepared and hence it is difficult to comment on the decrease or increase at higher weight fractions (indicated by grey line in Fig 5.15a).

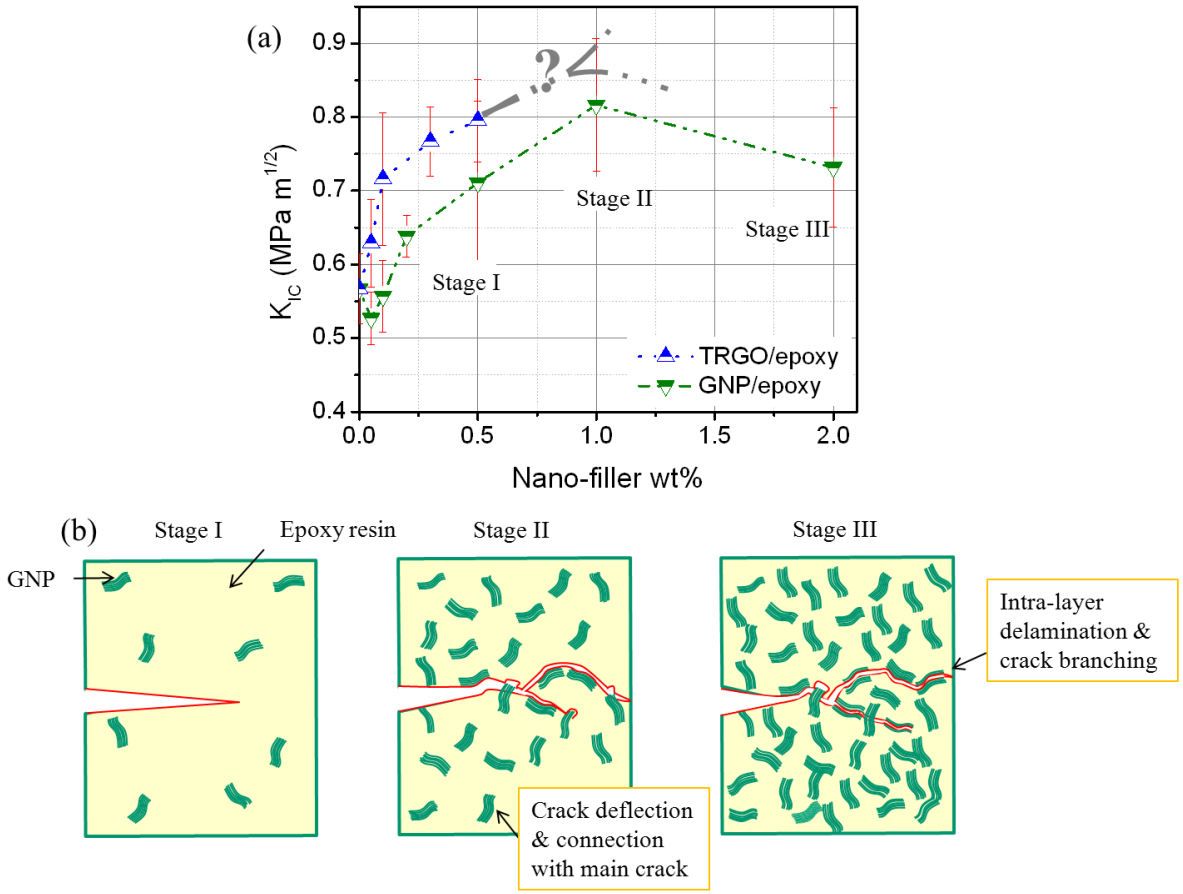

Figure 5.15: (a) Fracture toughness of TRGO/epoxy and GNP/epoxy as a function of filler content; (b) schematic of crack propagation that accounts for the fracture toughness variation with filler content for GNP/epoxy system.

The schematic in Fig. 5.15b is more suited for GNP/epoxy system where the toughening mechanism is divided into three main stages. At lower filler content, there is less volume of filler. Further, the inter-particle spacing between the agglomerates is high and hence the crack propagates almost in a linear manner similar to that of pure epoxy and only when it encounters a particle, the crack must pass by. Hence, the K_{IC} is also close to the K_{IC} of pure epoxy (Stage I). As the filler content increases, the failure mode is crack pinning at the vicinity of the GNP agglomerate, giving rise to narrow band formation and crack deflection by the GNP sheets as

observed in (Fig. 5.13c). Increasing the volume of filler, there is a regular deflection of the main crack by GNP agglomerates. The main crack and the deflected crack may or not combine; intra-layer delamination is also observed due to increased filler content which contributes to the increased K_{IC}, where it reaches a maximum (Stage II). Upon further increase in the filler content, the dominant failure mode is delamination between GNP sheets which leads to a dimpled fracture surface as in (Fig. 5.13f). Since the force between the sheets is a secondary force (van der Waals) the crack propagates similar to that in pure epoxy, leading to a decrease in fracture toughness (Stage III).

5.4.3 Fracture surface analysis GNP/epoxy after cryo-fracture

The above discussed failure mechanisms were not only observed in the fractured surface from SEN-3PB tests but also on the cryo-fractured surfaces in 0.3wt% GNP/epoxy system which are presented in Fig. 5.16. Dotted line indicates crack propagation direction.

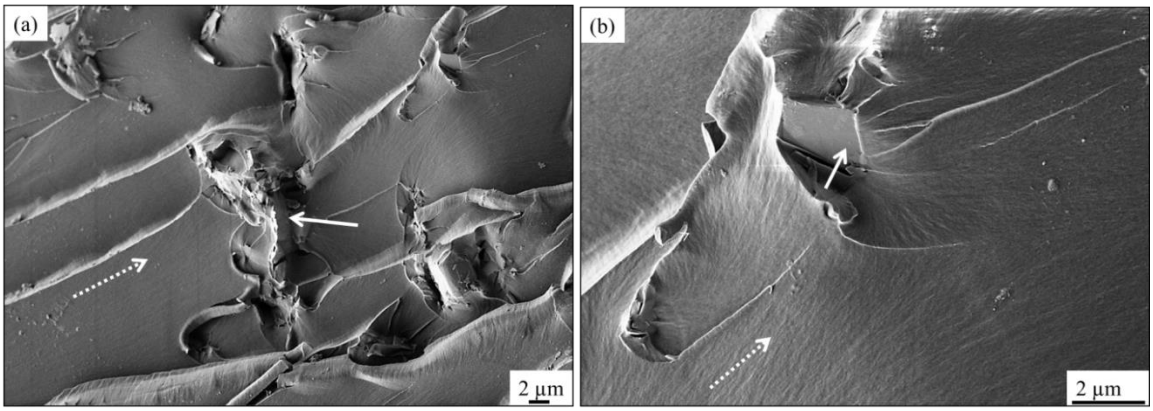

Figure 5.16: Scanning electron micrographs of cryo-fractured 0.3wt% GNP/epoxy; (a) hindering of crack propagation by GNP agglomerate, (b) trace from separation between the graphene layers.

In Fig. 5.16a the white arrow indicates one of the GNP agglomerates oriented perpendicular to the crack front hindering crack propagation. The situation in Figs. 5.16b represents a particle out of axis, but only partly in plane with fracture surface. It is seen that there is a region free from any of the flow patterns observed in the pure epoxy (indicated by white arrow). This region represents the intra-layer propagation through the graphitic nano-particle. Secondary cracks initiate from the edges of the GNP sheet. The flow pattern in the resin is in the direction of crack propagation and changes its direction when it is in the vicinity of GNP sheets. This change in the flow pattern is due to high shear forces that operate at the edges of the sheet and are also due to the ability of the GNP sheets to shear within themselves. These observations

from the cryo-fractured surface are consistent with the above explained schematic and the failure mechanism in general, for GNP or TRGO/epoxy systems.

5.5 R-curve

Fracture toughness vs. the crack length curves were presented in Fig. 4.26 in Chapter 4 Section 4.7.2. It must be noted that the 5 µm tip of the notch was not sharp enough and hence, first an unstable crack occurs and it produces a fast crack growth region. Only beyond this unstable crack growth region, the R-curve was obtained as mentioned earlier. Kinloch et al., reported two types of crack growth behaviour viz., stable crack growth and unstable crack growth [194]. The unstable crack growth occurs when the crack tip is blunted and under high degree of plasticization and the stable crack growth takes place under low degree of plasticization.

However, on close observation of the fracture surface, initial cracks near the raw notch, (Fig. 5.17a) along with a very small region of stable crack can be seen in Fig. 5.17c. First, upon loading, there is a localized plastic deformation ahead of the tip and it requires additional energy for the growth of the crack and thus the K_{IC} increases. Upon examination of the fracture surface near the raw notch as depicted in (Fig. 5.17), there is an increase in the roughness of the fracture surface for TRGO/epoxy. This is mainly due to localized plastic deformation and is more in the case of TRGO/epoxy due to the two-dimensional sheet geometry; this is reflected in the higher initial fracture toughness of the composite compared to MWCNT/epoxy and pure epoxy.

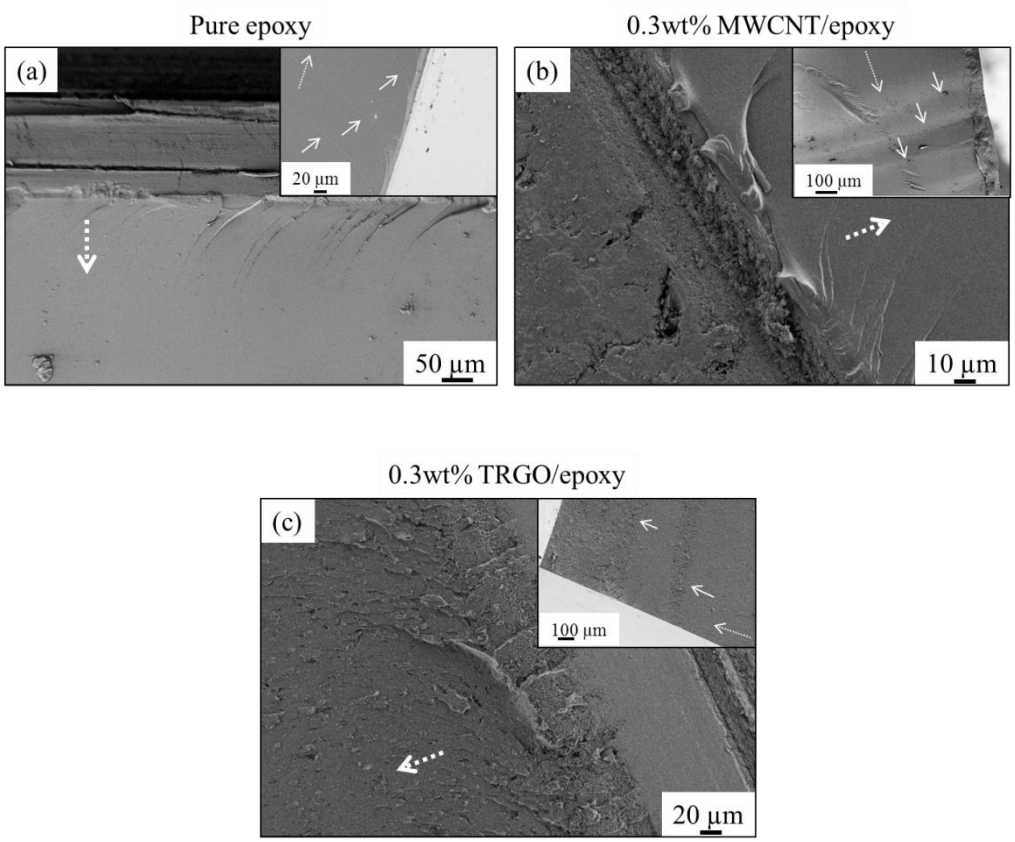

Figure 5.17: Scanning electron micrographs of the fracture surface near the raw notch of (a) pure epoxy; (b) 0.3wt% MWCNT/epoxy; (c) 0.3wt% TRGO/epoxy. Insets show the beach marks (white solid arrows). Dotted lines indicate the crack propagation direction.

Continuously loading further, the crack slowly propagates through the plastic zone and when this energy overcomes the crack resistance energy, the crack propagates faster until it is arrested again. In this case, due to effectively blunted crack tip, there is a fast preceding unstable crack growth followed by a crack arrest visible through beach marks as shown in the insets in Fig. 5.17. In the case of pure epoxy, these crack arrest lines are narrowly spaced whereas in the case of nano-composites they are more widely spaced and this is attributed to the presence of nano particles which provide additional crack resistance [218].

In general, the crack initiation and growth depends on intrinsic and extrinsic toughening mechanisms. An intrinsic mechanism is the one that operates ahead of the crack tip, whereas the extrinsic mechanism operates behind the crack tip, where the stress intensity factor is reduced by shielding the crack tip. In the case of TRGO/epoxy the crack initiation toughness or the K_{IC} from SEN-3PB is higher than MWCNT/epoxy because the size of the plastic

deformation zone for 2D filler is larger than for the 1D filler. The crack growth toughness, however, is governed by crack deflection of TRGO sheets and formation of micro-cracks [219].

As stated above, the leading causes for a rising R-curve in the case of TRGO/epoxy samples are reported to be micro-cracking by the TRGO sheets which reduce the stress at the crack tip. Optical micrographs of the crack tip show micro-cracks near the main crack, and this micro-cracking leads to an irregular crack with steps observed in the main crack. Formation of these micro-cracks releases strain energy and therefore more energy is required to propagate the crack and hence the K_{IC} increases. Apart from micro-cracking, crack deflection was also observed in TRGO/epoxy composites.

Micro crack formation has been extensively studied in brittle and quasi-brittle materials. These micro-cracks, which normally develop near the main crack tip, are formed due to the presence of external load and localised residual stresses. As the load is increased, a crack is initiated at the tip of a sharp pre-crack (in the present study it is the first fast crack growth). In the case of TRGO/epoxy, crack deflection occurs between the particles due to their 2D geometry. When the filler fraction increases, due to the presence of some dense primary agglomerates in the nano-composite, the crack deflection mechanism turns into crack bridging as the load level is increased. At this point, crack re-initiation takes place ahead of the primary crack tip, leaving an un-cracked bridge between the new crack and the primary crack [220]. Hence micro-cracking is one dominant mechanism for the increased R-curve. However, the position of these micro cracks affects the R-curve. This micro cracking in the case of TRGO/epoxy is due to delamination that occurs in between the graphitic layers.

While performing the SEN-4PB tests, the optical micrographs that were taken during the test contained a tulip-like structure developing along with the main crack. Crack tip phenomena in epoxies have been reported times in the literature. However, the cause for this phenomenon is still unclear and open for discussion. However, further investigation as to how the crack propagates in nano-composite reinforced with different fillers is required to be carried out.

6 Conclusion

This chapter brings out the main findings and corollaries of this work. The study was set to determine the potential of graphene as a filler material in composite structures. This dissertation has investigated different types of graphene (TRGO and GNP) dispersed in epoxy matrix and their comparison with MWCNT/epoxy nano-composite.

This study has found that generally, graphene/epoxy nano-composites have better mechanical properties than MWCNT/epoxy. When it comes to electrical properties, MWCNT dominates, and this is mainly due to filler geometry, ability to form a percolated network in matrix (or) formation of re-agglomerates after dispersion. Among the graphene types, TRGO/epoxy shows much higher fracture toughness (K_{IC}) and T_g than GNP/epoxy which is attributed to fewer number of layers and also due to the presence of partly functionalised oxide groups (12.0wt%) in TRGO. This aids in achieving a strong interaction between the filler and the matrix as reflected in T_g. However, GNP/epoxy shows higher electrical conductivity than TRGO/epoxy because the intrinsic filler conductivity of GNP is much higher than TRGO. As mentioned above, the presence of remnant oxide functionalities, structural defects during processing in TRGO and their ability to disperse well in the matrix, reduces the electrical conductivity of the nano-composite. A comparison pertaining to mechanical and electrical properties of different types of nano-composite is presented in Fig. 6.1. The plot shows the percentage of enhancement in properties with respect to pure epoxy for ease of comparison.

The second major finding is on the effect of dispersion method on the electrical property of the nano-composite. The most common processing route followed in graphene literature is through the use of solvent. Ultra-sonication of graphene filler under suitable solvent, aids in further exfoliation of agglomerates. However, the addition of solvent has its effects on the matrix system and hence complete removal of solvent has to be ensured. This part of work concentrates on the electrical and thermo-mechanical properties of GNP/epoxy using three different processing/dispersion methods. Three-roll milling technique gives better results in terms of electrical conductivity and storage modulus. Combining sonication with three-roll milling or sonication with high speed shear mixing yield nano-composites with better mechanical properties but with lower electrical conductivity.

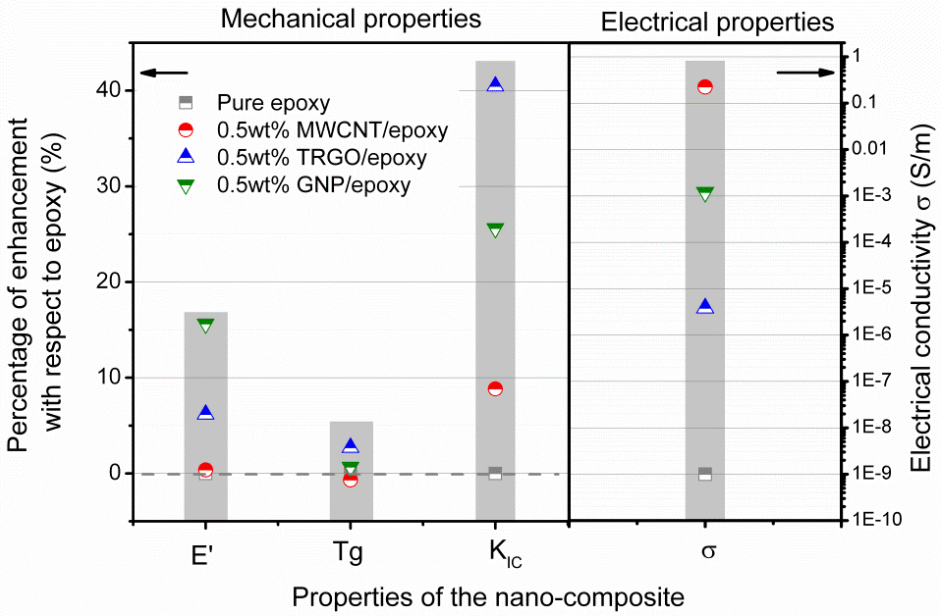

Figure 6.1: Mechanical and electrical property of 0.5wt% MWCNT/epoxy, TRGO/epoxy and GNP/epoxy nano-composites.

In a nutshell, the processing method can be tailored, depending on the application as in Fig. 6.2. There are two references used, viz., pure epoxy and pure epoxy with solvent. Though there is not much influence on the T_g with different processing methods, optimum results were achieved with three-roll milling method only.

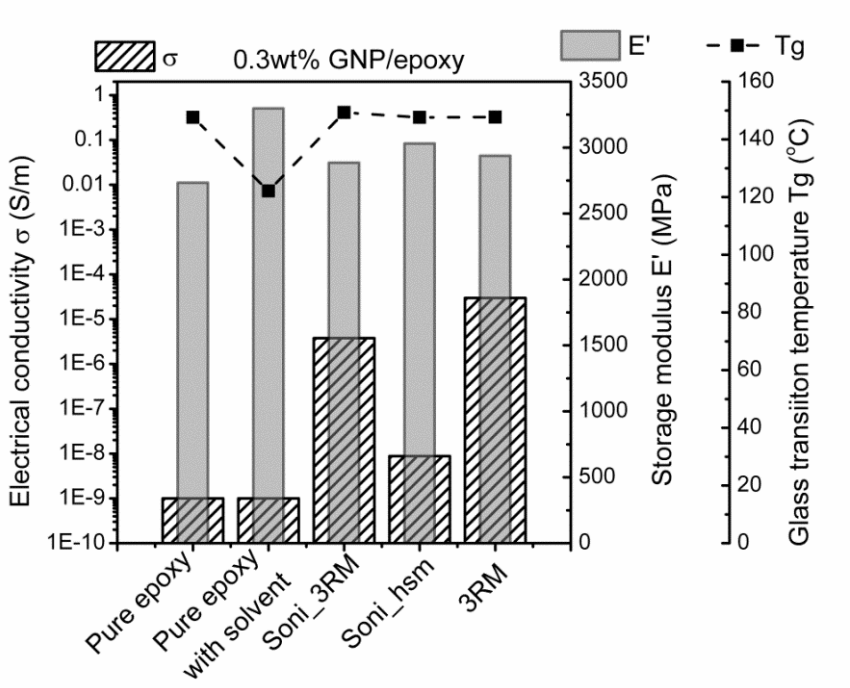

Figure 6.2: Effect of dispersion method on electrical conductivity, storage modulus and glass transition temperature of 0.3wt% GNP/epoxy.

Apart from the above mentioned findings, another study was performed combing TRGO and MWCNT fillers. The effect of addition of TRGO on the electrical percolation threshold of MWCNT/epoxy was studied through electro-rheological measurements. The empirical findings in this study provide a detailed understanding of the interactions between TRGO and MWCNT. The morphology of bi-filler composite showed the pinning of MWCNTs on to the TRGO sheets. This is due to the interactions through π electron clouds between TRGO and MWCNT. The lower electrical conductivity of the bi-filler (TRGO-MWCNT) system is because of lower intrinsic filler conductivity (TRGO) and filler-filler interaction.

It was apparent that the fracture toughness of the nano-composites follows the order of TRGO/epoxy > GNP/epoxy > MWCNT/epoxy. Hence, a major part of the work was done to understand the fracture behaviour that governs the toughening mechanism in TRGO or GNP/epoxy nano-composite.

Among the 2D fillers, TRGO showed a two-fold increase in K_{IC} compared to GNP toughened epoxy. This is mainly because of better dispersion ability of TRGO as these sheets are partly functionalized with oxide groups. The presence of functionalities on the edges and surface of the sheets aids in the formation of covalent bond with epoxy resin and thereby increasing the interaction between the filler and the matrix. Also, the number of layers in TRGO is far less than GNP and hence TRGO/epoxy has a higher number of dispersed nano-fillers.

From the fracture surface observation of graphene based epoxy nano-composites, evidence of crack deflection, crack pinning at the edges of the sheets, secondary cracks originating from the edges due to high shear forces were seen in both cryo-fractured and SEN-3PB fractured surfaces. The second most dominant deformation mechanism is the separation between graphitic layers that occurs at multiple places. Since the force between the graphitic layers is weak (van der Waals force) and the force between the polymer and matrix is high, it is easier for the GNP/TRGO sheets to shear within the graphitic layers. It is also possible that these separations which occur at multiple places can also combine to the main crack. However, the mechanism of separation that takes place within the sheets can either be shear or rupture of TRGO/GNP particles depending on orientation of the sheets to the load vector, crack plane and crack propagation direction.

For GNP/epoxy system the fracture toughness increases with filler content but starts to decrease at higher filler loadings (2.0wt%) though the surface roughness increases. As the filler loading is increased, separation between the graphitic layers occurs at several places which results in

local and extensive “dimple type” fractured surface due to the combination of crack deflection, separation between layers and lower distance between particles.

Based on the findings, it can be concluded that pure epoxy shows a more or less flat fracture surface. The deformation zone formed in a graphene nano-composite is higher, which may be due to the shearing in-between the graphitic sheets (particles), which in turn increases the fracture toughness of graphene toughened epoxies. Based on the above observation a schematic on the failure mechanism on graphene based epoxy nano-composites is proposed.

Taken together, these results suggest that the toughening effect of graphene fillers in epoxy matrix is significant when compared to other carbon nano-fillers. Though TRGO and GNP belong to the same family, their intrinsic properties widely affect the final property of the nano-composite. The use of graphene as a filler material was analysed from scratch, starting from filler characterisation to thermo-mechanical, electrical, rheological, and thermal properties of the composite. Combined electro-rheological investigations paved way to understand the filler-filler interaction in the case of a bi-filler nano-composite system. Despite its exploratory nature, this work also gave a glimpse of tailoring the nano-composite processing route to suit the application needs.

7 Outlook

The outcome of this work opened new perspectives in the field of nano-composite, especially on the toughening mechanisms in graphene based epoxy composites as well as in nano-modified fibre composite structures.

In terms of toughening of epoxies using graphene fillers, promising results were obtained. Hence, extending its reach beyond the nano-composite level to fibre based composite structures is already in progress. These nano-modified resins (TRGO/epoxy), when used as a matrix in manufacturing carbon fibre reinforced polymers (CFRP) showed improvement in compression after impact strength and also fatigue life [124,221]. Preliminary results on CFRP laminates prepared by vacuum infusion technique with TRGO/epoxy as the matrix showed 7% improvement in Young's modulus and 11% in flexural strength for 0.15wt% of TRGO in epoxy. The improvement in compression after impact tests for TRGO modified GFRP laminates was 55% (for 0.3wt% of TRGO in epoxy) when compared to unmodified resins [123]. With these preliminary results obtained from nano-modified matrices in composite structures, there remain open questions on fracture toughness of these laminates in both mode I and mode II.

Investigations were carried out on thermo-mechanical properties of an epoxy resin filled with thermally reduced graphene oxide (TRGO) and multi-wall carbon nanotubes (MWCNT) after exposure to hot distilled water [222]. Addition of low contents of TRGO and MWCNTs greatly reduces the water absorption capacity of epoxy polymer and improves its resistance to hydrothermal ageing. These initial results opens door for detailed investigations on the filler-matrix interactions.

Besides, the use of nano-modified resins, multi-functional composites can be prepared to achieve synergetic effects by combining graphene and MWCNT. This aspect was also partly covered in the dissertation, while explaining the filler-filler interaction (TRGO_MWCNT). Extending this concept further, paper composite with sandwiched structure made from the combination of MWCNT and GNPs was prepared. The storage modulus showed an improvement of 70% with increase in T_g of 10 °C, along with electrical conductivity. Most promising results were obtained with thermal conductivity, where the sandwiched structure showed 125% increase containing 13.0wt% of filler with respect to pure resin.

These are only a few areas where the ground work established in this thesis can be made use of. It was also shown that different types of graphene exhibit different properties based on the preparation of the filler itself. Other aspects that govern the final properties of a graphene based nano-composite like the number of layers present, order of stacking, orientation of these sheets in the polymeric matrix, and the presence of functionalities are yet to be explored.

Annexure

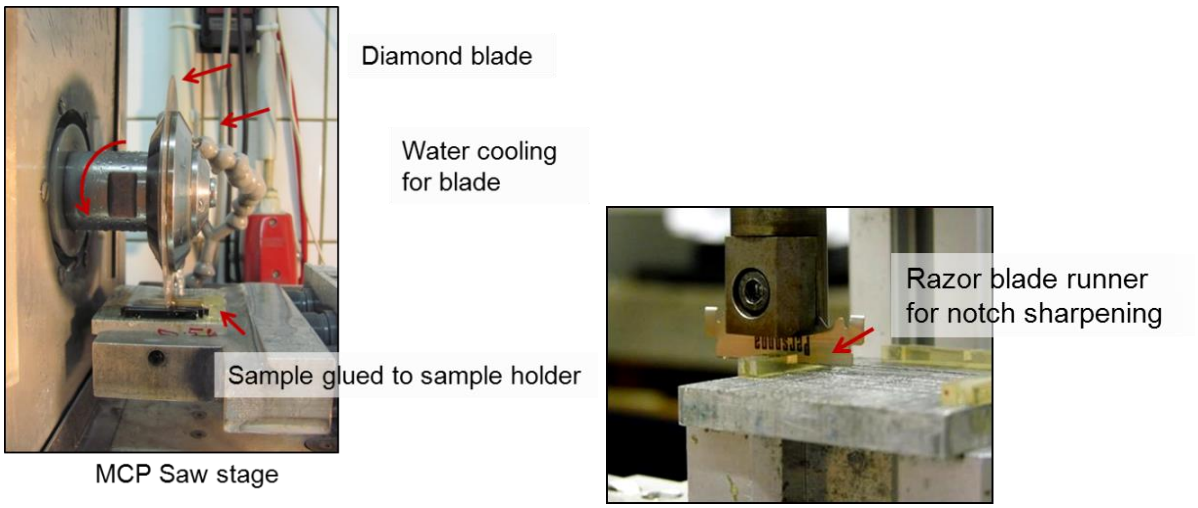

Figure A.1: Notch preparation for SEN-4PB tests; raw notch using diamond saw blade and V-notch using blade runner.

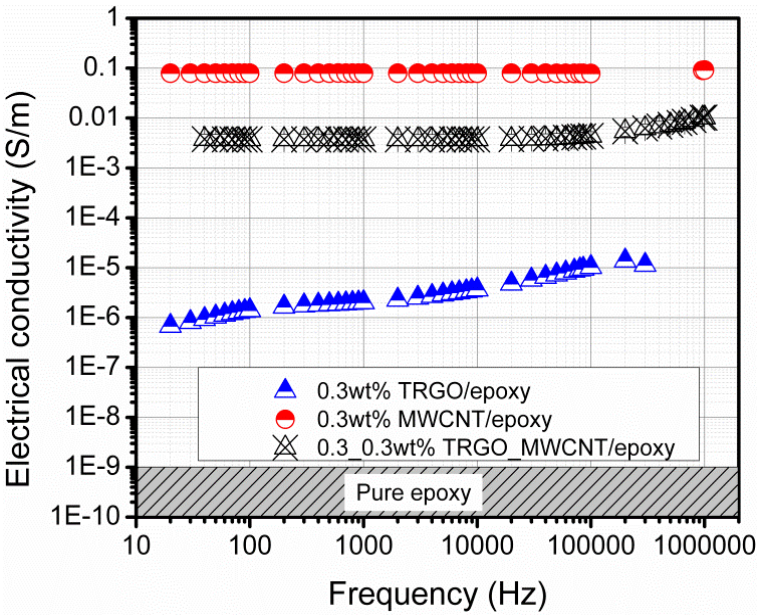

Figure A.2: Electrical conductivity of 0.3_0.3wt% TRGO_MWCNT/epoxy bi-filler composite compared with respective mono-filler composites as a function of frequency.

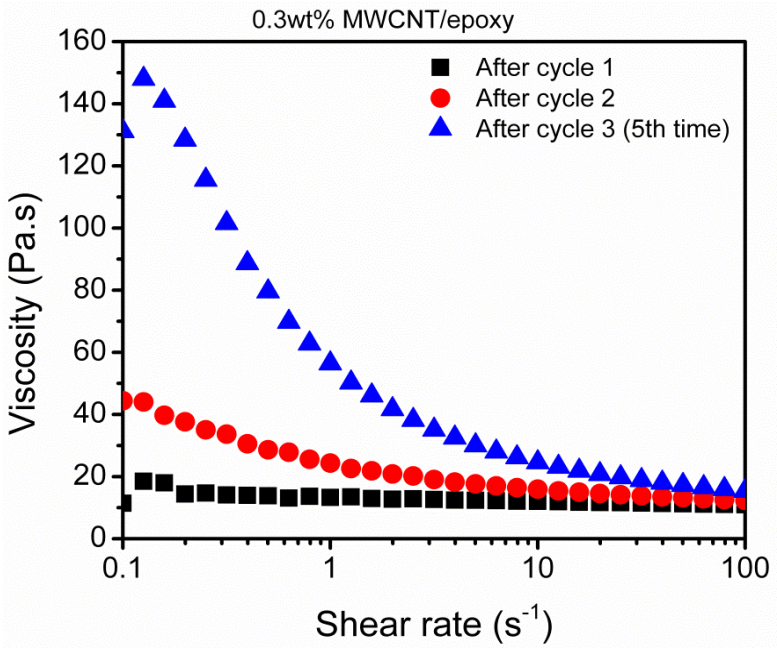

Figure A.3: Viscosity of 0.3wt% MWCNT/epoxy suspension prepared by 3RM process as a function of shear rate after each milling cycle.

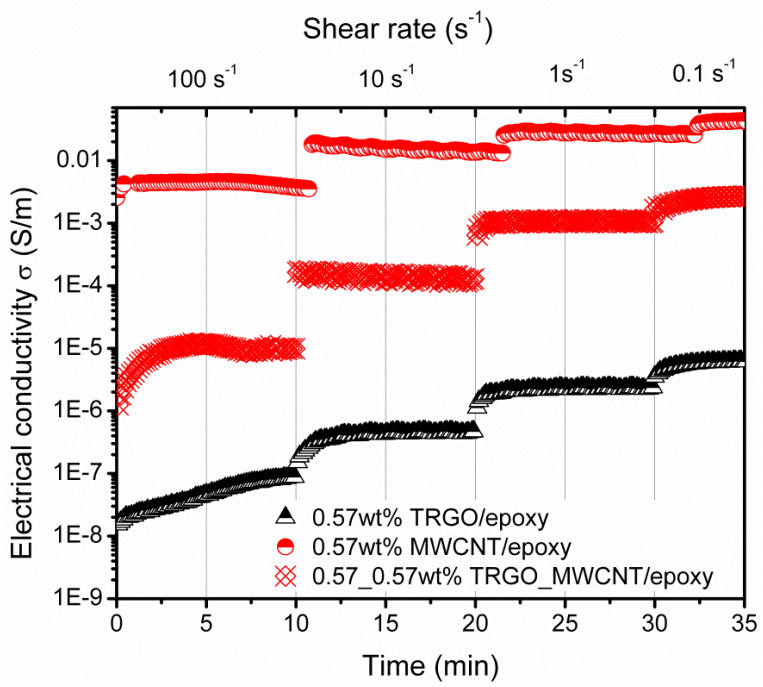

Figure A.4: Electrical conductivity at different shear rates for the MWCNT/epoxy, TRGO/epoxy and TRGO_MWCNT/epoxy suspensions at higher filler concentration respectively.

Annexure

The combined rheological and electrical measurements for pristine 0.02wt% TRGO/epoxy suspension are shown in Fig. A.5. The graph shows that the pristine 0.02wt% TRGO/epoxy is non-conducting nature and there is no evidence of shear induced agglomeration.

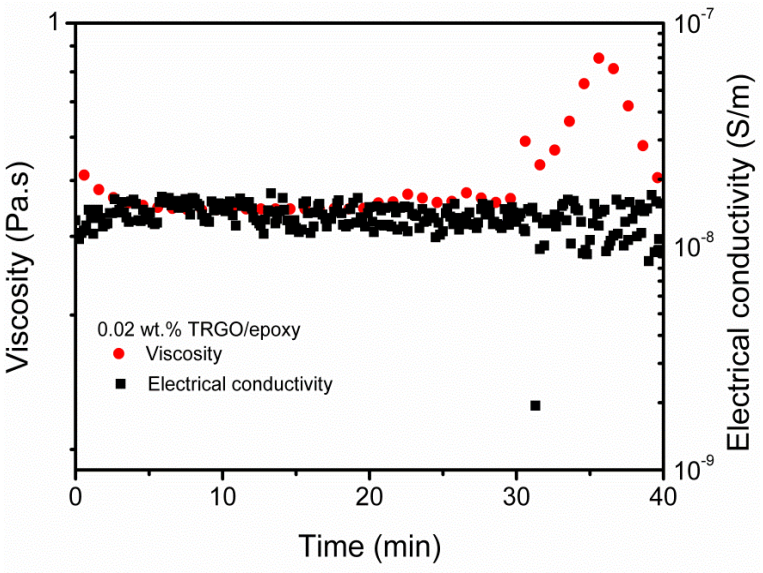

Figure A.5: Electrical conductivity and viscosity of 0.02wt% TRGO/epoxy suspensions as a function of shear rate and time.

Fig. A.6 shows the transmission optical micrographs of the 0.02wt% TRGO/epoxy suspensions and no percolated networks are formed.

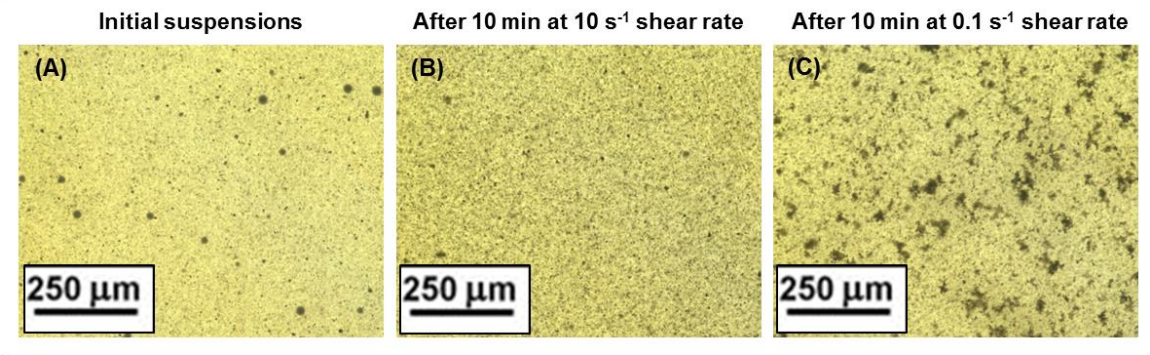

Figure A.6: Optical micrograph of 0.02wt% TRGO/epoxy suspension after 10 minute at (a) initial suspension (b) at 10 s^{-1} shear rate and (c) at 0.1 s^{-1} shear rate respectively.

Annexure

Table A.1: Thermo-mechanical properties of the nano-composite from DMTA analysis.

	E'_g (GPa), at 30 °C	**E'_r(Gpa), at 180 °C**	**T_g (°C),** From max. of tan δ peak
Pure epoxy	2.75±0.05	19.9±1.0	148
0.1wt% MWCNT/epoxy	2.60±0.01	19.9±0.3	149
0.3wt% MWCNT/epoxy	2.92±0.05	20.4±0.9	144
0.5wt% MWCNT/epoxy	2.76±0.13	21.8±1.1	147
0.1wt% TRGO/epoxy	2.76±0.04	18.5±0.3	149
0.3wt% TRGO/epoxy	2.96±0.04	25.6±0.2	149
0.5wt% TRGO/epoxy	2.92±0.06	26.7±0.2	152
0.1wt% GNP/epoxy	2.89±0.05	27.10±0.19	149
0.3wt% GNP/epoxy	2.94±0.01	29.11±0.31	148
0.5wt% GNP/epoxy	3.18±0.04	23.43±1.9	149
1.0wt% GNP/epoxy	3.01±0.04	32.35±0.08	151
2.0wt% GNP/epoxy	3.14±0.07	34.37±0.4	148

Table A.2: Fracture toughness values of nano-composite from SEN-3PB test.

	K_{IC} (MPa.m$^{1/2}$) from SEN-3PB test
Pure epoxy	0.567±0.048
0.05wt% MWCNT/epoxy	0.540±0.017
0.1wt% MWCNT/epoxy	0.547±0.037
0.2wt% MWCNT/epoxy	0.598±0.026
0.5wt% MWCNT/epoxy	0.616±0.053
0.05wt% TRGO/epoxy	0.629±0.060
0.1wt% TRGO/epoxy	0.716±0.090
0.3wt% TRGO/epoxy	0.767±0.047
0.5wt% TRGO/epoxy	0.795±0.056
0.05wt% GNP/epoxy	0.527±0.036
0.1wt% GNP/epoxy	0.557±0.049
0.2wt% GNP/epoxy	0.638±0.028
0.5wt% GNP/epoxy	0.711±0.110
1.0wt% GNP/epoxy	0.816±0.090
2.0wt% GNP/epoxy	0.732±0.080

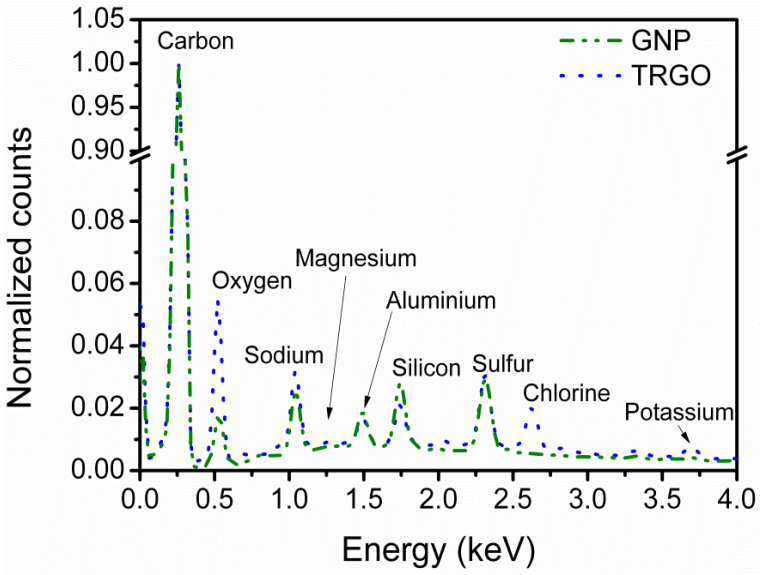

Figure A.7: Energy dispersive spectrum for the as-received TRGO and GNP nano-fillers.

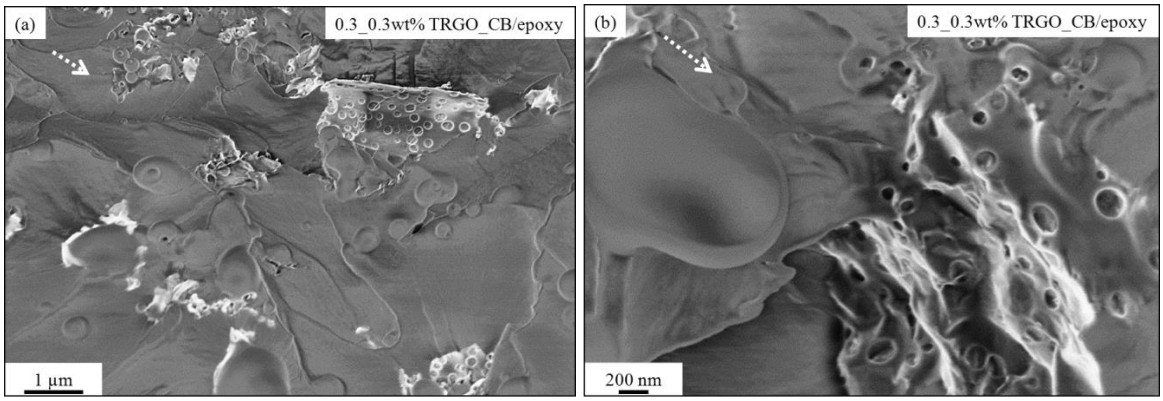

Figure A.8: Scanning electron micrograph of cryo-fractured 0.3_0.3wt% TRGO_CB/epoxy in "in-lens" mode where (a) impression of CB agglomerates on graphene sheets and (b) higher magnification micrograph. Dotted lines indicate crack propagation direction.

Publications from this work

List of publications

1. **Swetha Chandrasekaran**, Gabriella Faiella, L.A.S.A. Prado, Folke Tölle, Rolf Mülhaupt, Karl Schulte. "Thermally reduced graphene oxide acting as a trap for multiwall carbon nanotubes in bi-filler epoxy composites". Composites: Part A 49 (2013) 51-57.
2. **Swetha Chandrasekaran**, Christian Seidel, Karl Schulte. "Preparation and characterization of graphite nano-platelet (GNP)/epoxy nano-composite: Mechanical, electrical and thermal properties". European Polymer Journal, 49(12), (2013) 3878-3888.
3. Olesja Starkova, **Swetha Chandrasekaran**, L.A.S.A. Prado, Folke Tölle, Rolf Mülhaupt, Karl Schulte. "Hydrothermally resistant thermally reduced graphene oxide and multi-wall carbon nanotube based epoxy nanocomposites". Polymer Degradation and Stability 98 (2013) 519-526.
4. Evegenij Mannov, Henrik Schmutzler, **Swetha Chandrasekaran**, Christian Viets, Samuel Buschhorn, Folke Tölle, Rolf Mülhaupt ,Karl Schulte. "Improvement of compressive strength after impact in fibre reinforced polymer composites by matrix modification with thermally reduced graphene oxide". Composites Science and Technology 87 (2013) 36-41.
5. **Swetha Chandrasekaran**, Narumichi Sato, Folke Tölle, Rolf Mülhaupt, Karl Schulte. "Fracture toughness and failure mechanism of graphene based epoxy composites". Composites science and technology 97 (2014) 90-99.
6. Narumichi Sato, **Swetha Chandrasekaran**, Folke Tölle, Rolf Mülhaupt, Masaki Hojo, Karl Schulte. "The toughening effect of carbon nanofillers on the fracture toughness of Epoxy / PA6 microparticles composite" – Submitted (under review).

List of Conferences

1. **Swetha Chandrasekaran**, Narumichi Sato, Christian Seidel and Karl Schulte. Preparation and characterisation of graphite nano-platelet (GNP)/epoxy nano-composite: Mechanical, electrical and thermal properties. 6th International Conference on Carbon NanoParticle Based Composites (CNPComp2013), Dresden, Germany (September 21-25, 2013). Oral.
2. **Swetha Chandrasekaran**, Gabriella Faiella, L.A.S.A. Prado, Folke Tölle, Rolf Mülhaupt, Karl Schulte. Mechanical and Electrical Properties of a Few Layer Thermally Reduced Graphene Oxide based Bi-filler Nanocomposite. 4th International Conference On Recent

Advances In Composite Materials (ICARCM 2013), Goa, India (February 18-21, 2013). Oral.

3. **Swetha Chandrasekaran**, L. A. S. A. Prado, Samuel T. Buschhorn, Rolf Mülhaupt, Heinz Zeininger, Karl Schulte. Fracture toughness and thermo-mechanical properties of thermally reduced graphene oxide/epoxy nano-composites. 15th European Conference on Composite Materials (ECCM15), Venice, Italy (June 24-28, 2012). Oral.
4. **Swetha Chandrasekaran**, Thea I. W. Schnoor, L. A. S. A. Prado, Karl Schulte. Preparation of Graphene Nano-ribbons By Chemical Unzipping of Carbon Nanotubes. Eurofillers 2011, Dresden (August 21-25, 2011). Poster.

References

[1] Balazs AC, Emrick T, Russell TP. Nanoparticle Polymer Composites: Where Two Small Worlds Meet. Science 2006;314(5802):1107–10.

[2] Chung D. Carbon materials for structural self-sensing, electromagnetic shielding and thermal interfacing. Carbon 2012;50(9):3342–53.

[3] Dresselhaus MS, Dresselhaus G, Charlier JC, Hernandez E. Electronic, thermal and mechanical properties of carbon nanotubes. Philosophical Transactions of the Royal Society A: Mathematical, Physical and Engineering Sciences 2004;362(1823):2065–98.

[4] Terrones M. Science and technology of the twenty-first century: Synthesis, Properties, and Applications of Carbon Nanotubes. Annual review of Materials Research 2003;33(1):419–501.

[5] Novoselov KS, Fal′ko VI, Colombo L, Gellert PR, Schwab MG, Kim K. A roadmap for graphene. Nature 2012;490(7419):192–200.

[6] Stankovich S, Dikin DA, Dommett GHB, Kohlhaas KM, Zimney EJ, Stach EA, Piner RD, Nguyen ST, Ruoff RS. Graphene-based composite materials. Nature 2006;442(7100):282–6.

[7] Jancar J, Douglas J, Starr FW, Kumar SK, Cassagnau P, Lesser AJ, Sternsteinh SS, Buehler MJ. Current issues in research on structure–property relationships in polymer nanocomposites. Polymer 2010;51(15):3321–43.

[8] Gojny FH, Wichmann MHG, Fiedler B, Schulte K. Influence of different carbon nanotubes on the mechanical properties of epoxy matrix composites – A comparative study. Composites Science and Technology 2005;65(15-16):2300–13.

[9] Yasmin A, Abot JL, Daniel IM. Processing of clay/epoxy nanocomposites by shear mixing. Scripta Materialia 2003;49(1):81–6.

[10] Wetzel B, Haupert F, Zhang MQ. Epoxy nanocomposites with high mechanical and tribological performance. Composites Science and Technology 2003;63(14):2055–67.

[11] Mackay ME, Tuteja A, Duxbury PM, Hawker CJ, Van Horn B, Guan Z, Chen G, Krishnan RS. General strategies for nanoparticle dispersion. Science 2006;311(5768):1740–3.

[12] Coleman JN, Khan U, Blau WJ, Gun'ko YK. Small but strong: A review of the mechanical properties of carbon nanotube–polymer composites. Carbon 2006;44(9):1624–52.

[13] Coleman JN, Khan U, Gun'ko YK. Mechanical reinforcement of polymers using carbon nanotubes. Advanced Materials 2006;18(6):689–706.

[14] Bauhofer W, Kovacs JZ. A review and analysis of electrical percolation in carbon nanotube polymer composites. Composites Science and Technology 2009;69(10):1486–98.

[15] Gojny FH, Wichmann MHG, Köpke U, Fiedler B, Schulte K. Carbon nanotube-reinforced epoxy-composites: enhanced stiffness and fracture toughness at low nanotube content. Composites Science and Technology 2004;64(15):2363–71.

[16] Fidelus JD, Wiesel E, Gojny FH, Schulte K, Wagner HD. Thermo-mechanical properties of randomly oriented carbon/epoxy nanocomposites. Composites Part A: Applied Science and Manufacturing 2005;36(11):1555–61.

[17] Martone A, Formicola C, Giordano M, Zarrelli M. Reinforcement efficiency of multi-walled carbon nanotube/epoxy nano composites. Composites Science and Technology 2010;70(7):1154–60.

[18] Chae HG, Sreekumar TV, Uchida T, Kumar S. A comparison of reinforcement efficiency of various types of carbon nanotubes in polyacrylonitrile fiber. Polymer 2005;46(24):10925–35.

[19] Geim AK, Novoselov KS. The rise of graphene. Nature Materials 2007;6:183–91.

[20] Allen MJ, Tung VC, Kaner RB. Honeycomb carbon: A review of graphene. Chemical Reviews 2010;110(1):132–45.

[21] Li D, Müller MB, Gilje S, Kaner RB, Wallace GG. Processable aqueous dispersions of graphene nanosheets. Nature Nanotechnology 2008;3(2):101–5.

[22] Du J, Cheng H. The fabrication, properties, and uses of graphene/polymer composites. Macromolecular Chemistry and Physics 2012;213(10-11):1060–77.

[23] Debelak B, Lafdi K. Use of exfoliated graphite filler to enhance polymer physical properties. Carbon 2007;45(9):1727–34.

[24] Du J, Zhao L, Zeng Y, Zhang L, Li F, Liu P, Liu C. Comparison of electrical properties between multi-walled carbon nanotube and graphene nanosheet/high density polyethylene composites with a segregated network structure. Carbon 2011;49(4):1094–100.

[25] Wu C, Huang X, Wang G, Lv L, Chen G, Li G, Jiang P. Highly conductive nanocomposites with three-dimensional, compactly interconnected graphene networks via a self-assembly process. Advanced Functional Materials 2013;23(4):506–13.

[26] Wallace PR. The band theory of graphite. Physical Review 1947;71(9):622–34.

[27] Boehm HP, Setton R, Stumpp E. Nomenclature and terminology of graphite intercalation compounds. Carbon 1986;24(2):241–5.

[28] H.P. Boehm ACGFaUH. Das Adsorptionsverhalten sehr dünner Kohlenstoff-Folien. Zeitschrift fuer anorganische und allgemeine Chemie. 1962;316:120-127.

[29] Novoselov KS, Geim AK, Morozov SV, Jiang D, Zhang Y, Dubonos SV, Grigorieva IV, Firsov AA. Electric field effect in atomically thin carbon films. Science 2004;306(5696):666–9.

[30] Dreyer DR, Ruoff RS, Bielawski CW. From conception to realization: An historial account of graphene and some perspectives for its future. Angewandte Chemie International Edition 2010;49(49):9336–44.

[31] Zhu Y, James DK, Tour JM. New Routes to Graphene, Graphene Oxide and Their Related Applications. Adv. Mater. 2012;24(36):4924–55.

[32] Rümmeli MH, Rocha CG, Ortmann F, Ibrahim I, Sevincli H, Börrnert F et al. Graphene: Piecing it Together. Adv. Mater. 2011;23(39):4471–90.

[33] Wang X, You H, Liu F, Li M, Wan L, Li S, Li Q, Xu Y, Tian R, Yu Z, Xiang D, Cheng J. Large-scale synthesis of few-layered graphene using CVD. Chemical Vapor Deposition 2009;15(1-3):53–6.

[34] Shelton JC, Patil R, Blakely JM. Equilibrium segregation of carbon to a nickel (111) surface: a surface phase transition. Surface Science 1974;43(2):493–520.

[35] Eizenberg M, Blakely JM. Carbon monolayer phase condensation on Ni (111). Surface Science 1979;82(1):228–36.

[36] Guermoune A, Chari T, Popescu F, Sabri SS, Guillemette J, Skulason HS, Szkopek T, Siaj M. Chemical vapor deposition synthesis of graphene on copper with methanol, ethanol, and propanol precursors. Carbon 2011;49(13):4204–10.

[37] Hu Y, Ruan M, Guo Z, Dong R, Palmer J, Hankinson J, Berger C, Heer W. Structured epitaxial graphene: growth and properties. Journal of Physics D: Applied Physics 2012;45(15):154010:1-12.

[38] Kim KS, Zhao Y, Jang H, Lee SY, Kim JM, Kim KS, Ahn J, Kim P, Choi J, Hong BH. Large-scale pattern growth of graphene films for stretchable transparent electrodes. Nature Letters 2009;457(5):706–10.

[39] Camara N, Rius G, Huntzinger JR, Tiberj A, Mestres N, Godignon P, Camassel J. Selective epitaxial growth of graphene on SiC. Applied Physics Letters 2008;93(12):123503.

[40] Kosynkin DV, Higginbotham AL, Sinitskii A, Lomeda JR, Dimiev A, Price BK, Tour JM. Longitudinal unzipping of carbon nanotubes to form graphene nanoribbons. Nature Letters 2009;458(7240):872–6.

[41] Cataldo F, Compagnini G, Patané G, Ursini O, Angelini G, Ribic PR, Margaritondoe G, Cricentif A, Palleschig G, Valentini F. Graphene nanoribbons produced by the oxidative unzipping of single-wall carbon nanotubes. Carbon 2010;48(9):2596–602.

[42] Subrahmanyam KS, Panchakarla LS, Govindaraj A, Rao CNR. Simple method of preparing graphene flakes by an arc-discharge method. Journal of Physical Chemistry C 2009;113(11):4257–9.

[43] Liao C, Lu Y, Tamalampudi SR, Cheng H, Chen Y. Chemical vapor deposition synthesis and Raman spectroscopic characterization of large-area graphene sheets. Journal of Physical Chemistry A 2013;117(39):9454–61.

[44] Wu Y, Wang B, Ma Y, Huang Y, Li N, Zhang F, Chen Y. Efficient and large-scale synthesis of few-layered graphene using an arc-discharge method and conductivity studies of the resulting films. Nano Research 2010;3(9):661–9.

[45] Edwards RS, Coleman KS. Graphene synthesis: relationship to applications. Nanoscale 2013;5(1):38-51.

[46] Emtsev KV, Bostwick A, Horn K, Jobst J, Kellogg GL, Ley L, McChesney JL et al. Towards wafer-size graphene layers by atmospheric pressure graphitization of silicon carbide. Nature Materials 2009;8(3):203–7.

[47] Nie S, Wu W, Xing S, Yu Q, Bao J, Pei S, McCarty F. Growth from below: bilayer graphene on copper by chemical vapor deposition. New Journal of Physics 2012;14(9):93028.

[48] Ju H, Huh SH, Choi SH, Lee H. Structures of thermally and chemically reduced graphene. Materials Letters 2010;64(3):357–60.

[49] http://www.drilube.co.jp/english/common/img/product/img_graphitized.jpg.

[50] Zhang Y, Small JP, Pontius WV, Kim P. Fabrication and electric-field-dependent transport measurements of mesoscopic graphite devices. Applied Physics Letters 2005;86(7):73104.

[51] Lu X, Yu M, Huang H, Ruoff RS. Tailoring graphite with the goal of achieving single sheets. Nanotechnology 1999;10(3):269–72.

[52] Jayasena B, Subbiah S. A novel mechanical cleavage method for synthesizing few-layer graphenes. Nanoscale Research Letters 2011;6(1):95.

[53] Choucair M, Thordarson P, Stride JA. Gram-scale production of graphene based on solvothermal synthesis and sonication. Nature Nanotechnology 2008;4(1):30–3.

[54] Du W, Jiang X, Zhu L. From graphite to graphene: direct liquid-phase exfoliation of graphite to produce single- and few-layered pristine graphene. Journal of Materials Chemistry A 2013;1(36):10592.

[55] Hummers WS, Offeman RE. Preparation of graphitic oxide. Journal of American Chemical Society 1958;80(6):1339.

[56] Heyong He, Klinowski J, Forster M, Lerf A. A new structural model for graphite oxide. Chemical Physics Letters 1998;287(1-2):53–6.

[57] Lerf A, He H, Forster M, Klinowski J. Structure of graphite oxide revisited. Journal of physical Chemistry B 1998;102(23):4477–82.

[58] Ju H, Choi S, Huh SH. X-ray diffraction patterns of thermally-reduced graphenes. Journal of the Korean Physical Society, 2010;57(61):1649.

[59] Brodie BC. On the atomic weight of graphite. Philosophical Transactions of the Royal Society of London 1859;149(0):249–59.

[60] Dreyer DR, Park S, Bielawski CW, Ruoff RS. The chemistry of graphene oxide. Chemical Society Reviews 2009;39(1):228.

[61] Pei S, Cheng H. The reduction of graphene oxide. Carbon 2012;50(9):3210–28.

[62] McAllister MJ, Li J, Adamson DH, Schniepp HC, Abdala AA, Liu J, Herrera-Alonso M, Milius DL, Car R , Prud'homme RK, Aksay IA. Single Sheet Functionalized Graphene by Oxidation and Thermal Expansion of Graphite. Chemistry of Materials 2007;19(18):4396–404.

[63] Sridhar V, Jeon JH, Oh I. Synthesis of graphene nano-sheets using eco-friendly chemicals and microwave radiation. Carbon 2010;48(10):2953–7.

[64] Hu H, Zhao Z, Zhou Q, Gogotsi Y, Qiu J. The role of microwave absorption on formation of graphene from graphite oxide. Carbon 2012;50(9):3267–73.

[65] Chua CK, Pumera M. Chemical reduction of graphene oxide: a synthetic chemistry viewpoint. Chemical Society Reviews 2013;43(1):291.

[66] Gao W, Alemany LB, Ci L, Ajayan PM. New insights into the structure and reduction of graphite oxide. Nature Chemistry 2009;1(5):403–8.

[67] Ambrosi A, Chua CK, Bonanni A, Pumera M. Lithium aluminum hydride as reducing agent for chemically reduced graphene oxides. Chemistry of Materials 2012;24(12):2292–8.

[68] Zhang J, Yang H, Shen G, Cheng P, Zhang J, Guo S. Reduction of graphene oxide via L-ascorbic acid. Chemical Communications 2010;46(7):1112.

[69] Pei S, Zhao J, Du J, Ren W, Cheng H. Direct reduction of graphene oxide films into highly conductive and flexible graphene films by hydrohalic acids. Carbon 2010;48(15):4466–74.

[70] Dreyer DR, Murali S, Zhu Y, Ruoff RS, Bielawski CW. Reduction of graphite oxide using alcohols. Journal of Materials Chemistry 2011;21(10):3443.

[71] Rourke JP, Pandey PA, Moore JJ, Bates M, Kinloch IA, Young RJ, Wilson NR. The real graphene oxide revealed: stripping the oxidative debris from the graphene-like sheets. Angewandte Chemie International Edition 2011;123(14):3231–5.

[72] Sangermano M, Tagliaferro A, Foix D, Castellino M, Celasco E. In situ reduction of graphene oxide in an epoxy resin thermally cured with amine. Macromolecular Materials and Engineering 2013:Available online.

[73] Traina M, Pegoretti A. In situ reduction of graphene oxide dispersed in a polymer matrix. Journal of Nanoparticle Research 2012;14(4):801.

[74] Xu Y, Sheng K, Li C, Shi G. Highly conductive chemically converted graphene prepared from mildly oxidized graphene oxide. Journal of Materials Chemistry. 2011;21(20):7376.

[75] Varela-Rizo H, Rodriguez-Pastor I, Merino C, Martin-Gullon I. Highly crystalline graphene oxide nano-platelets produced from helical-ribbon carbon nanofibers. Carbon 2010;48(12):3640–3.

[76] Viculis LM, Mack JJ, Mayer OM, Hahn HT, Kaner RB. Intercalation and exfoliation routes to graphite nanoplatelets. Journal of Materials Chemistry. 2005;15(9):974.

[77] Chen J, Jang C, Xiao S, Ishigami M, Fuhrer MS. Intrinsic and extrinsic performance limits of graphene devices on SiO_2. Nature Nanotechnology 2008;3(4):206–9.

[78] Tse W, Qiao Z, Yao Y, MacDonald AH, Niu Q. Quantum anomalous Hall effect in single-layer and bilayer graphene. Physical Review B 2011;83(15).

[79] Balandin AA, Ghosh S, Bao W, Calizo I, Teweldebrhan D, Miao F, Lau CN. Superior thermal conductivity of single-layer graphene. Nano Letters 2008;8(3):902–7.

[80] Lee C, Wei X, Kysar JW, Hone J. Measurement of the elastic properties and intrinsic strength of monolayer graphene. Science 2008;321(5887):385–8.

[81] Pascault J, Sautereau H, Verdu J, Williams RJJ. Thermosetting Polymers. CRC Press, 2002.

[82] Hernandez A. Evaluation of electrical conductivity of graphene and CNT in epoxy composites. Bachelor Thesis at Instituts M-11: Kunststoffe und Verbundwerkstoffe, TUHH, Germany, 2012.

[83] Boyle MA, Martin CJ, and Neuner JD. Epoxy resins. ASM Handbook, Volume 21: Composites. Miracle DB and Donaldson SL, editors, 2001, 78-89.

[84] Data Sheet: Hot curing epoxy system based on Araldite LY 556 / Aradur 917 /

Accelerator DY 070. Huntsman LLC, Basel, Switzerland, March 2004. Available at:

http://www.astorit.ch/fileadmin/publikationen_f/composite_heisshaertend/ LY556-906-DY070_E_2007.pdf.

[85] Das TK, Prusty S. Graphene-based polymer composites and their applications. Polymer-Plastics Technology and Engineering 2013;52(4):319–31.

[86] Ma PC, Siddiqui NA, Marom G, Kim JK. Dispersion and functionalization of carbon nanotubes for polymer-based nanocomposites: A review. Composites Part A: Applied Science and Manufacturing 2010;41(10):1345–67.

[87] Villar-Rodil S, Paredes JI, Martínez-Alonso A, Tascón JMD. Preparation of graphene dispersions and graphene-polymer composites in organic media. Journal of Materials Chemistry 2009;19(22):3591.

[88] Monti M, Rallini M, Puglia D, Peponi L, Torre L, Kenny JM. Morphology and electrical properties of graphene–epoxy nanocomposites obtained by different solvent assisted processing methods. Composites Part A: Applied Science and Manufacturing 2013;46:166–72.

[89] Liang J, Huang Y, Zhang L, Wang Y, Ma Y, Guo T, Chen Y. Molecular-level dispersion of graphene into poly(vinyl alcohol) and effective reinforcement of their nanocomposites. Advanced Functional Materials 2009;19(14):2297–302.

[90] Zhao X, Zhang Q, Chen D. Enhanced mechanical properties of graphene-based poly(vinyl alcohol) composites. Macromolecules 2010;43(5):2357–63.

[91] Ramanathan T, Abdala AA, Stankovich S, Dikin DA, Herrera-Alonso M, Piner RD, Adamson DH, Schniepp HC, Chen X, Ruoff RS, Nguyen ST, Aksay IA, Prud'Homme RK, Brinson LC. Functionalized graphene sheets for polymer nanocomposites. Nature Nanotechnology 2008;3(6):327–31.

[92] Luo J, Jiang S, Wu Y, Chen M, Liu X. Synthesis of stable aqueous dispersion of graphene/polyaniline composite mediated by polystyrene sulfonic acid. Journal of Polymer Science Part A: Polymer Chemistry 2012;50(23):4888–94.

[93] Kim H, Miura Y, Macosko CW. Graphene/polyurethane nanocomposites for improved gas barrier and electrical conductivity. Chemistry of Materials 2010;22(11):3441–50.

[94] Gudarzi MM, Sharif F. Enhancement of dispersion and bonding of graphene-polymer through wet transfer of functionalized graphene oxide. eXPRESS Polymer Letters 2012;6(12):1017–31.

[95] Fang M, Zhang Z, Li J, Zhang H, Lu H, Yang Y. Constructing hierarchically structured interphases for strong and tough epoxy nanocomposites by amine-rich graphene surfaces. Journal of Materials Chemistry. 2010;20(43):9635.

[96] Greco A, Timo A, Maffezzoli A. Development and characterization of amorphous thermoplastic matrix graphene nanocomposites. Materials 2012;5(12):1972–85.

[97] Kim H, Kobayashi S, AbdurRahim MA, Zhang MJ, Khusainova A, Hillmyer MA, Abdala AA, Macosko CW. Graphene/polyethylene nanocomposites: Effect of polyethylene functionalization and blending methods. Polymer 2011;52(8):1837–46.

[98] Steurer P, Wissert R, Thomann R, Mülhaupt R. Functionalized graphenes and thermoplastic nanocomposites based upon expanded graphite oxide. Macromolecular Rapid Communications 2009;30(4-5):316–27.

[99] Araby S, Zaman I, Meng Q, Kawashima N, Michelmore A, Kuan HC, Majewski P, Ma J, Zhang L. Melt compounding with graphene to develop functional, high-performance elastomers. Nanotechnology 2013;24(16):165601.

[100] Feng L, Guan G, Li C, Zhang D, Xiao Y, Zheng L, Zhu W. In-situ synthesis of poly(methyl methacrylate)/graphene oxide nanocomposites using thermal-initiated and graphene oxide-initiated polymerization. Journal of Macromolecular Science, Part A: Pure and Applied Chemistry 2013;50(7):720–7.

[101] Aldosari MA, Othman AA, Alsharaeh EH. Synthesis and characterization of the in situ bulk polymerization of PMMA containing graphene sheets using microwave irradiation. Molecules 2013;18(3):3152–67.

[102] Fim F, Basso NRS, Graebin AP, Azambuja DS, Galland GB. Thermal, electrical, and mechanical properties of polyethylene-graphene nanocomposites obtained by in situ polymerization. Journal of Applied Polymer Science 2013;128(5):2630–7.

[103] Chen G, Wu D, Weng W, He B, Yan W. Preparation of polystyrene-graphite conducting nanocomposites via intercalation polymerization. Polymer international 2001;50(9):980–5.

[104] Glover AJ, Cai M, Overdeep KR, Kranbuehl DE, Schniepp HC. In-situ reduction of graphene oxide in polymers. Macromolecules 2011;44(24):9821–9.

[105] Weiss NO, Zhou H, Liao L, Liu Y, Jiang S, Huang Y, Duan X. Graphene: An emerging electronic material. Advanced Materials 2012;24(43):5782–825.

[106] Cong H, Ren X, Wang P, Yu S. Flexible graphene–polyaniline composite paper for high-performance supercapacitor. Energy Environmental Science 2013;6(4):1185.

[107] Li J, Xie H, Li Y, Liu J, Li Z. Electrochemical properties of graphene nanosheets/polyaniline nanofibers composites as electrode for supercapacitors. Journal of Power Sources 2011;196(24):10775–81.

[108] Wang X, Wang T, Yang C, Li H, Liu P. Well-defined flake-like polypyrrole grafted graphene nanosheets composites as electrode materials for supercapacitors with enhanced cycling stability. Applied Surface Science 2013;287:242–51.

[109] Bora C, Dolui SK. Interfacial synthesis of polypyrrole/graphene composites and investigation of their optical, electrical and electrochemical properties. Polymer International 2013: Available online.

[110] Chatterjee S, Nüesch FA, Chu BTT. Comparing carbon nanotubes and graphene nanoplatelets as reinforcements in polyamide 12 composites. Nanotechnology 2011;22(27):275714.

[111] Pang H, Chen T, Zhang G, Zeng B, Li Z. An electrically conducting polymer/graphene composite with a very low percolation threshold. Materials Letters 2010;64(20):2226–9.

[112] Gojny FH, Wichmann MHG, Fiedler B, Kinloch IA, Bauhofer W, Windle AH and Schulte K. Evaluation and identification of electrical and thermal conduction mechanisms in carbon nanotube/epoxy composites. Polymer 2006;47(6):2036–45.

[113] Shahil KMF, Balandin AA. Thermal properties of graphene and multilayer graphene: Applications in thermal interface materials. Solid State Communications 2012;152(15):1331–40.

[114] Raza MA, Westwood AVK, Brown AP, Stirling C. Texture, transport and mechanical properties of graphite nanoplatelet/silicone composites produced by three roll mill. Composites Science and Technology 2012;72(3):467–75.

[115] Corcione CE, Maffezzoli A. Transport properties of graphite/epoxy composites: Thermal, permeability and dielectric characterization. Polymer Testing 2013;32(5):880–8.

[116] Teng C, Ma CM, Lu C, Yang S, Lee S, Hsiao M, Yen M, Chiou K, Lee T. Thermal conductivity and structure of non-covalent functionalized graphene/epoxy composites. Carbon 2011;49(15):5107–16.

[117] Luo T, Lloyd JR. Enhancement of thermal energy transport across graphene/graphite and polymer interfaces: a molecular dynamics study. Advanced Functional Materials 2012;22(12):2495–502.

[118] Chatterjee S, Nafezarefi F, Tai NH, Schlagenhauf L, Nüesch FA, Chu BTT. Size and synergy effects of nanofiller hybrids including graphene nanoplatelets and carbon nanotubes in mechanical properties of epoxy composites. Carbon 2012;50(15):5380–6.

[119] Rafiee MA, Rafiee J, Wang Z, Song H, Yu Z, Koratkar N. Enhanced mechanical properties of nanocomposites at low graphene content. ACS Nano 2009;3(12):3884–90.

[120] Vadukumpully S, Paul J, Mahanta N, Valiyaveettil S. Flexible conductive graphene/poly(vinyl chloride) composite thin films with high mechanical strength and thermal stability. Carbon 2011;49(1):198–205.

[121] Wang Y, Shi Z, Yin J. Unzipped Multiwalled Carbon Nanotubes for Mechanical Reinforcement of Polymer Composites. Journal of Physical Chemistry C 2010;114(46):19621–8.

[122] Fan J, Shi Z, Ge Y, Wang Y, Wang J, Yin J. Mechanical reinforcement of chitosan using unzipped multiwalled carbon nanotube oxides. Polymer 2012;53(2):657–64.

[123] Mannov E, Schmutzler H, Chandrasekaran S, Viets C, Buschhorn ST, Tölle F, Mülhaupt, Schulte K. Improvement of compressive strength after impact in fibre reinforced polymer composites by matrix modification with thermally reduced graphene oxide. Composites Science and Technology 2013;87:36–41.

[124] Yavari F, Rafiee MA, Rafiee J, Yu Z, Koratkar N. Dramatic Increase in Fatigue Life in Hierarchical Graphene Composites. ACS Applied Materials and Interfaces 2010;2(10):2738–43.

[125] Rafiee MA, Rafiee J, Yu Z, Koratkar N. Buckling resistant graphene nanocomposites. Applied Physics Letters 2009;95(22):223103,1-3.

[126] Jana S, Zhong W. Graphite particles with a "puffed" structure and enhancement in mechanical performance of their epoxy composites. Materials Science and Engineering: A 2009;525(1-2):138–46.

[127] Wetzel B, Rosso P, Haupert F, Friedrich K. Epoxy nanocomposites – fracture and toughening mechanisms. Engineering Fracture Mechanics 2006;73(16):2375–98.

[128] Garg AC, Mai Y. Failure mechanisms in toughened epoxy resins—A review. Composites Science and Technology 1988;31(3):179–223.

[129] Lee J, Yee AF. Inorganic particle toughening I: micro-mechanical deformations in the fracture of glass bead filled epoxies. Polymer 2001;42(2):577–88.

[130] Kinloch AJ, Shaw SJ, Tod DA, Hunston DL. Deformation and fracture behaviour of a rubber-toughened epoxy: 1. Microstructure and fracture studies. Polymer 1983;24(10):1341–54.

[131] Yee AF, Pearson RA. Toughening mechanisms in elastomer-modified epoxies Part 1. Journal of Materials Science 1986(21):2462–74.

[132] Pearson RA, Yee AF. Toughening mechanisms in elastomer-modified epoxies Part 2. Journal of Materials Science 1986(21):2475–88.

[133] Zhao Q, Hoa SV. Toughening mechanism of epoxy resins with micro/nano particles. Journal of Composite Materials 2006;41(2):201–19.

[134] Hsieh TH, Kinloch AJ, Taylor AC, Kinloch IA. The effect of carbon nanotubes on the fracture toughness and fatigue performance of a thermosetting epoxy polymer. Journal of Materials Science 2011;46(23):7525–35.

[135] Johnsen BB, Kinloch AJ, Mohammed RD, Taylor AC, Sprenger S. Toughening mechanisms of nanoparticle-modified epoxy polymers. Polymer 2007;48(2):530–41.

[136] Wichmann MHG, Schulte K, Wagner HD. On nanocomposite toughness. Composites Science and Technology 2008;68(1):329–31.

[137] Liang YL, Pearson R. Toughening mechanisms in epoxy–silica nanocomposites (ESNs). Polymer 2009;50(20):4895–905.

[138] Srivastava I, Koratkar N. Fatigue and fracture toughness of epoxy nanocomposites. Journal of materials 2010;62(2):50–7.

[139] Ayatollahi MR, Shokrieh MM, Shadlou S, Kefayati AF, Chitsazzadeh M. Mechanical and electrical properties of epoxy/ multi-walled carbon nanotube/nanoclay nanocomposites. Iranian Polymer Journal 2011;20(10):835–43.

[140] Wang K, Chen L, Wu J, Toh ML, He C, Yee AF. Epoxy nanocomposites with highly exfoliated clay: mechanical properties and fracture mechanisms. Macromolecules 2005;38(3):788–800.

[141] Kim BC, Park SW, Lee DG. Fracture toughness of the nano-particle reinforced epoxy composite. Composite Structures 2008;86(1-3):69–77.

[142] Swaminathan G, Shivakumar K. Thermomechanical and fracture properties of exfoliated nanoclay nanocomposites. Journal of Reinforced Plastics and Composites 2011;30(3):256–68.

[143] Morales AG, Taylor AC, Fu M, Hyde A. Nanoclay-filled epoxy composites for electrical insulation applications. Proceedings of the 9th International Conference on Properties and Applications of Dielectric Materials 2009:868–71.

[144] Lachman N, Wagner HD. Correlation between interfacial molecular structure and mechanics in CNT/epoxy nano-composites. Composites Part A: Applied Science and Manufacturing 2010;41(9):1093–8.

[145] Bortz DR, Heras EG, Martin-Gullon I. Impressive fatigue life and fracture toughness improvements in graphene oxide/epoxy composites. Macromolecules 2012;45(1):238–45.

[146] Tang L, Wan Y, Yan D, Pei Y, Zhao L, Li Y, Wu L, Jiang J, Lai G. The effect of graphene dispersion on the mechanical properties of graphene/epoxy composites. Carbon 2013;60:16–27.

[147] Zaman I, Phan TT, Kuan H, Meng Q, Bao La LT, Luong L, Youssf O, Ma J. Epoxy/graphene platelets nanocomposites with two levels of interface strength. Polymer 2011;52(7):1603–11.

[148] Rafiee MA, Rafiee J, Srivastava I, Wang Z, Song H, Yu Z, Koratkar N. Fracture and fatigue in graphene nanocomposites. Small 2010;6(2):179–83.

[149] Schulz S, Faiella G, Buschhorn ST, Prado LASA, Giordano M, Schulte K, Bauhofer W. Combined electrical and rheological properties of shear induced multiwall carbon nanotube agglomerates in epoxy suspensions. European Polymer Journal 2011;47(11):2069–77.

[150] Bauhofer W, Schulz S, Eken A, Skipa T, Lellinger D, Alig I, Tozzi EJ, Klingenberg DJ. Shear-controlled electrical conductivity of carbon nanotubes networks suspended in low and high molecular weight liquids. Polymer 2010;51(22):5024–7.

[151] Alig I, Pötschke P, Lellinger D, Skipa T, Pegel S, Kasaliwal GR, Villmow T. Establishment, morphology and properties of carbon nanotube networks in polymer melts. Polymer 2012;53(1):4–28.

[152] Jelitto H, , Swain MV, Balke H, Schneider GA, Felten F. Measurement of the total energy release rate for cracks in PZT under combined mechanical and electrical loading. Journal of Applied Mechanics 2007;74(6):1197.

[153] Özcoban H, Jelitto H, Schneider GA. Influence of finite notch root radius and optically determined crack length on the measured fracture toughness of brittle materials. Journal of the European Ceramic Society 2010;30(7):1579–83.

[154] Jiang B, Liu C, Zhang C, Liang R, Wang B. Maximum nanotube volume fraction and its effect on overall elastic properties of nanotube-reinforced composites. Composites Part B: Engineering 2009;40(3):212–7.

[155] Schueler R, Petermann J, Schulte K, Wentzel H. Agglomeration and electrical percolation behavior of carbon black dispersed in epoxy resin. Journal of Applied Polymer Science 1997;63(13):1741–6.

[156] Huang YY, Terentjev EM. Dispersion of carbon nanotubes: mixing, sonication, stabilization, and composite properties. Polymers 2012;4(4):275–95.

[157] Shaffer M, Fan X, Windle AH. Dispersion and packing of carbon nanotubes. Carbon 1998;36(11):1603–12.

[158] He L, Tjong S. Carbon nanotube/epoxy resin composite: Correlation between state of nanotube dispersion and Zener tunneling parameters. Synthetic Metals 2012;162(24):2277–81.

[159] Fu X, Wang J, Ding J, Wu H, Dong Y, Fu Y. Quantitative evaluation of carbon nanotube dispersion through scanning electron microscopy images. Composites Science and Technology 2013;87:170–3.

[160] Zhang K, Park B, Fang F, Choi H. Sonochemical preparation of polymer nanocomposites. Macromolecules 2009;14(6):2095–10.

[161] Li YB, Wei BQ, Liang J, Yu Q, Wu DH. Transformation of carbon nanotubes to nanoparticles by ball milling process. Carbon 1999;37(3):493–7.

[162] Ma PC, Tang BZ, Kim J. Conversion of semiconducting behavior of carbon nanotubes using ball milling. Chemical Physics Letters 2008;458(1-3):166–9.

[163] Villmow T, Pötschke P, Pegel S, Häussler L, Kretzschmar B. Influence of twin-screw extrusion conditions on the dispersion of multi-walled carbon nanotubes in a poly(lactic acid) matrix. Polymer 2008;49(16):3500–9.

[164] Orloff J (Editor). Handbook of charged particle optics. CRC press 2008.

[165] Li W, Buschhorn ST, Schulte K, Bauhofer W. The imaging mechanism, imaging depth, and parameters influencing the visibility of carbon nanotubes in a polymer matrix using an SEM. Carbon 2011;49(6):1955–64.

[166] Martin C, Sandler J, Shaffer M, Schwarz M, Bauhofer W, Schulte K, Windle AH. Formation of percolating networks in multi-wall carbon-nanotube–epoxy composites. Composites Science and Technology 2004;64(15):2309–16.

[167] Flandin L, Prasse T, Schueler R, Schulte K, Bauhofer W, Cavaille J.-Y. Anomalous percolation transition in carbon-black–epoxy composite materials. Physical Review B 1999;59(22):14349–55.

[168] Bunde A, Dieterich W. Percolation in composites. Journal of Electroceramics 2000;5(2):81–92.

[169] Faiella G, Piscitelli F, Lavorgna M, Antonucci V, Giordano M. Tuning the insulator to conductor transition in a multiwalled carbon nanotubes/epoxy composite at substatistical percolation threshold. Applied Physics Letters 2009;95(15):153106.

[170] Dang Z, Shehzad K, Zha J, Mujahid A, Hussain T, Nie J, Shi C. Complementary percolation characteristics of carbon fillers based electrically percolative thermoplastic elastomer composites. Composites Science and Technology 2011;72(1):28–35.

[171] Ruschau GR, Newnham RE. Critical volume fractions in conductive composites. Journal of Composite Materials 1992;26(18):2727–35.

[172] Aguilar JO, Bautista-Quijano JR, Avilés F. Influence of carbon nanotube clustering on the electrical conductivity of polymer composite films. eXPRESS Polymer Letters 2010;4(5):292–9.

[173] Bao WS, Meguid SA, Zhu ZH, Pan Y, Weng GJ. A novel approach to predict the electrical conductivity of multifunctional nanocomposites. Mechanics of Materials 2012;46:129–38.

[174] Li J, Kim J. Percolation threshold of conducting polymer composites containing 3D randomly distributed graphite nanoplatelets. Composites Science and Technology 2007;67(10):2114–20.

[175] Sandler JKW, Kirk JE, Kinloch IA, Shaffer M, Windle AH. Ultra-low electrical percolation threshold in carbon-nanotube-epoxy composites. Polymer 2003;44(19):5893–9.

[176] Terrones M, Martín O, González M, Pozuelo J, Serrano B, Cabanelas JC, Vega-Diaz SM, Baselga J. Interphases in graphene polymer-based nanocomposites: achievements and challenges. Advanced Marterials 2011;23(44):5302–10.

[177] Sumfleth J, Adroher XC, Schulte K. Synergistic effects in network formation and electrical properties of hybrid epoxy nanocomposites containing multi-wall carbon nanotubes and carbon black. Journal of Materials Science 2009;44(12):3241–7.

[178] Sumfleth J, Buschhorn ST, Schulte K. Comparison of rheological and electrical percolation phenomena in carbon black and carbon nanotube filled epoxy polymers. Journal of Materials Science 2011;46(3):659–69.

[179] Mueller S, Llewellin EW, Mader HM. The rheology of suspensions of solid particles. Proceedings of the Royal Society A: Mathematical, Physical and Engineering Sciences 2010;466(2116):1201–28.

[180] Starý Z, Krückel J, Schubert DW. Shear induced electrical behaviour of conductive polymer composites. AIP Conference Proceddings – Novel Trends in Rheology V:258–67.

[181] Schulz SC, Schlutter J, Buschhorn ST, Schulte K, Bauhofer W. Rheological properties and irreversible dispersion changes in carbon nanotube/epoxy systems. Polymer Engineering and Science 2012;52(4):849–55.

[182] Kim JA, Seong DG, Kang TJ, Youn JR. Effects of surface modification on rheological and mechanical properties of CNT/epoxy composites. Carbon 2006;44(10):1898–905.

[183] Schulz SC, Faiella G, Buschhorn ST, Schulte K, Giordano M, Bauhofer W. Determination of dispersion state of carbon nanotubes/epoxy suspensions prepared by different mixing techniques. Annual Transactions of The Nordic Rheology Society 2011;19:95-100.

[184] Seo J, Cha J, Kim S. Enhancement of the thermal conductivity of adhesives for wood flooring using xGnP. Energy and Buildings 2012;51:153–6.

[185] Yu A, Ramesh P, Itkis M, Bekyarova E, Haddon R. Graphite nanoplatelet-epoxy composite thermal interface materials. Journal of Physical Chemistry C 2007;111(21):7565–9.

[186] Yu L, Park JS, Lim YS, Lee CS, Shin K, Moon HJ, Yanng CM, Lee YS, Han JH. Carbon hybrid fillers composed of carbon nanotubes directly grown on graphene nanoplatelets for effective thermal conductivity in epoxy composites. Nanotechnology 2013;24(15):155604.

[187] Huang X, Zhi C, Jiang P. Toward effective synergetic effects from graphene nanoplatelets and carbon nanotubes on thermal conductivity of ultrahigh volume fraction nanocarbon epoxy composites. Journal of Physical Chemistry C 2012;116(44):23812–20.

[188] Zhou S, Xu J, Yang Q, Chiang S, Li B, Du H, Xu C and Kang F. Experiments and modeling of thermal conductivity of flake graphite/polymer composites affected by adding carbon-based nano-fillers. Carbon 2013;57:452–9.

[189] Sun Y, Zhang Z, Moon KS, Wong CP. Glass transition and relaxation behavior of epoxy nanocomposites. Journal of Polymer Science Part B: Polymer Physics 2004;42(21):3849–58.

[190] Rahaman A, Mohanty A. Effect of carbon nanotubes on the curing and thermomechanical behavior of epoxy/carbon nanotubes composites. Polymer composites 2013:Available online.

[191] Srivastava I, Yu Z, Koratkar NA. Viscoelastic properties of graphene-polymer composites. Advanced Science Engineering and Medicine 2012;4(1):10–4.

[192] Prado LASA, Kwiatkowska M, Funari SS, Roslaniec Z, Broza G, Schulte K. Studies on morphology and interphase of poly(butylene terephthalate)/carbon nanotubes nanocomposites. Polymer Engineering and Science 2010;50(8):1571–6.

[193] Venditti A, Gillham JK, Jean YC, Lou Y. Free volume after cure vs. fractional conversion for a high-Tg epoxy/amine thermosetting system. Journal of Applied Polymer Science 1995;56(10):1207–20.

[194] Kinloch AJ, Williams JG. Crack blunting mechanisms in polymers. Journal of Materials Science 1980;15(4):987–96.

[195] Munz D. What Can We Learn from R-Curve Measurements? Journal of American Ceramic Society 2007;90(1):1–15.

[196] Xiao K, Yee L, Kwok YS. Effects of pre-cracking methods on fracture behaviour of an Araldite-F epoxy and its rubber-modified systems. Journal of Materials Science;33(11):2831–6.

[197] Behr S. Investigation on effects of carbon nanoparticles on fracture properties of epoxies. Grosse Studienarbeit at Instituts M-11: Kunststoffe und Verbundwerkstoffe, TUHH, Germany, 2011.

[198] Saito R, Hofmann M, Dresselhaus G, Jorio A, Dresselhaus MS. Raman spectroscopy of graphene and carbon nanotubes. Advances in Physics 2011;60(3):413–550.

[199] Ferrari AC, Basko DM. Raman spectroscopy as a versatile tool for studying the properties of graphene. Nature Nanotechnology 2013;8:235–46.

[200] Ferrari AC, Meyer JC, Scardaci V, Casiraghi C, Lazzeri M, Mauri F, Piscanec S, Jiang D, Novoselov KS, Roth S, and Geim AK. Raman spectrum of graphene and graphene layers. Physical Review Letters 2006;97(18):1-4.

[201] Tuinstra F, Koenig JL. Raman spectrum of graphite. The journal of chemical physics 1970;53(3):1126.

[202] Tai FC, Wei C, Chang SH, Chen WS. Raman and X-ray diffraction analysis on unburned carbon powder refined from fly ash. Journal of Raman Spectroscopy 2010;41(9):933–7.

[203] Cançado LG, Jorio A, Ferreira EHM, Stavale F, Achete CA, Capaz RB, Moutinho MVO, Lombardo A, Kulmala TS, Ferrari AC. Quantifying defects in graphene via Raman spectroscopy at different excitation energies. Nano Leters 2011;11(8):3190–6.

[204] Knight DS, White WB. Characterization of diamond films by Raman spectroscopy. Journal of Materials Research 1989;4(2):385–93.

[205] Kim K, Park S. Influence of multi-walled carbon nanotubes on the electrochemical performance of graphene nanocomposites for supercapacitor electrodes. Electrochimica Acta 2011;56(3):1629–35.

[206] Cote LJ, Kim J, Tung VC, Luo J, Kim F, Huang J. Graphene oxide as surfactant sheets. Pure and Applied Chemistry 2011;83(1):95–110.

[207] Erickson K, Erni R, Lee Z, Alem N, Gannett W, Zettl A. Determination of the Local Chemical Structure of Graphene Oxide and Reduced Graphene Oxide. Advanced Materials 2010;22(40):4467–72.

[208] Tang LC, Zhang H, Sprenger S, Ye L, Zhang Z. Fracture mechanisms of epoxy-based ternary composites filled with rigid-soft particles. Composites Science and Technology 2012;72(5):558–65.

[209] Hull D. The effect of mixed mode I/III on crack evolution in brittle solids. International Journal of Fracture 1995;70(1):59–79.

[210] Fiedler B, Gojny FH, Wichmann MHG, Nolte MC, Schulte K. Fundamental aspects of nano-reinforced composites. Composites Science and Technology 2006;66(16):3115–25.

[211] Wagner HD, Ajayan PM, Schulte K. Nanocomposite toughness from a pull-out mechanism. Composites Science and Technology 2013;83:27–31.

[212] Shtein M, Nadiv R, Lachman N, Wagner HD, Regev O. Fracture behavior of nanotube–polymer composites: Insights on surface roughness and failure mechanism. Composites Science and Technology 2013;87:157–63.

[213] Yasmin A, Daniel IM. Mechanical and thermal properties of graphite platelet/epoxy composites. Polymer 2004;45(24):8211–9.

[214] Prolongo SG, Jimenez-Suarez A, Moriche R, Ureña A. In situ processing of epoxy composites reinforced with graphene nanoplatelets. Composites Science and Technology 2013;86:185–91.

[215] Parashar A, Mertiny P. Multiscale model to study of fracture toughening in graphene/polymer nanocomposite. International Journal of Freacture 2013;179(1-2):221–8.

[216] Gong L, Kinloch IA, Young RJ, Riaz I, Jalil R, Novoselov KS. Interfacial stress transfer in a graphene monolayer nanocomposite. Advanced Materials 2010;22(24):2694–7.

[217] Gong L, Young RJ, Kinloch IA, Riaz I, Jalil R, Novoselov KS. Optimizing the reinforcement of polymer-based nanocomposites by graphene. ACS Nano 2012;6(3):2086–95.

[218] Chandrasekaran S, Behr S, Buschhorn ST, Özcoban H, Tölle F, Mülhaupt R, Schneider G and Schulte K. R-curve measurements of thermally reduced graphene oxide based epoxy nanocomposite (to be published).

[219] Kruzic JJ, Nalla RK, Kinney JH, Ritchie RO. Crack blunting, crack bridging and resistance-curve fracture mechanics in dentin: Effect of hydration. Biomaterials 2003;24(28):5209–21.

[220] De Souza JA, Goutianos S, Skovgaard M, Sørensen BF. Fracture resistance curves and toughening mechanisms in polymer based dental composites. Journal of the Mechanical Behavior of Biomedical Materials 2011;4(4):558–71.

[221] Shen M, Chang T, Hsieh T, Li Y, Chiang C, Yang H, Yip M. Mechanical properties and tensile fatigue of graphene nanoplatelets reinforced polymer nanocomposites. Journal of Nanomaterials 2013;4:1–9.

[222] Starkova O, Chandrasekaran S, Prado L, Tölle F, Mülhaupt R, Schulte K. Hydrothermally resistant thermally reduced graphene oxide and multi-wall carbon nanotube based epoxy nanocomposites. Polymer Degradation and Stability 2013;98(2):519–26.